Jet Vectoring and Vorticity Generation Using Plasma Actuators

By

MICHAEL BOLITHO

Bachelor of Science in Mechanical Engineering
Oklahoma State University
Stillwater, OK, USA
2006

Submitted to the Faculty of the
Graduate College of
Oklahoma State University
in partial fulfillment of
the requirements for
the Degree of
MASTER OF SCIENCE
May, 2008

Jet Vectoring and Vorticity Generation Using Plasma Actuators

Thesis Approved:

Dr. Jamey Jacob

Thesis Advisor

Dr. Andrew Arena

Dr. Frank Chambers

Dr. A. Gordon Emslie

Dean of the Graduate College

ACKNOWLEDGMENTS

There are many people that I would like to thank that have made this journey much easier and more enjoyable than it would have been otherwise. First of all, I would like to express my sincere thanks to my advisor, Dr. Jamey Jacob, for being a better teacher and mentor than I could have ever imagined, who helped me to become a better scientist and engineer. I would also like to thank everybody that helped me in the lab, or at least kept me company – Nathan Lunsford, Ben Loh, Craig Williamson, Andrew Contreras, Grant Heimbach, Carlton Heard, and especially Ceren Ozturk who has been of tremendous help over the last year of this research. My thanks also go out to my parents and parents in-law for all the assistance and support they have given me. Thank you to Dr. Andy Arena and Dr. Frank Chambers for serving on my committee and giving constructive advice on my research. Finally, and most of all, I would like to thank my wife, Kirby Bolitho, for all of the help, support, and love she has given me throughout graduate school and otherwise.

TABLE OF CONTENTS

Chapter Page

1 Introduction **1**

2 Previous Work **5**

2.1 Plasma Flow Control 5

2.2 Vortex Generator Jets 9

3 Experimental Setup **11**

3.1 Plasma Actuator Construction 11

3.2 PIV Measurements 11

3.3 Benchtop Setup 12

3.4 Wind Tunnel Setup 13

3.5 Power Measurement 14

3.6 Derived Quantities 16

4 Jet Vectoring Plasma Actuator **19**

4.1 Benchtop 19

4.1.1 Steady Actuation 19

4.1.2 Unsteady Actuation 30

4.1.3 Critical Pulsing Frequency 45

4.2 Wind Tunnel 60

4.2.1 Duty Cycle 61

4.2.2 Pulsing Frequency 65

4.2.3 Sideslip Angle 67

4.2.4 Wind Tunnel Speed 72

5 Summary and Conclusions **79**

A Appendix **82**

A.1 PSJA Arrays 82

BIBLIOGRAPHY **86**

LIST OF FIGURES

Figure Page

1.1 Linear plasma actuator cross section schematic. 2

1.2 Plasma region generated by a plasma actuator 2

1.3 Jet vectoring plasma actuator cross section schematic. 3

1.4 Vortex generation using jet vectoring plasma actuator. 4

3.1 Raw PIV image from benchtop testing. 13

3.2 Schematic of benchtop experimental setup. 14

3.3 Schematic of wind tunnel experimental setup. 15

3.4 Raw PIV image from wind tunnel testing. 16

3.5 Current measurement of jet vectoring plasma actuator. 17

3.6 Voltage measurement of jet vectoring plasma actuator. 17

4.1 Example of jet vectoring using plasma actuators 20

4.2 Instantaneous PIV results for equal power to each side. 20

4.3 Instantaneous PIV results for slightly asymmetric power. 21

4.4 Instantaneous PIV results for highly asymmetric power. 21

4.5 Instantaneous PIV results for highly asymmetric power. 22

4.6 Averaged PIV results for the baseline (equal plasma) case. 23

4.7 Averaged PIV results for operating frequency of one side 250Hz below maximum output. 24

4.8 Averaged PIV results for operating frequency of one side 500Hz below maximum output. 25

4.9 Averaged PIV results for operating frequency of one side 750Hz below maximum output. 26
4.10 Averaged PIV results for operating frequency of one side 1000Hz below maximum output. 27
4.11 Averaged PIV results for operating frequency of one side 1500Hz below maximum output. 28
4.12 Angle of jet produced by decreasing the operating frequency of one side of the jet vectoring plasma actuator. 29
4.13 Smoke flow visualization of a pulsed jet vectoring plasma actuator. . . 30
4.14 Averaged PIV results for pulsing frequency of 10Hz, 1/2in spacing . . 31
4.15 Averaged PIV results for pulsing frequency of 50Hz, 1/2in spacing . . 32
4.16 Averaged PIV results for pulsing frequency of 100Hz, 1/2in spacing . 32
4.17 Averaged PIV results for pulsing frequency of 150Hz, 1/2in spacing . 33
4.18 Averaged PIV results for pulsing frequency of 200Hz, 1/2in spacing . 33
4.19 Averaged PIV results for pulsing frequency of 250Hz, 1/2in spacing . 34
4.20 Averaged PIV results for pulsing frequency of 500Hz, 1/2in spacing . 34
4.21 Averaged PIV results for pulsing frequency of 10Hz, 3/4in spacing . . 35
4.22 Averaged PIV results for pulsing frequency of 25Hz, 3/4in spacing . . 36
4.23 Averaged PIV results for pulsing frequency of 50Hz, 3/4in spacing . . 36
4.24 Averaged PIV results for pulsing frequency of 100Hz, 3/4in spacing . 37
4.25 Averaged PIV results for pulsing frequency of 150Hz, 3/4in spacing . 37
4.26 Averaged PIV results for pulsing frequency of 200Hz, 3/4in spacing . 38
4.27 Averaged PIV results for pulsing frequency of 250Hz, 3/4in spacing . 38
4.28 Averaged PIV results for pulsing frequency of 500Hz, 3/4in spacing . 39
4.29 Averaged PIV results for pulsing frequency of 10Hz, 1in spacing . . . 39
4.30 Averaged PIV results for pulsing frequency of 25Hz, 1in spacing . . . 40
4.31 Averaged PIV results for pulsing frequency of 50Hz, 1in spacing . . . 40

4.32 Averaged PIV results for pulsing frequency of 100Hz, 1in spacing . . 41
4.33 Averaged PIV results for pulsing frequency of 150Hz, 1in spacing . . 41
4.34 Averaged PIV results for pulsing frequency of 200Hz, 1in spacing . . 42
4.35 Averaged PIV results for pulsing frequency of 250Hz, 1in spacing . . 42
4.36 Averaged PIV results for pulsing frequency of 500Hz, 1in spacing . . 43
4.37 Vertical momentum flux induced by a jet vectoring plasma actuator with 1in exposed electrode spacing. 43
4.38 Vertical momentum flux induced by a jet vectoring plasma actuator with 3/4in exposed electrode spacing. 44
4.39 Averaged PIV results for duty cycles of 50% and 50% 45
4.40 Averaged PIV results for duty cycles of 50% and 45% 46
4.41 Averaged PIV results for duty cycles of 50% and 40% 47
4.42 Averaged PIV results for duty cycles of 50% and 35% 48
4.43 Averaged PIV results for duty cycles of 50% and 30% 49
4.44 Averaged PIV results for duty cycles of 50% and 25% 50
4.45 Jet angle produced with varying duty cycle. 51
4.46 Maximum vertical jet velocity decay for 50 Hz pulsing frequency. . . . 53
4.47 Maximum vertical jet velocity decay for 100 Hz pulsing frequency. . . 54
4.48 Maximum vertical jet velocity decay for 150 Hz pulsing frequency. . . 55
4.49 Maximum vertical jet velocity decay for 200 Hz pulsing frequency. . . 56
4.50 Maximum vertical jet velocity decay for 250 Hz pulsing frequency. . . 57
4.51 Maximum vertical jet velocity decay for 500 Hz pulsing frequency. . . 58
4.52 Schematic of jet produced at low pulsing frequencies. 59
4.53 Schematic of jet produced at pulsing frequencies near the critical frequency. 59
4.54 Schematic of jet produced at high pulsing frequencies. 60
4.55 Averaged PIV results for both channels operated at 50% DC. 61

4.56 Averaged PIV results for one channel at 50% and the other at 40% DC. 62
4.57 Averaged PIV results for one channel at 50% and the other at 30% DC. 62
4.58 Averaged PIV results for one channel at 50% and the other at 20% DC. 63
4.59 Averaged PIV results for one channel at 50% and the other at 10% DC. 63
4.60 Circulation induced by the jet vectoring plasma actuator at a 5° sideslip angle for different duty cycles. 64
4.61 Averaged PIV results for 1Hz pulsing frequency (below critical frequency). 66
4.62 Averaged PIV results for 100Hz pulsing frequency (near critical frequency). 66
4.63 Averaged PIV results for 250Hz pulsing frequency (above critical frequency). 67
4.64 Circulation induced by the jet vectoring plasma actuator at a 5° sideslip angle for different pulsing frequencies. 68
4.65 Averaged PIV results for both channels at 50% DC, 0° yaw. 69
4.66 Averaged PIV results for both channels at 50% DC, 5° yaw. 70
4.67 Averaged PIV results for both channels at 50% DC, 10° yaw. 70
4.68 Averaged PIV results for two channels at 50% and 20% DC, 0° yaw. . 71
4.69 Averaged PIV results for two channels at 50% and 20% DC, 5° yaw. . 71
4.70 Averaged PIV results for two channels at 50% and 20%, 10° yaw. . . 72
4.71 Circulation induced by the jet vectoring plasma actuator at different sideslip angles under symmetric operation. 73
4.72 Circulation induced by the jet vectoring plasma actuator at different sideslip angles under asymmetric operation (50% and 20% duty cycles). 74
4.73 Averaged PIV results for both channels at 50%, 1.7m/s tunnel speed. 75
4.74 Averaged PIV results for two channels at 50%, 3.4m/s tunnel speed. . 76

4.75 Averaged PIV results for two channels at 50% and 20%, 1.7m/s tunnel speed. 76
4.76 Averaged PIV results for two channels at 50% and 20%, 3.4m/s tunnel speed. 77
4.77 Circulation induced by the jet vectoring plasma actuator at different tunnel speeds, under asymmetric operation (50% and 20% duty cycles). 78

A.1 (a) Plasma ring created by pulsed annular actuator in blowing configuration. (b) Plasma ring created by pulsed annular actuator in suction configuration. 82
A.2 (a) Vortices induced by chevron actuator. (b) Cross-stream vortex structures. 83
A.3 PIV data of right side of PSJA in suction configuration. Left: phase-locked at $t = 13$ ms. Right: time-averaged. 83
A.4 Array of PSJAs: construction (left) and actuation (right). 83
A.5 Grid of alternating blowing and sucking PSJAs. 84
A.6 Cross section of a staged PSJA. 84
A.7 2 stage PSJA. 85

CHAPTER 1

Introduction

Plasma actuators refer to a number of devices that use atmospheric pressure electrical discharges. Types of discharges included in the plasma actuator category are glow discharges (such as one atmosphere uniform glow discharge plasma, OAUGDP), corona discharges, and dielectric barrier discharges (DBDs). DBD plasma actuators are of particular interest in the current study and are shown in Fig. 1.1; they consist of one electrode exposed to the atmosphere, and one electrode embedded under a dielectric material. Plasma is created along the interface of the electrodes by applying a high voltage, high frequency ac signal to the actuator to ionize the surrounding air. This region of plasma creates a body force on the surrounding air which induces a near wall jet. The intensity of the jet created is controlled by the input signal (as seen in Fig. 1.2 by varying the input power), dielectric material, electrode width, electrode gap, etc, while the type of jet produced is controlled by the arrangement of the plasma actuator. A number of researchers have studied the linear plasma actuator, but several other geometries have been studied, including annular, cylindrical, and chevron geometries, among others. Plasma actuators have been shown to be effective flow control devices primarily in the near wall region, adding momentum to the boundary layer, suppressing or delaying separation. Arrangements of the plasma actuator which affect the flow away from the near wall region have been studied in recent years, and will be the primary focus of the current study.

Similar in application to plasma actuators, conventional synthetic jet actuators, which create zero net mass flux jets, have been shown to be useful in certain flow con-

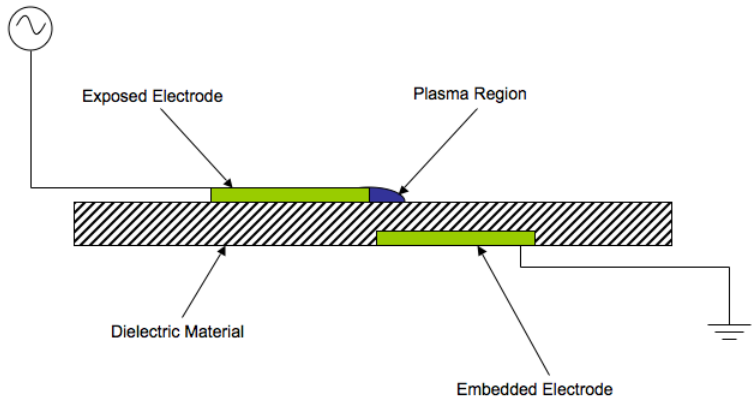

Figure 1.1: Linear plasma actuator cross section schematic.

Figure 1.2: Plasma region generated by a plasma actuator

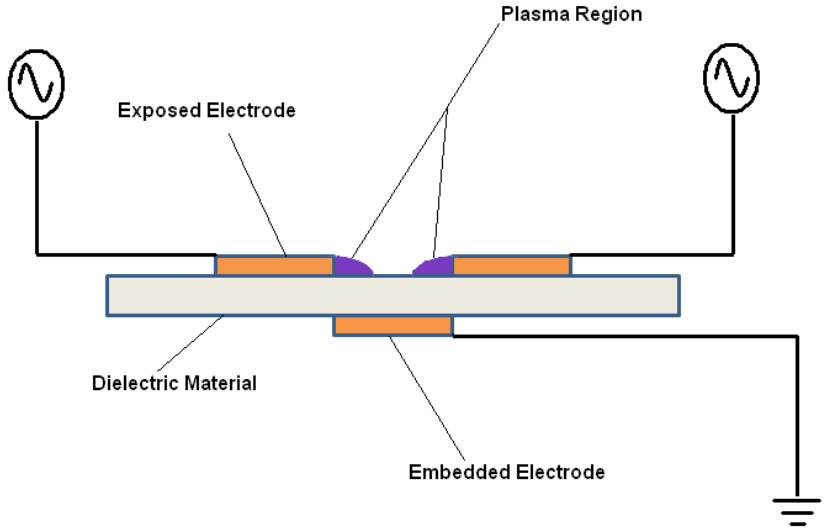

Figure 1.3: Jet vectoring plasma actuator cross section schematic.

trol applications [1]. Synthetic jet actuators utilize an oscillating diaphragm mounted inside of a cavity which alternately suck air in and blow air out of the cavity. While synthetic jet actuators are useful, with much higher jet velocities than that of plasma actuators, there are drawbacks when compared to plasma synthetic jet actuators (PSJAs) in that they have moving parts and require volume in which to be mounted.

The current study investigates the plasma actuator arranged such that it utilizes a single embedded electrode and an electrode exposed to the atmosphere on either side of the embedded electrode (shown in Fig. 1.3). Arranging the plasma actuator in this manner produces a synthetic jet similar to that of a conventional synthetic jet actuator. The plasma actuator investigated in the current study is shown to vector thrust over the entire spectrum from -90° to 90° in quiescent conditions, as well as create pulsed vortex generating jets in external flow, as shown in Fig. 1.4.

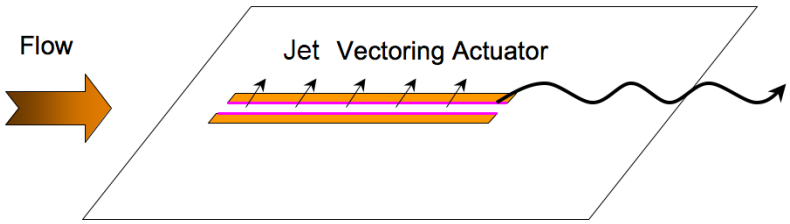

Figure 1.4: Vortex generation using jet vectoring plasma actuator.

CHAPTER 2

Previous Work

2.1 Plasma Flow Control

A number of researchers have investigated the use of plasma actuators as flow control devices, primarily for the addition of momentum to the boundary layer during separation. Some early work in the field of plasma flow control was done by Malik *et al.* [2]. The study used ionic wind produced by a dc corona discharge as a flow control device to modify the boundary layer over a flat plate. They found that at low speeds, up to 30 m/s, there were drag reductions of 20% for an applied voltage of 15 kV. Plasma flow control has since come to include dielectric barrier discharges, glow discharges, and arc discharges as well as the dc corona discharges investigated by Malik *et al.* .

Enloe *et al.* made several findings on the behavior of plasma actuators [3, 4]. In these two studies, they made numerous conclusions about the characteristics of the plasma actuator. In the paper covering plasma morphology, they found that the thrust provided by the actuator is directly proportional to the input power, which is proportional $V^{7/2}$. They also clearly determined that the aerodynamic plasma actuator produces a dielectric barrier discharge, and discounted bulk heating as a mechanism for affecting the flow. Their final conclusion in the paper over plasma morphology was that an electrostatic body force is created by the plasma actuator which is proportional to the net charge density and the strength of the electric field; the body force is given by $f = \rho E = -\frac{\epsilon_0}{\lambda_D^2}\phi E$ where ϵ_0 is the permittivity of free space and λ_D is the Debye length. In their paper over the geometric effects of plasma

actuators, they found that the largest force density is in a small region adjacent to the exposed electrode and that the exposed electrode edge has a considerable impact on the performance of the actuator.

The force created is a critical parameter in examining the effectiveness of the plasma actuator, and has been studied by Porter *et al.* [5], Gregory *et al.* [6], and Baughn *et al.* [7]. Porter *et al.* measured both the time-averaged force and the temporal force while varying operating frequency and voltage. They found that for constant voltage, the time-averaged body force and power dissipation are proportional to the frequency, but that the impulse during one cycle, energy dissipation during one cycle, and efficiency are independent of frequency. They also found that their data supports the theory of Font [8], that is, the plasma actuator produces one relatively large "push" and one relatively small "pull" (force in the opposite direction) during a cycle. Gregory *et al.* investigated the effects of pressure on the force created by the plasma actuator, and found that the efficiency of the actuator decreases linearly with decreasing pressure. Baughn *et al.* measured velocity profiles upstream and downstream of the actuator, and observed that for low freestream velocities (on the order of a few m/s), the force created by the actuator was not affected by the crossflow.

Corke and Post [9] presented an overview of several different flow control techniques using plasma actuators including leading-edge separation control on a wing section, separation control for low-pressure turbine blades, and control of dynamic stall on oscillating airfoils. They found that using the plasma actuator for leading-edge separation flow control at angles of attack well beyond stall increased the lift-to-drag ratio by as much as 400%. They also found that applying the plasma actuator near the leading edge of an oscillating airfoil improved the cycle-integrated lift by as much as 13%, and that the plasma actuator completely suppressed separation that occurs near the mid-chord of blades in a linear cascade. Finally, Corke and Post found that the plasma actuator operated with a short duty cycle was more effective than steady

actuation, which is particularly important to the current study.

Post and Corke [10] conducted a set of experiments, observing the effects of a leading-edge plasma actuator operated under steady and unsteady conditions for open- and closed-loop control. The actuator was placed on a NACA 0015 airfoil. They found that pulsing the actuator at 20 Hz gave a 10.1% improvement in lift, and using closed-loop 'smart' control improved the lift by 12.6%, each compared to the case with the actuator off. Experiments carried out by Corke *et al.* [11] attained similar results using leading-edge separation control on a NACA 0009 airfoil, and showed that the stall angle was increased.

While many researchers investigating the use of plasma actuators as leading-edge separation control devices primarily focus on adding momentum to the boundary layer, Porter *et al.* [12] argue that the plasma actuator is more useful when used as a boundary layer trip. They found that in laminar flow, the plasma actuator can sufficiently trip the boundary layer at a duty cycle of 10%. This is done by stealing momentum rather than adding it to the boundary layer to suppress separation.

Most of the research on plasma actuators completed thus far has been focused on using the actuator within the boundary layer, while there are some researchers, including Segawa *et al.* [13]and Santhanakrishnan and Jacob [14], that have investigated the use of plasma actuators outside of the boundary layer. Segawa *et al.* studied an arrangement of the linear plasma actuator that they found clearly created mushroom cloud plumes at temperatures of 20 and 200°C. Santhanakrishnan and Jacob investigated a plasma actuator that consists of an inner embedded circular electrode and an outer exposed annular electrode. The jet created by this actuator is normal to the wall with similar flow characteristics to that of a conventional synthetic jet actuator, and is referred to as a plasma synthetic jet actuator (PSJA). They found that the maximum jet velocity was on the order of 1 m/s and that the effectiveness of the PSJA decreased with increasing Re.

One Atmosphere Uniform Glow Discharge Plasma (OAUGDP), studied by Roth *et al.* [15], are glow discharge plasma actuators. They studied the OAUGDP in spanwise and streamwise arrays in laminar, transitional, and fully turbulent boundary layer flow over an operating frequency range of 2 kHz to 10 kHz. It was shown that drag is increased using a symmetric streamwise array compared to that of an asymmetric spanwise array.

Jacob *et al.* [16] studied boundary layer flow control using plasma actuators. They noted that to maximize the plasma output, the horizontal spacing between the embedded and exposed electrodes should be zero. They placed the actuator on a low pressure turbine blade at low Re to eliminate separation. Another investigation. done by Jacob *et al.* [17], examined plasma generation under ac and pulsed dc sources. They showed that using pulsed dc allows higher peak power levels compared to that when using an ac signal.

Roth and Dai [18] make detailed investigations on the effects of several dielectric and input signal parameters including dielectric material, electrode horizontal spacing, embedded electrode width, input frequency, and input voltage on the flow velocity induced by the OAUGDP actuator. They noticed that the choice of dielectric material affects the plasma volume, distribution of electric field lines, and heating power loss (the fraction of total input power dissipated as dielectric heating for a single plasma actuator was found by Roth *et al.* [19] to range from 48% to 100%). Roth and Dai stated that the optimum dielectric material would have a higher dielectric constant value, higher dielectric strength , and a lower heating loss factor. They found that using Teflon as the dielectric created a stronger jet when compared to quartz, and proceeded with the remainder of their experiments using Teflon as the dielectric material. The width of the embedded electrode was found to have a negligible effect on both the maximum induced velocity and input power required for the given actuator. The horizontal distance between the edge of the exposed and embedded

electrodes was adjusted to have a slight gap, zero gap, and slight overlap between electrodes. It was found that this variation had a significant effect on the induced velocity, and a 1 to 2 mm gap width was discovered to produce the maximum output for the particular actuator used. At constant frequency, it was found that increasing voltage to the actuator resulted in higher induced velocities. At constant voltage, the input frequency was varied, and they found that as the frequency was increased, the induced velocity would increase to a maximum, then drop with any increase in frequency beyond that.

Porter *et al.*[20] made measurements in quiescent conditions on a steady jet vectoring plasma actuator with by changing the voltage applied to one of the exposed electrodes. They found that by controlling the voltage differential between the two exposed electrodes, the angle of the jet can be controlled. Bolitho and Jacob [21] made similar measurements in quiescent flow, as well as measurements of the jet vectoring plasma actuator while being pulsed. They found that the angle of the jet produced by the actuator can be controlled by changing the power, operating frequency and duty cycle of one side of the jet vectoring plasma actuator. They also found that by varying the pulsing frequency, the type of jet produced by the actuator changes.

2.2 Vortex Generator Jets

Pulsed vortex generator jets (VGJs) have been used by researchers to reattach separated flow, commonly applied to low pressure turbine blades. McQuilling and Jacob [22] studied the use of VGJs applied to low pressure turbine blades placed at 69% and 10.5% of the suction surface length. They investigated both steady and pulsed VGJs, where the duty cycle of the pulsed VGJs was varied. They found that the case with the VGJ placed at 69% of the suction surface length under steady operation controlled separation the entire time, while pulsed blowing of 10% and 50% duty cycles were also effective at the same location. They investigated the second location

to explore the possibility of controlling separation with VGJs near the leading edge. When placed at this location, they were found to be ineffective. It was also noticed that the average diameter of the vortices created at the 69% location was 0.51 cm, while the average size of the vortices created at the 10.5% location was 0.39 cm, creating much less vorticity.

Gross and Fasel [23] studied the effects of pulsed vortex generator jets (PVGJs) and harmonic blowing applied to low pressure turbine blades at low Re. They showed that PVGJs trigger earlier flow transition which increases the turbulent momentum and allows the boundary layer to better deal with the adverse pressure gradient, therefore proving that this method effectively controls separation.

Bons *et al.* [24] conducted experiments in which they created strong vortices using VGJs and PVGJs for $Re = 25000$ to $Re = 100000$ applied to low pressure turbine blades. Similar to the findings of Gross and Fasel, they found that PVGJs, as well as VGJs, initiate early transition, effectively attaching the flow on the aft section of the suction side of the blade. They also discovered that the pulsed case provides separation control comparable to that of the steady case, but with an order of magnitude less required mass flow.

Using PIV measurements, McQuilling *et al.* [25] study the effects of VGJs and PVGJs applied to a low pressure turbine blade for $Re = 30000$ to $Re = 300000$. They observed that the location of separation without control is between 63.4% and 67.6% of the suction side length. With the location of the ejector nozzles set at 46% of the suction side length, when either VGJ or PVGJ control is applied, separation was completely eliminated for all the cases they examined.

CHAPTER 3

Experimental Setup

3.1 Plasma Actuator Construction

The plasma actuator arrangement studied in the current investigation consists of a single embedded electrode with an electrode on either side exposed to the atmosphere. The embedded electrode is separated from the exposed electrodes by a dielectric material. The dielectric material used in the current study is either 1/16 in thick Teflon or 0.025 in thick alumina. Teflon is used in the benchtop experiments, and alumina is used in the wind tunnel tests due to its robustness. For all tests, copper tape of width 1/2 in is utilized for the exposed electrodes, while the embedded electrode is 1/4 in, 1/2 in, 3/4 in, or 1 in width copper tape. The embedded electrode is grounded, and two separate high voltage (approximately 80kV PP), high frequency (5 to 10 kHz) ac signals are sent to each of the exposed electrodes.

3.2 PIV Measurements

Particle image velocimetry (PIV) is used to examine the entire flow field of a 2-D cross section of the flow above the plasma actuator. The flow field is seeded with particles on the order of 1 micron diameter, produced by a Turbofog fog generator. A laser light sheet is projected over the cross section of the plasma actuator, using a dual-head Nd:YAG laser from Big Sky Lasers pulsed in sync with a high speed, high resolution Kodak Megaplus ES 1.0 CCD camera using a Quantum Composer timing box. The camera being used for PIV measurements aquires images that are 1008 x

1018 pixels, captured using Epix frame grabbing software. The laser sheet is created by passing the laser emitted from the Big Sky laser through a set of three lenses. The first lense, a converging lense, is used to focus the laser. The second, a diverging lens, is placed at the focal length of the first lens and creates a more concentrated, thinner beam. The final lens, a cylindrical lens, is used to spread the beam into a 2-D laser sheet. Pairs of laser sheets are pulsed at 10Hz, while the delay between the two laser pulses within a pair is 50 or 100 microseconds. The field of view being examined is 5 to 6 cm, with a resolution of 125 to 205 pixels per cm. For each PIV run, 63 or 191 image pairs are captured, and averaged over each run.

The PIV algorithm used herein utilizes the wall adaptive Lagrangian parcel tracking algorithm (WaLPT), developed by Sholl and Savas [26]. This algorithm treats the seeding as fluid parcels and determines their translations and deformations. Fluid parcels registered by CCD pixels with individually estimated velocities and accelerations. A standard DPIV algorithm is used to determine the initial velocity field, and the routines in WaLPT allow for highly accurate measurements of velocities near surfaces by mirroring the flow about the wall using an image parity exchange routine. Velocity and vorticity, of specific interest, are calculated as part of the PIV algorithm and are scaled accordingly. Vorticity is determined spectrally and does not suffer from typical numerical differentiation problems. A typical raw PIV image can be seen in Fig. 3.1. Further details of the algorithm and error estimates are provided elsewhere [27].

3.3 Benchtop Setup

Using the PIV techniques described, the jet vectoring plasma actuator is characterized in a quiescent environment. The actuator is placed within a clear 20 in x 10 in x 12 in glass container, and fog is ducted into the container. The laser sheet is passed over the midspan of the actuator, which is placed perpindicular to the laser sheet such that

Figure 3.1: Raw PIV image from benchtop testing.

a cross section of the jet produced can be captured. The Kodak Megaplus camera is placed perpendicular to the laser sheet, as shown in Fig. 3.2. For all benchtop tests, the pulse delay between lasers within a single pair is 50 microseconds. 191 image pairs are captured for each run and averaged over the entire run. The field of view for all benchtop tests is approximately 6cm, with a resolution of approximately 165 pixels per cm.

3.4 Wind Tunnel Setup

The wind tunnel experiments utilize a low speed wind tunnel. The plasma actuator is placed near the front (upstream side) of the 12 in x 12 in test section, while the laser and camera equipment are placed outside of the wind tunnel. The fog is generated and diffused near the inlet of the wind tunnel, then passes through the wind tunnel and over the actuator. The laser sheet is passed over the actuator, perpendicular to the direction of the wind tunnel flow. A prism is placed inside the wind tunnel,

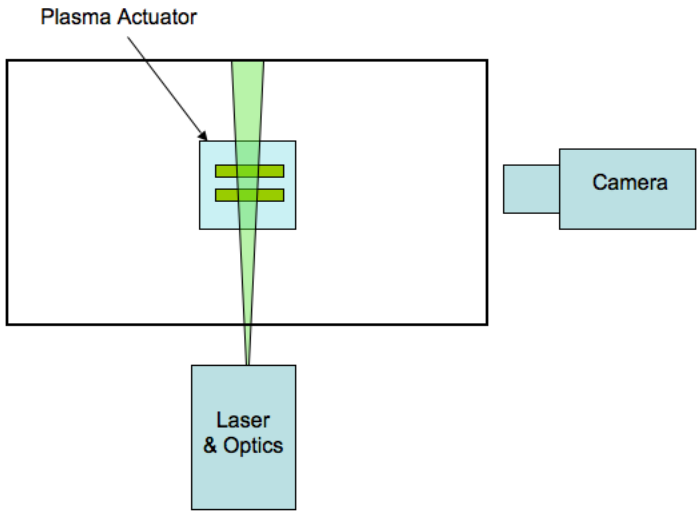

Figure 3.2: Schematic of benchtop experimental setup.

downstream of the plasma actuator, to allow the Kodak Megaplus camera to be mounted outside of the tunnel, as seen in Fig. 3.3. For all wind tunnel tests, the delay between laser pulses within a single pair is 100 microseconds. The field of view for the tests carried out in the wind tunnel is approximately 5 cm to 6 cm, with a resolution of 165 to 205 pixels per cm. The images captured in the wind tunnel tests contain small circular flow structures most likely due to the small amount of mixing at low wind tunnel speeds; this can be seen in the raw PIV image, shown in Fig. 3.4. Due to the WaLPT algorithm used, the flow structures did not present themselves as a problem, with correlations in wind tunnel tests similar to those of the benchtop tests.

3.5 Power Measurement

Power measurements are taken by measuring the current and voltage with a NK Technologies AC current transducer and a North Star PVM-11 1000:1 high voltage

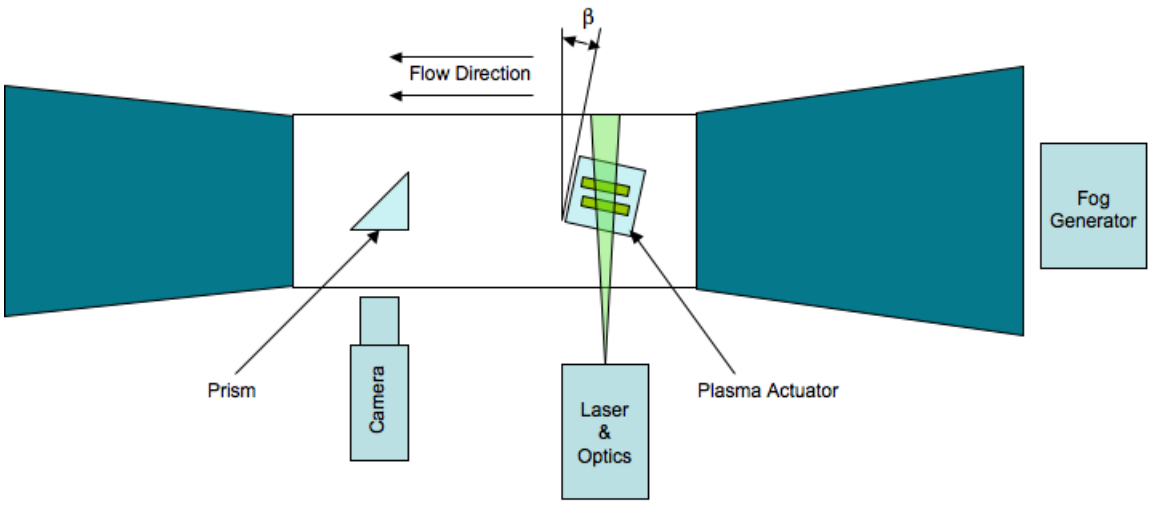

Figure 3.3: Schematic of wind tunnel experimental setup.

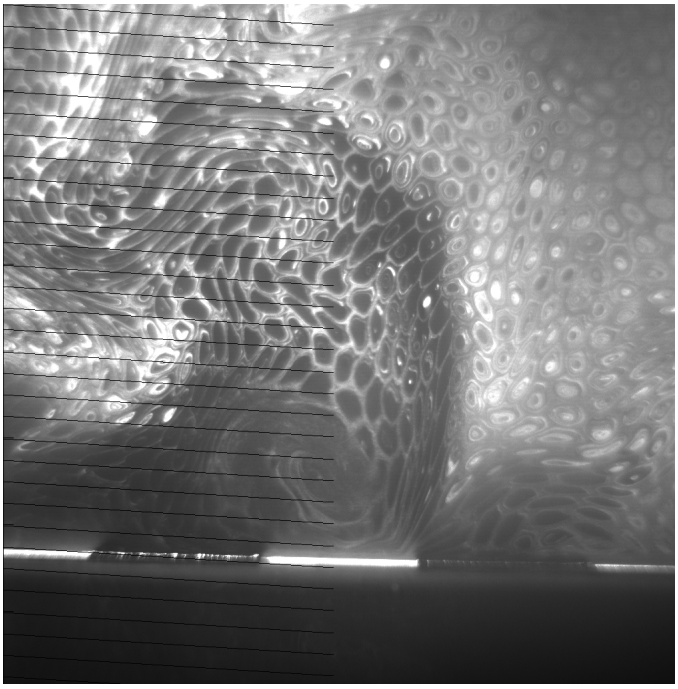

Figure 3.4: Raw PIV image from wind tunnel testing.

probe, respectively. Values of current and voltage are attained using an oscilloscope. Sample current and voltage readings are shown in Fig. 3.5 and Fig. 3.6, respectively. Average power consumption is calculated with the product of the means of current and voltage. Throughout this study, the input power is not varied extensively.

3.6 Derived Quantities

Several flow field parameters are calculated and shown throughout this study, including momentum flux, and circulation. These values are calculated using the velocity and velocity gradients output by the PIV algorithm. Momentum flux is particularly studied during the benchtop testing, while circulation is used to characterize the flow field created while the actuator is used for vortex generation in the wind tunnel.

The momentum flux is calculated for the plasma actuator while it is under symmetric operation by Eq. 3.1. Since this is only calculated under symmetric time averaged conditions and the control volume is outside of the plasma actuator, the

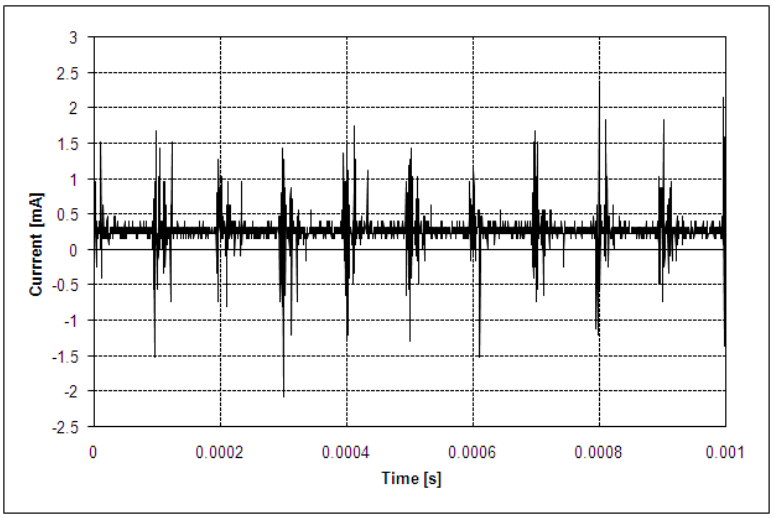

Figure 3.5: Current measurement of jet vectoring plasma actuator.

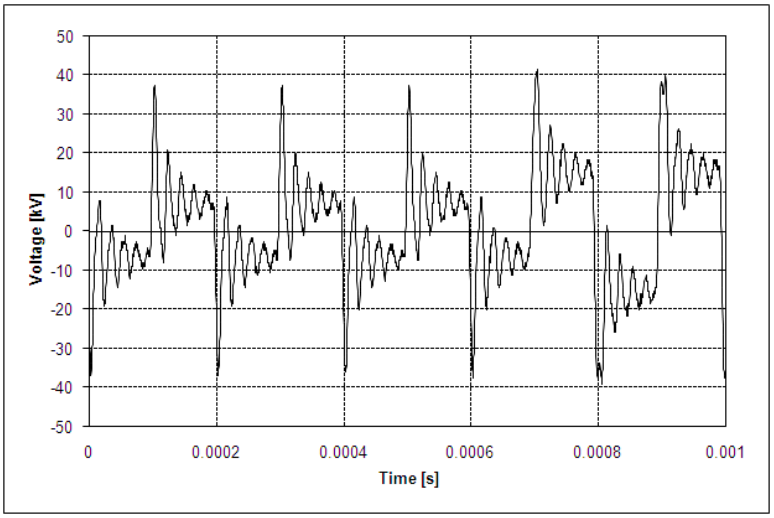

Figure 3.6: Voltage measurement of jet vectoring plasma actuator.

momentum flux contribution from the left and right sides of the control volume cancels. Additionally, the momentum flux at the bottom boundary of the control volume is zero due to the wall. Therefore, only the top of the control volume contributes to the momentum flux. Considering the momentum flux per unit span and discrete values, Eq. 3.1 becomes Eq. 3.2. Where dx is the space between two adjacent velocity vectors.

$$F = \int\int \rho\, V(V \cdot \hat{n})dA \tag{3.1}$$

$$F/z = \Sigma\, \rho\, V(V \cdot \hat{n})dx \tag{3.2}$$

The circulation is calculated by Eq. 3.3.

$$\Gamma = \int \vec{\omega} \cdot d\hat{A} \tag{3.3}$$

Using discrete values for vorticity output by the PIV algorithm, Eq. 3.3 can be written as Eq. 3.4.

$$\Gamma = \Sigma\, \omega_z dxdy \tag{3.4}$$

The circulation results are shown as a function of the radius of the vortex.

CHAPTER 4

Jet Vectoring Plasma Actuator

4.1 Benchtop

It is of interest, for the current study, to know how each parameter of the input signal and exposed electrode spacing affects the flow field induced by the jet vectoring plasma actuator. This is done by varying input power, operating frequency, duty cycle, pulsing frequency, and exposed electrode spacing independently. The results are obtained using PIV, either averaged over the entire run or instantaneous. The dielectric used in all benchtop tests is 1/16 in thick Teflon ($\epsilon \sim 2.1$), the exposed electrodes are 1/2 in wide copper tape, the embedded electrode is 1/2 in copper tape, except where it is specified to be 3/4 in or 1 in wide copper tape, and the horizontal spacing between the embedded electrode and exposed electrodes is nominally 0 in. Throughout the experimental results, several vorticity contours are shown, and are measured in units of 1/s.

4.1.1 Steady Actuation

Power

As a preliminary test, to determine the usefulness of varying the input signal parameters and to prove the jet vectoring concept, the power to each side of the jet vectoring plasma actuator is varied independently. The body force induced by linear plasma actuators has been shown by a number of researchers to scale linearly with input power. Fig. 4.1 shows the concept of using symmetric and asymmetric input power

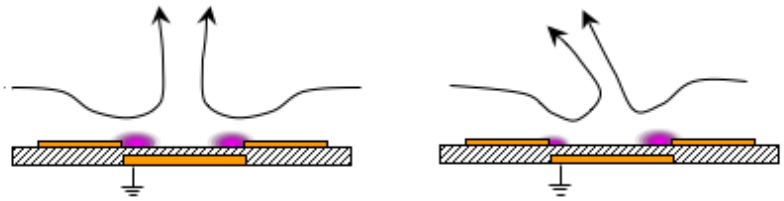

Figure 4.1: Example of jet vectoring using plasma actuators

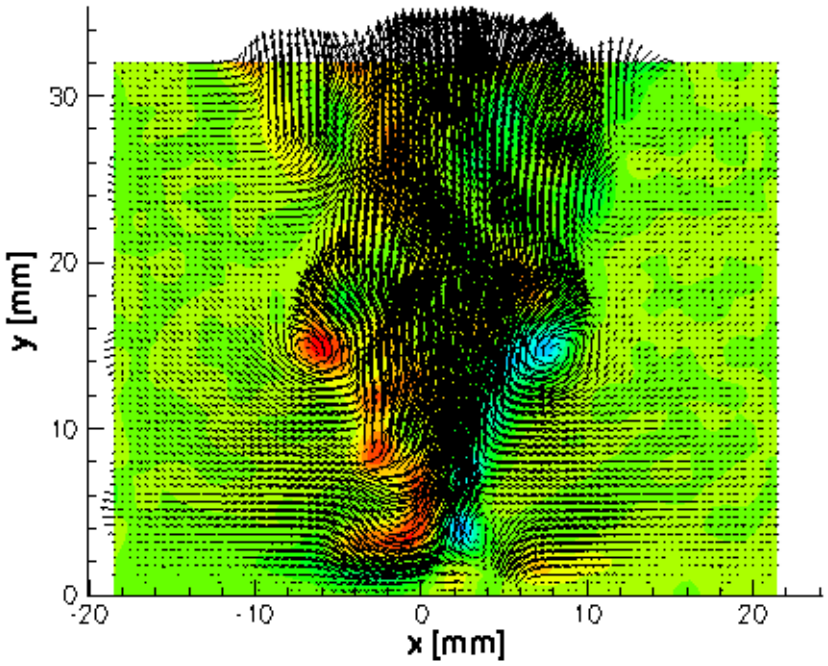

Figure 4.2: Instantaneous PIV results for equal power to each side.

to the jet vectoring plasma actuator. Fig. 4.2 shows an actuator being operated under symmetric power, both sides of the actuator have equal input power. By lowering the input power to one side of the actuator, a jet such as the one shown in Fig. 4.3 is produced. By operating only one side of the actuator, a near wall jet (-90° or 90°) is produced as seen in Fig. 4.4 and Fig. 4.5. By varying input power only, the jet vectoring plasma actuator produces a jet angle from -90° to 90° with respect to the normal to the wall.

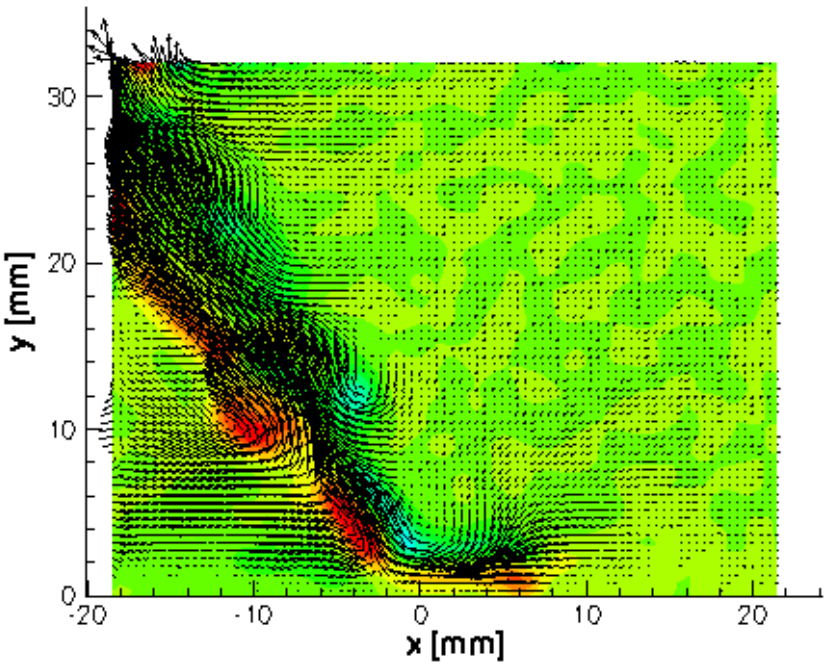

Figure 4.3: Instantaneous PIV results for slightly asymmetric power.

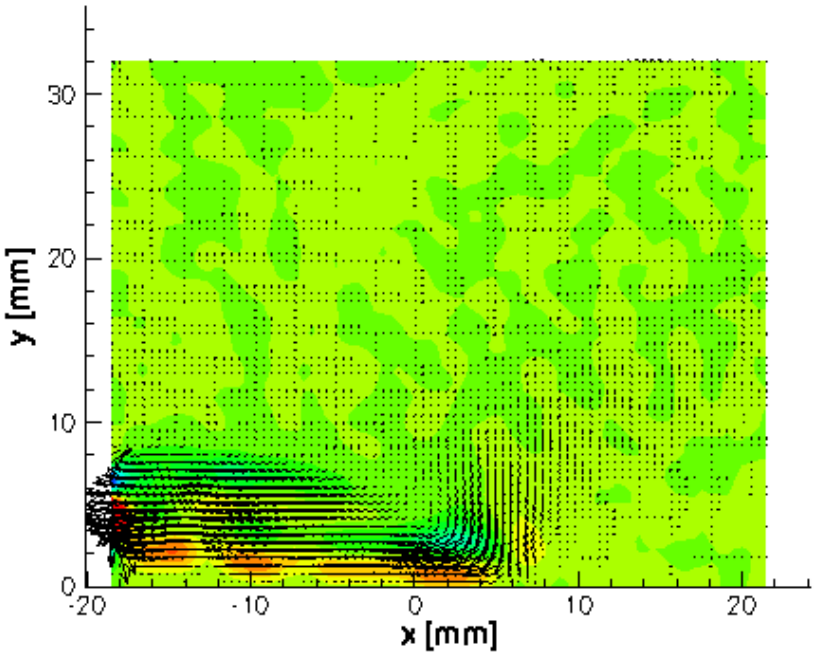

Figure 4.4: Instantaneous PIV results for highly asymmetric power.

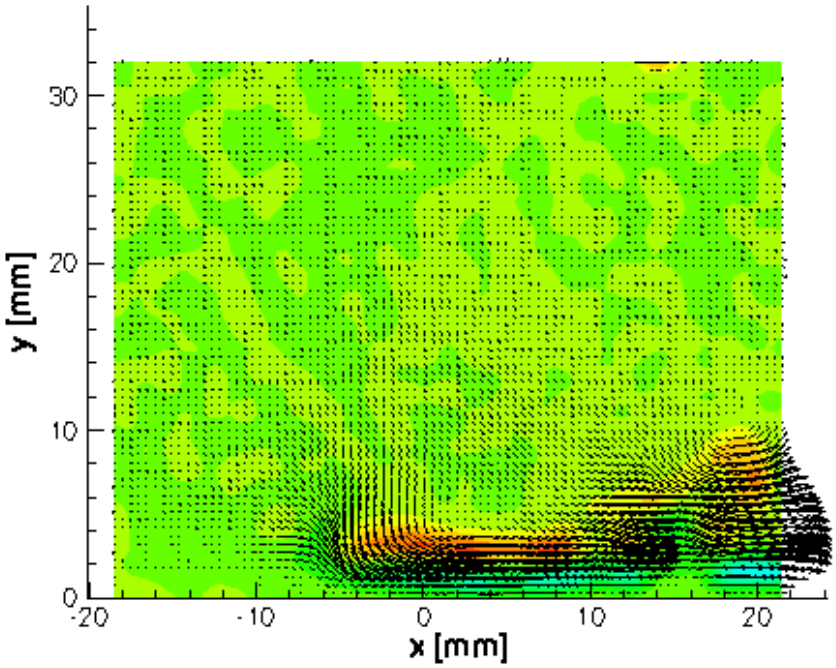

Figure 4.5: Instantaneous PIV results for highly asymmetric power.

Operating Frequency

By varying the operating frequency of a plasma actuator, the strength of the plasma can be controlled, hence the strength and direction of the jet produced by the jet vectoring plasma actuator. For the plasma actuator investigated currently, there is some case in which the jet produced is normal to the wall, as in the symmetric case shown in Fig. 4.2. By changing the operating frequency of either side of the actuator, the jet produced is not normal to the wall, as in the asymmetric case in Fig. 4.3. The baseline, or symmetric case, is shown in Fig. 4.6, which shows averaged PIV results. In this case, the operating frequency of each side is adjusted until the maximum plasma strength is obtained, as determined by the strength of the glow emitted by the actuator. The following cases, shown in Fig. 4.7 - Fig. 4.11, show how the flow field is affected when the driving frequency of the actuator on the right is decreased up to 1500 Hz away from its maximum plasma generation in steps of 250 Hz. These

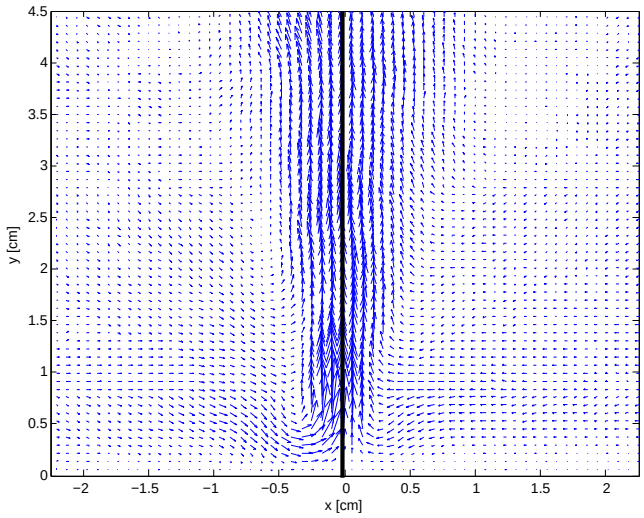

Figure 4.6: Averaged PIV results for the baseline (equal plasma) case.

figures show that as the driving frequency of the actuator on the right is decreased away from its maximum output, the angle of the jet becomes increasingly skewed toward the weaker side of the jet vectoring plasma actuator.

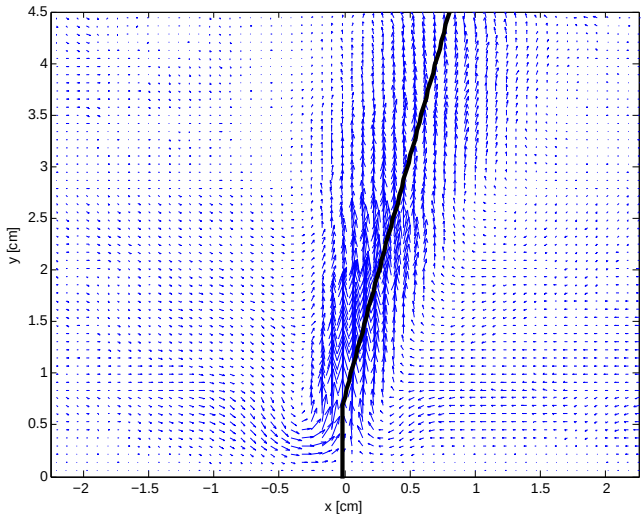

Figure 4.7: Averaged PIV results for operating frequency of one side 250Hz below maximum output.

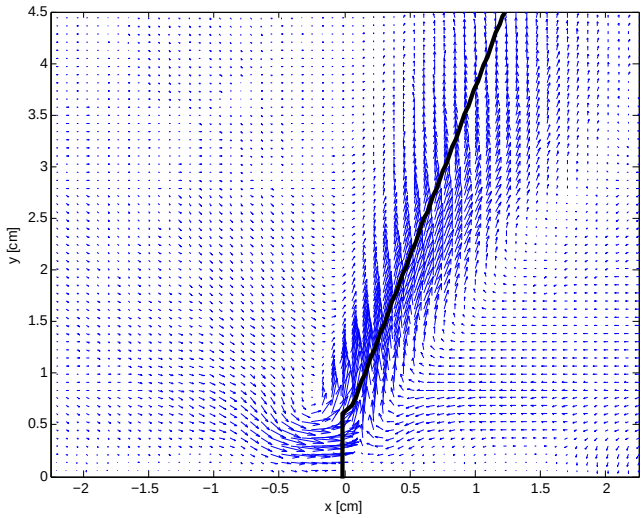

Figure 4.8: Averaged PIV results for operating frequency of one side 500Hz below maximum output.

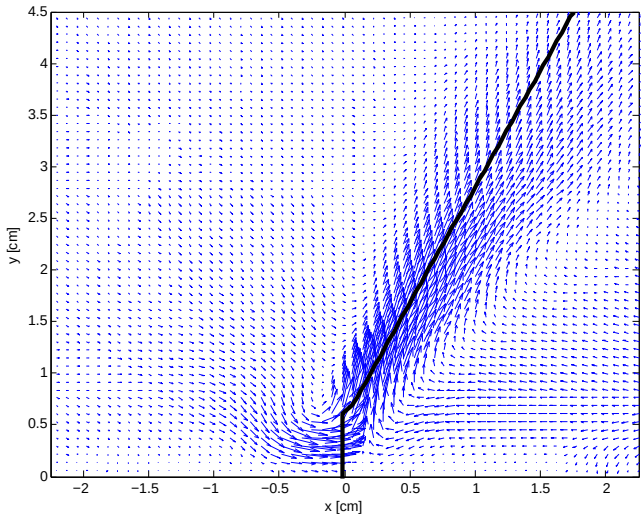

Figure 4.9: Averaged PIV results for operating frequency of one side 750Hz below maximum output.

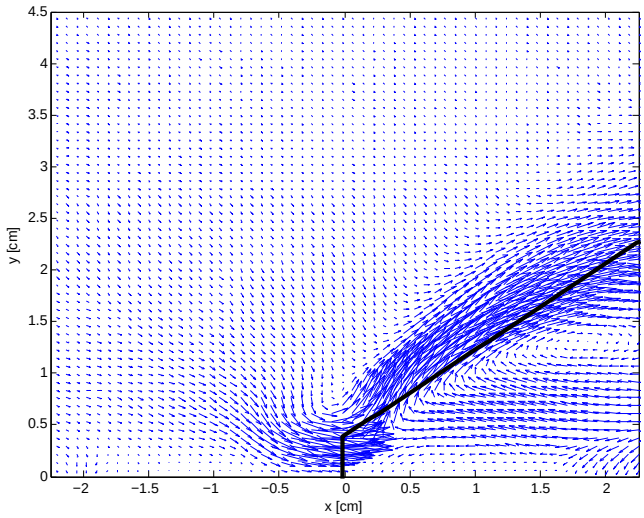

Figure 4.10: Averaged PIV results for operating frequency of one side 1000Hz below maximum output.

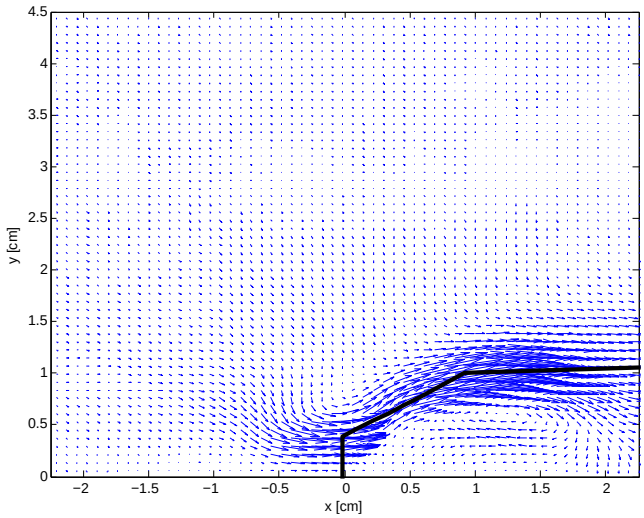

Figure 4.11: Averaged PIV results for operating frequency of one side 1500Hz below maximum output.

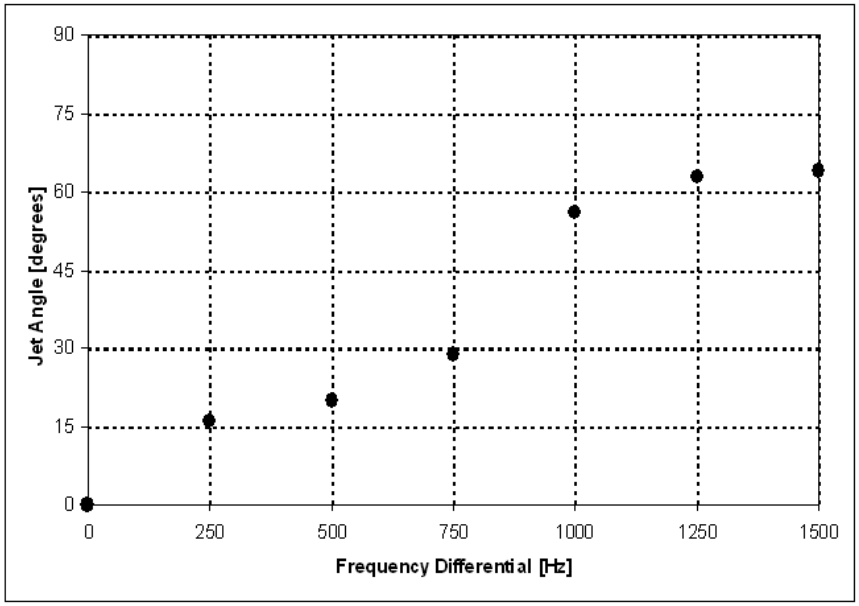

Figure 4.12: Angle of jet produced by decreasing the operating frequency of one side of the jet vectoring plasma actuator.

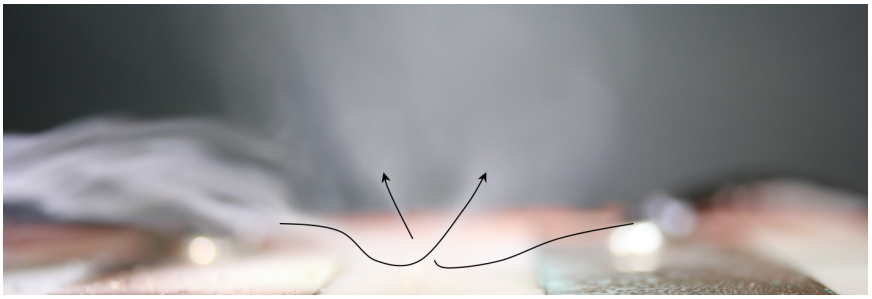

Figure 4.13: Smoke flow visualization of a pulsed jet vectoring plasma actuator.

It is shown that by decreasing the operating frequency of one side of the actuator away from its optimum, and holding the other side at a constant frequency, the angle of jet is changed. Fig. 4.12 shows how the angle is changed while changing the frequency of one side of the actuator. The relationship between the angle of the jet and the frequency differential, over the span studied, is approximately linear.

4.1.2 Unsteady Actuation

Jet vectoring through unsteady actuation is achieved, in the current study, by pulsing each side of the jet vectoring plasma actuator alternately. Fig 4.13 shows an example of smoke flow visualization of a jet vectoring plasma actuator while being pulsed. It shows that a jet is induced by one side of the actuator which is then redirected upward as the other side of the actuator is turned on. The effects of pulsing frequency, duty cycle, and exposed electrode spacing (embedded electrode width) on the jet characteristics are investigated.

Modulation Frequency

For the investigation of the effects of modulation frequency, the duty cycle of both channels (both sides of the actuator) is held at 50%, the phase angle between the two channels is 180°, and the driving frequency is 7kHz. The pulsing frequency is varied from 10 Hz to 500 Hz.

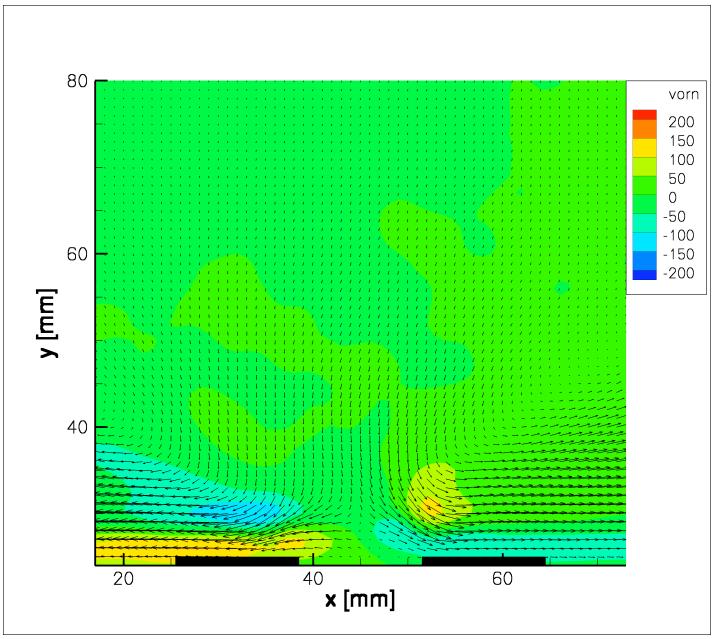

Figure 4.14: Averaged PIV results for pulsing frequency of 10Hz, 1/2in spacing

Characteristic instantaneous PIV results are shown for several different pulsing frequencies in Fig. 4.14 - Fig. 4.20. At low frequencies, a near wall jet is created, at high frequencies, a wall normal jet is produced, and at mid range pulsing frequencies, there is very little created by the plasma actuator.

To examine the effects of exposed electrode spacing on the jet produced by the jet vectoring plasma actuator, the embedded electrode width was varied simultaneously with the electrode spacing. In addition to the 1/2 in embedded electrode width studied, embedded electrode widths of 3/4 in and 1 in are also investigated. The duty cycle of each channel is again held at 50%, the operating frequency is 7kHz, and the phase angle between the two channels is 180°. The pulsing frequency is varied from 10Hz to 500Hz.

Averaged PIV results for the 3/4 in and 1 in embedded electrode width can be seen in Fig. 4.21 - Fig. 4.28 and Fig. 4.29 - Fig. 4.36, respectively. At higher pulsing frequencies, the jet created is normal to the wall, and at very low pulsing frequencies

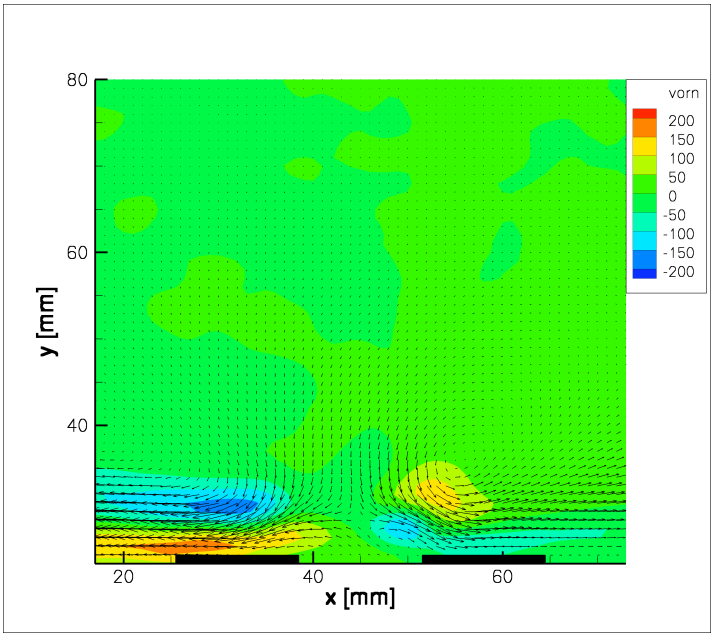

Figure 4.15: Averaged PIV results for pulsing frequency of 50Hz, 1/2in spacing

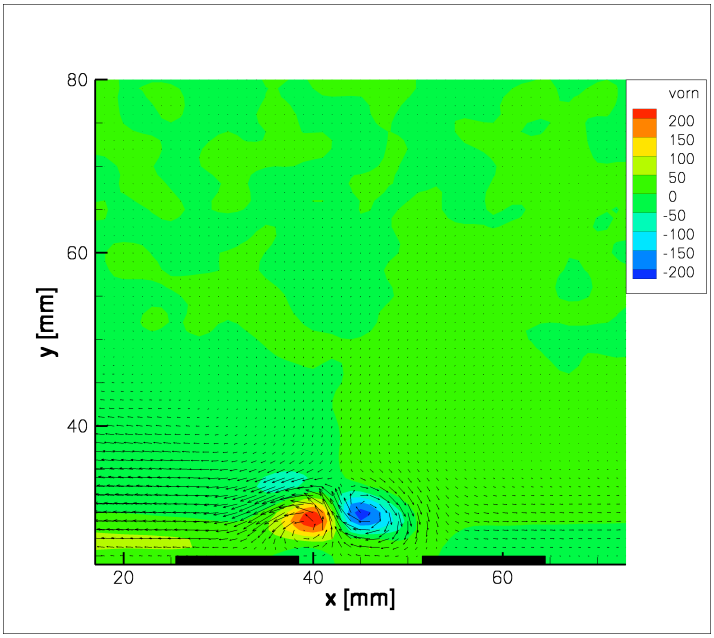

Figure 4.16: Averaged PIV results for pulsing frequency of 100Hz, 1/2in spacing

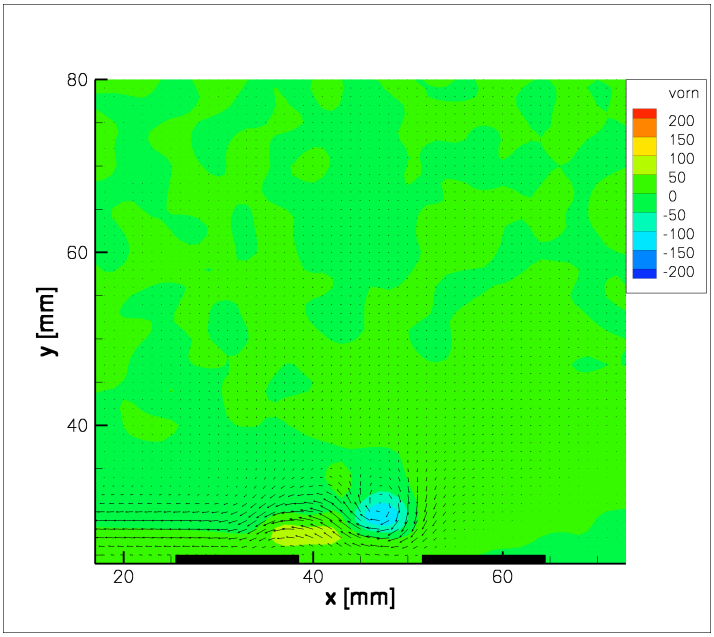

Figure 4.17: Averaged PIV results for pulsing frequency of 150Hz, 1/2in spacing

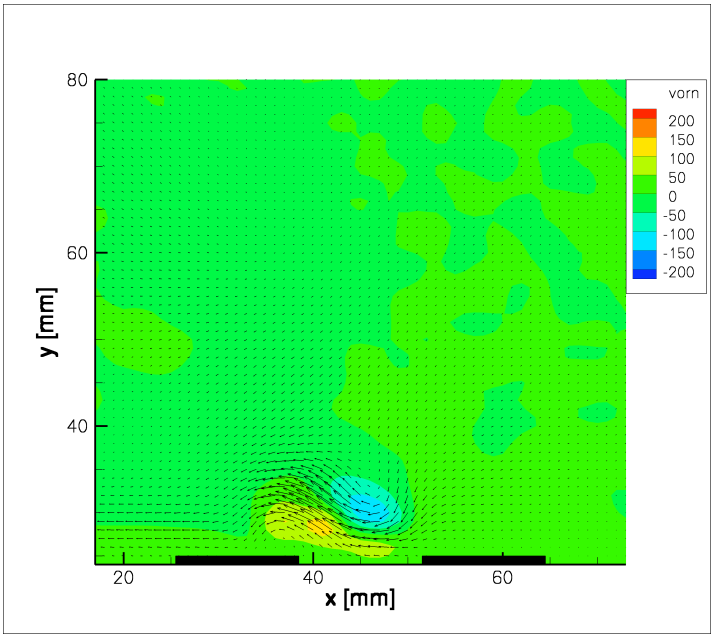

Figure 4.18: Averaged PIV results for pulsing frequency of 200Hz, 1/2in spacing

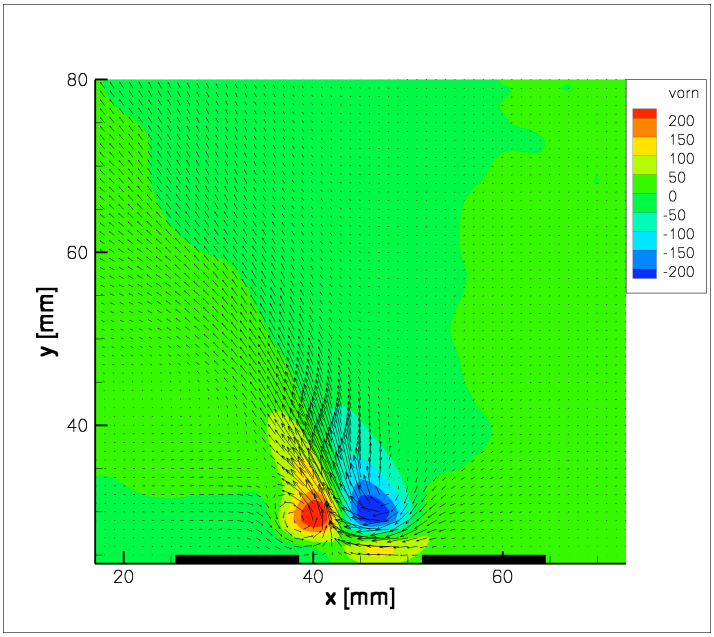

Figure 4.19: Averaged PIV results for pulsing frequency of 250Hz, 1/2in spacing

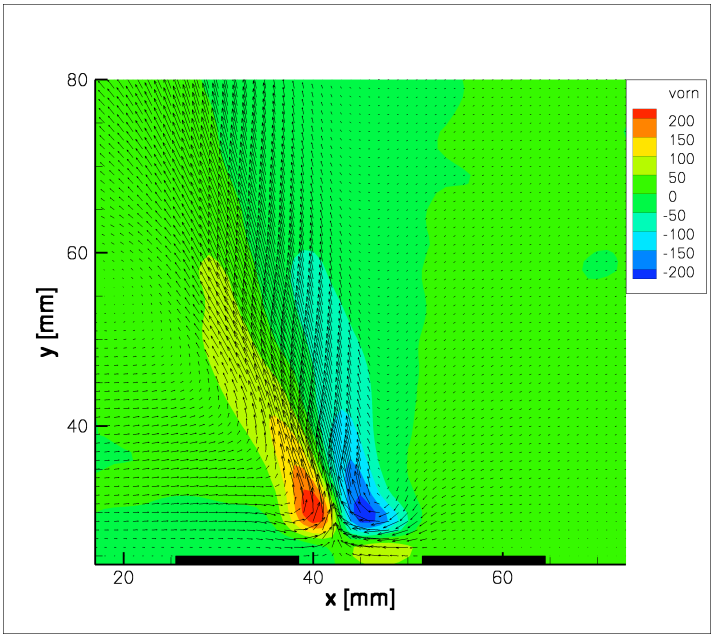

Figure 4.20: Averaged PIV results for pulsing frequency of 500Hz, 1/2in spacing

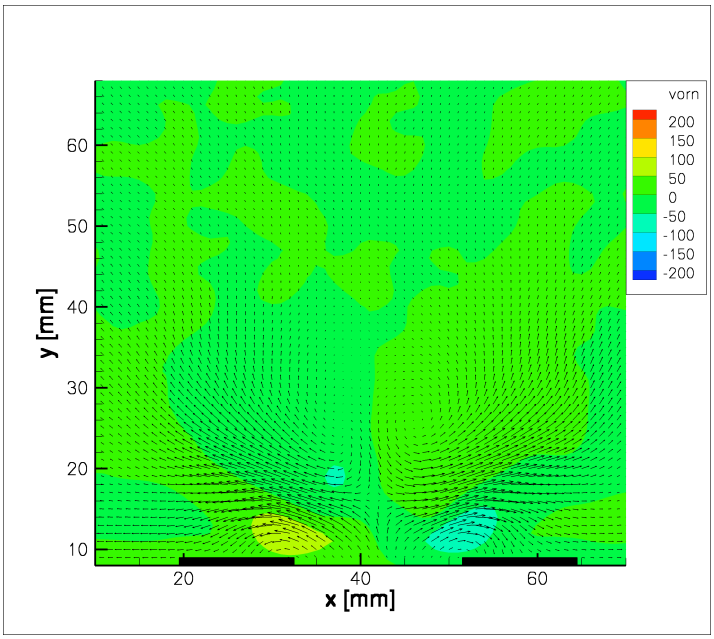

Figure 4.21: Averaged PIV results for pulsing frequency of 10Hz, 3/4in spacing

the jet created is parallel to the wall. Each of the different actuator sizes (1/2 in, 3/4 in, and 1 in embedded electrode width) has a unique pulsing frequency at which a wall normal jet is produced.

Fig. 4.37 and Fig. 4.38 show the momentum flux produced for the actuators with exposed electrode spacing sizes of 3/4 in and 1 in against the vertical distance from the actuator. Each actuator produces its peak momentum flux at 50Hz, below which there is a very small amount of momentum flux. Beyond 50Hz, in both cases, the actuators have a lower peak momentum flux, but affect the air over a greater vertical distance from the actuator.

Duty Cycle

While the investigation of the effects of pulsing frequency primarily focused on the type of jet produced, the investigation of duty cycle variation is focused on the angle of jet created by the plasma actuator. While holding the duty cycle of one channel

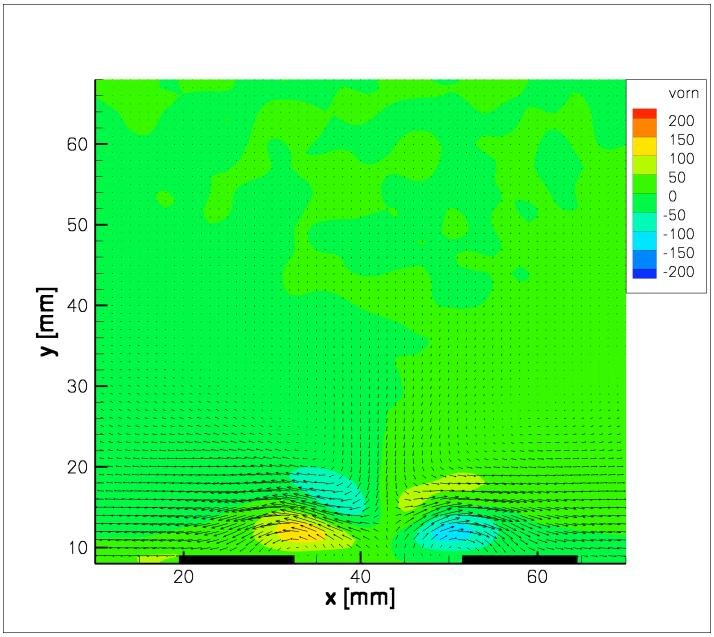

Figure 4.22: Averaged PIV results for pulsing frequency of 25Hz, 3/4in spacing

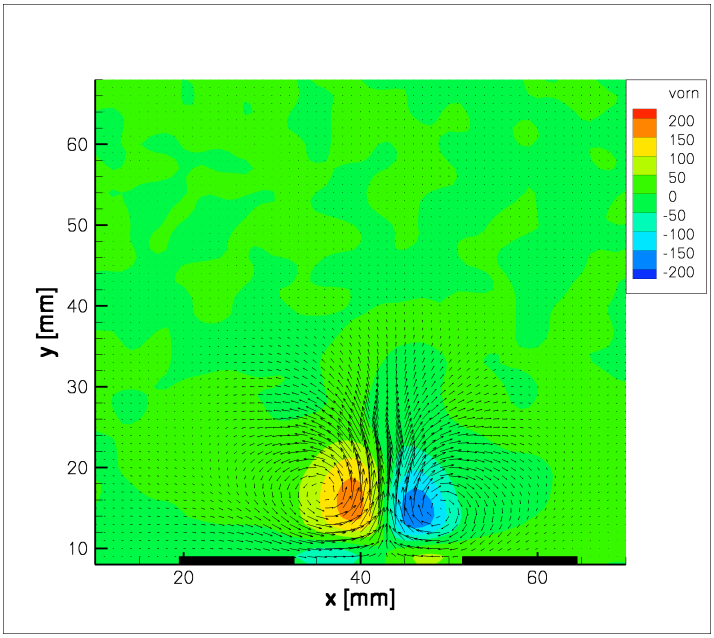

Figure 4.23: Averaged PIV results for pulsing frequency of 50Hz, 3/4in spacing

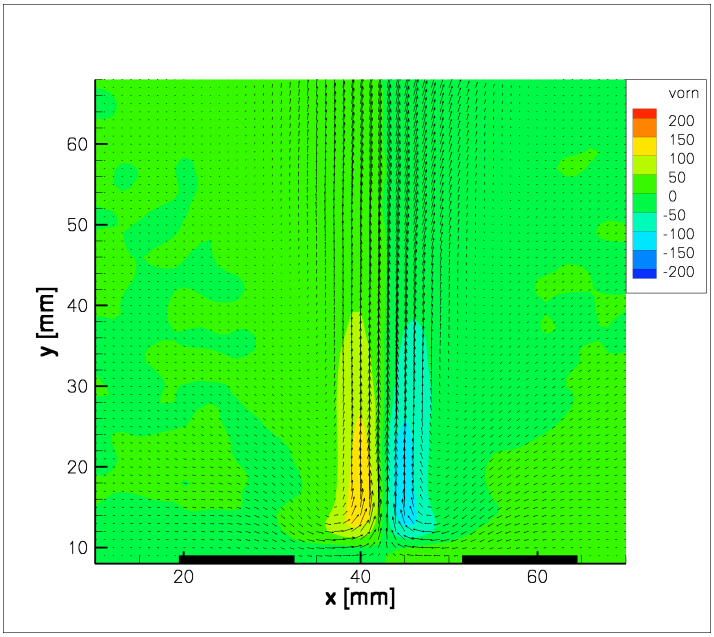

Figure 4.24: Averaged PIV results for pulsing frequency of 100Hz, 3/4in spacing

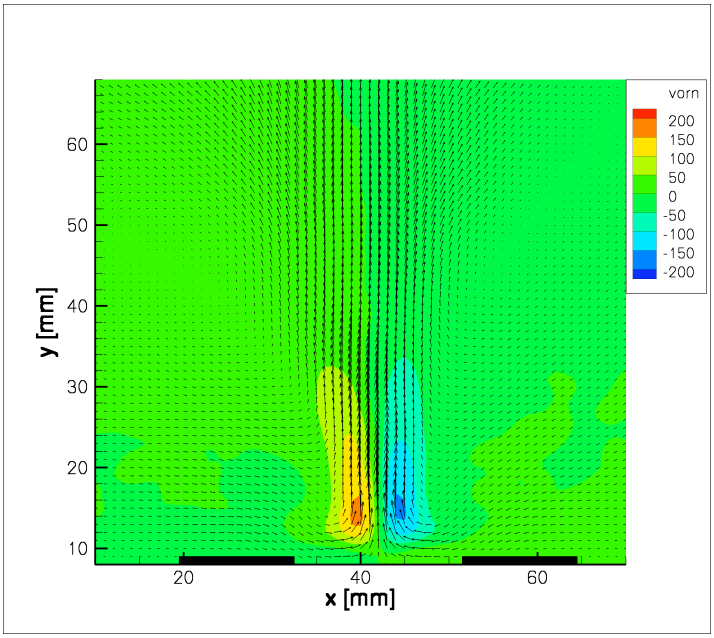

Figure 4.25: Averaged PIV results for pulsing frequency of 150Hz, 3/4in spacing

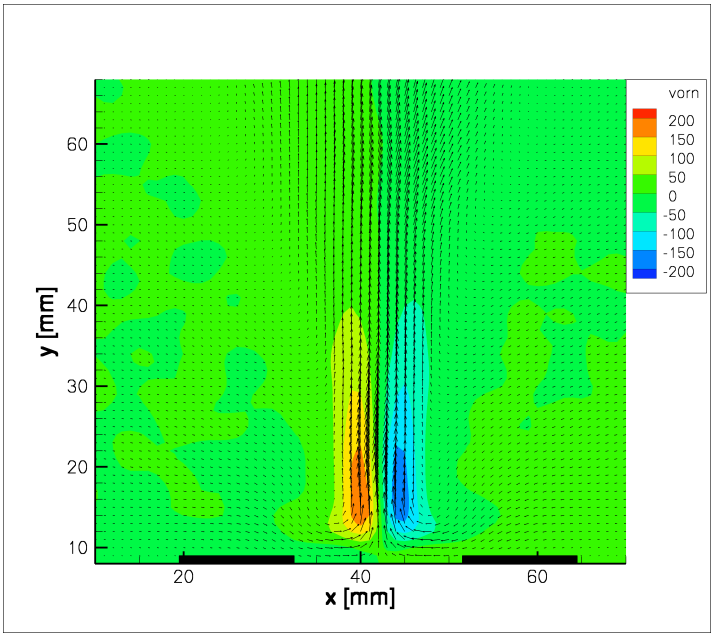

Figure 4.26: Averaged PIV results for pulsing frequency of 200Hz, 3/4in spacing

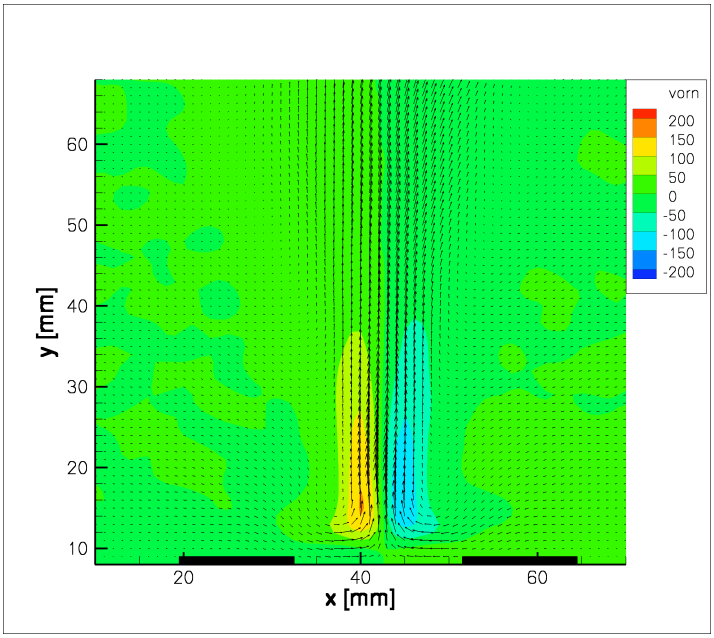

Figure 4.27: Averaged PIV results for pulsing frequency of 250Hz, 3/4in spacing

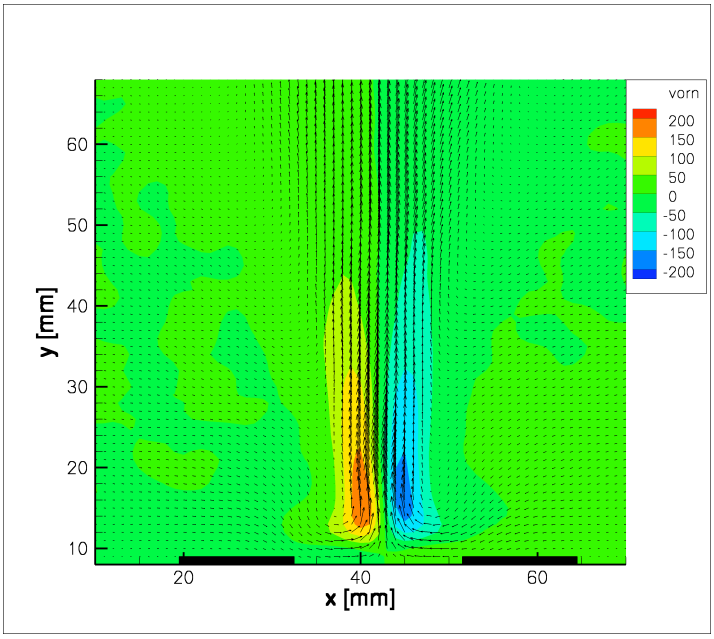

Figure 4.28: Averaged PIV results for pulsing frequency of 500Hz, 3/4in spacing

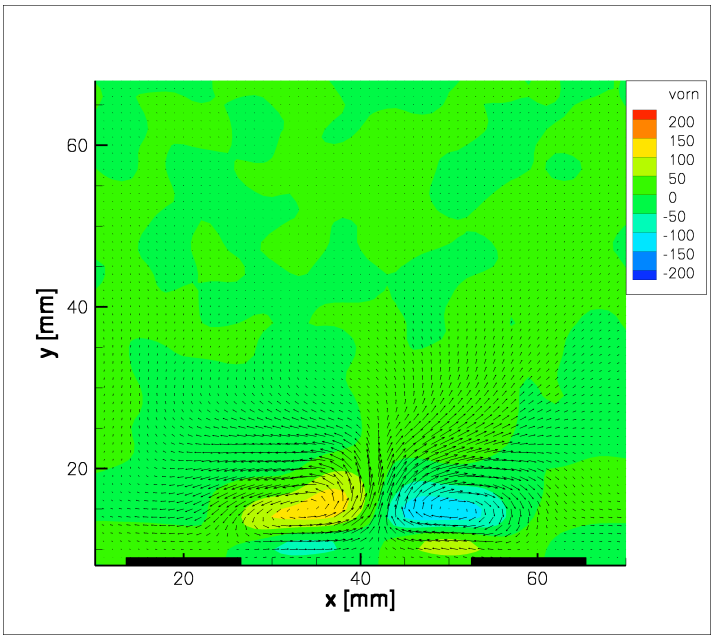

Figure 4.29: Averaged PIV results for pulsing frequency of 10Hz, 1in spacing

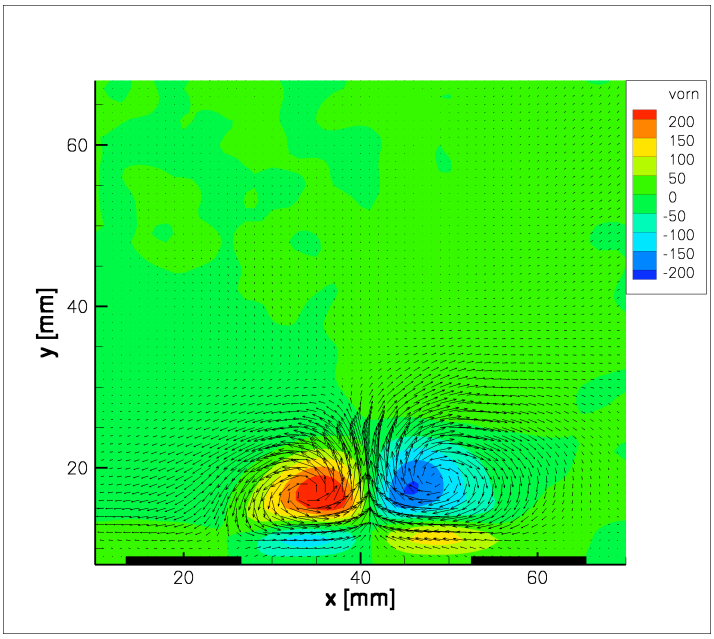

Figure 4.30: Averaged PIV results for pulsing frequency of 25Hz, 1in spacing

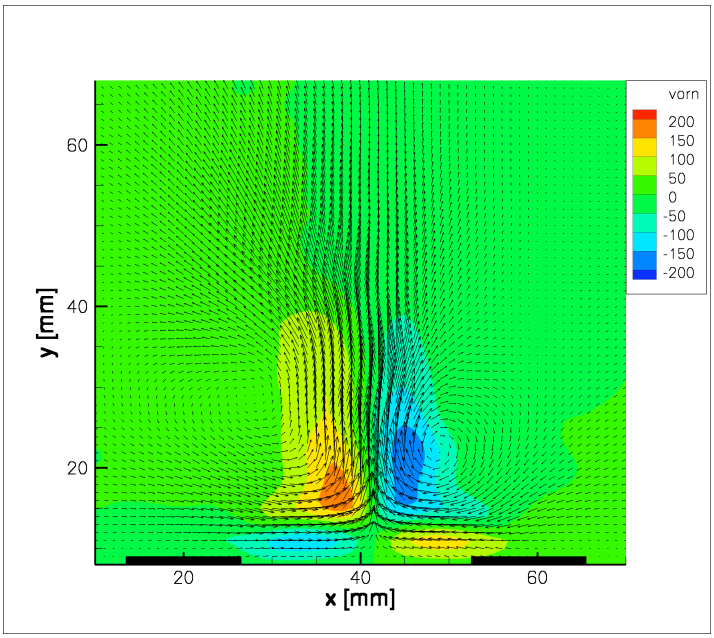

Figure 4.31: Averaged PIV results for pulsing frequency of 50Hz, 1in spacing

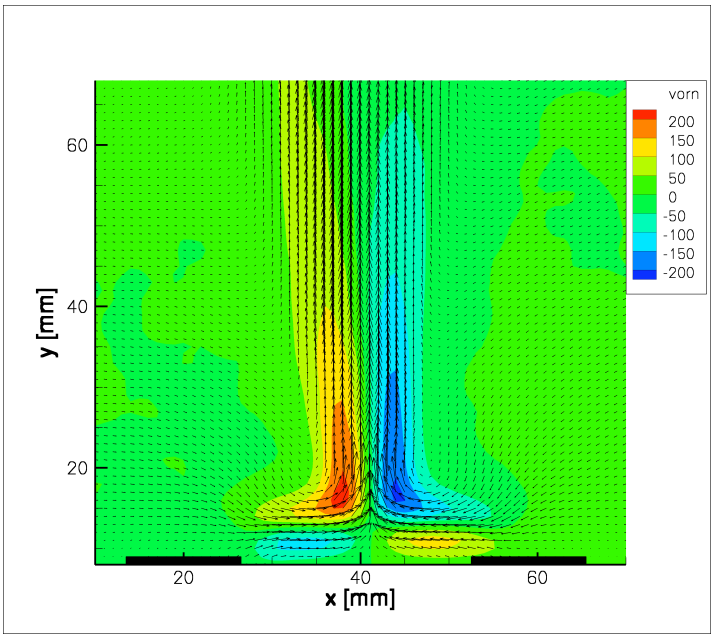

Figure 4.32: Averaged PIV results for pulsing frequency of 100Hz, 1in spacing

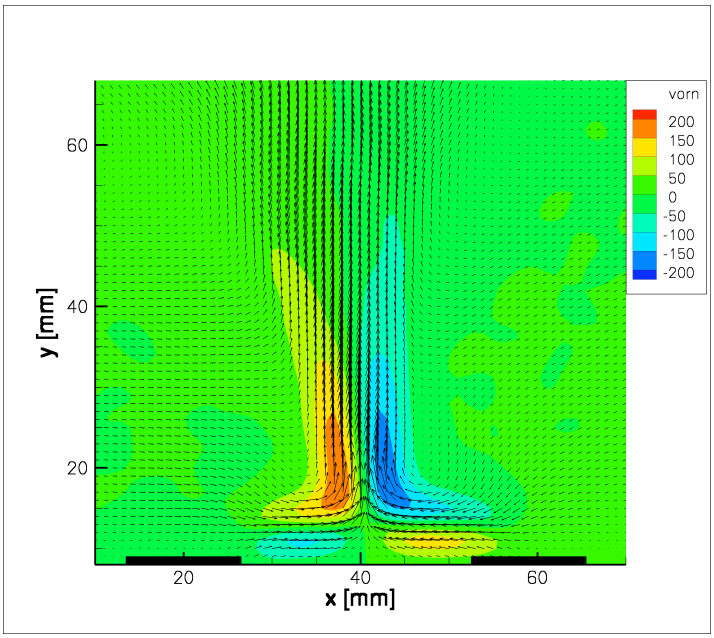

Figure 4.33: Averaged PIV results for pulsing frequency of 150Hz, 1in spacing

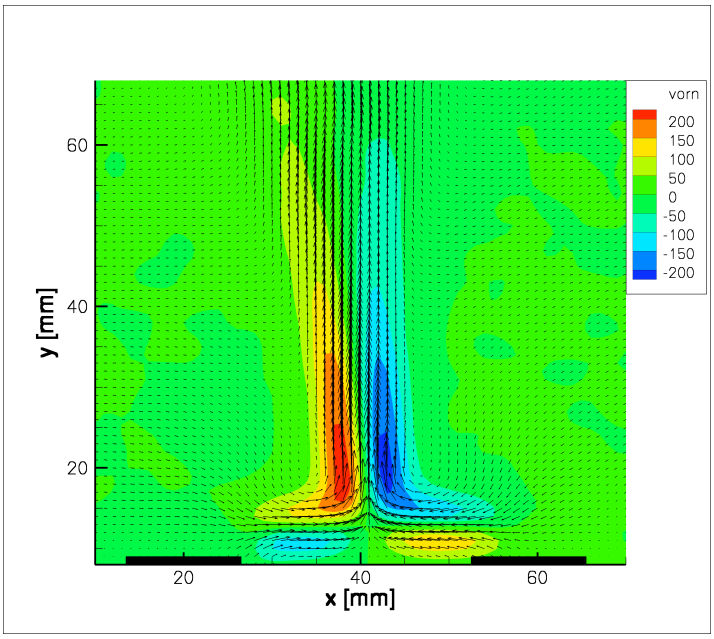

Figure 4.34: Averaged PIV results for pulsing frequency of 200Hz, 1in spacing

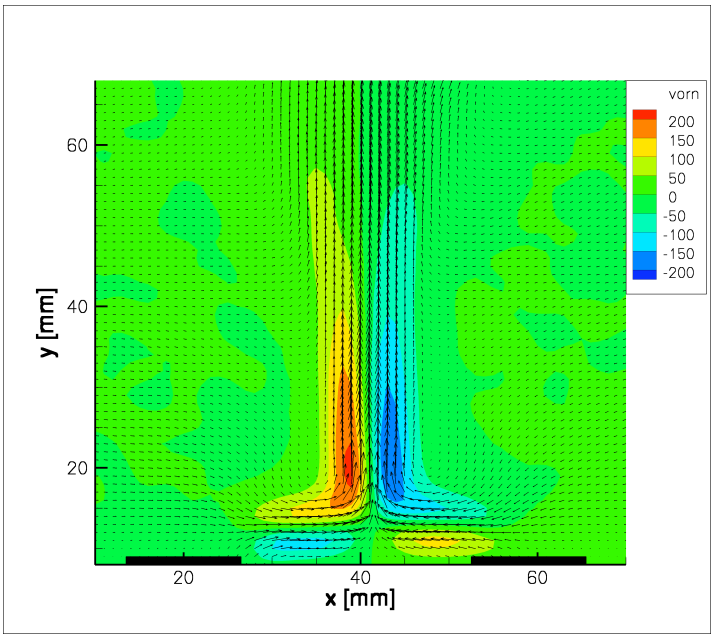

Figure 4.35: Averaged PIV results for pulsing frequency of 250Hz, 1in spacing

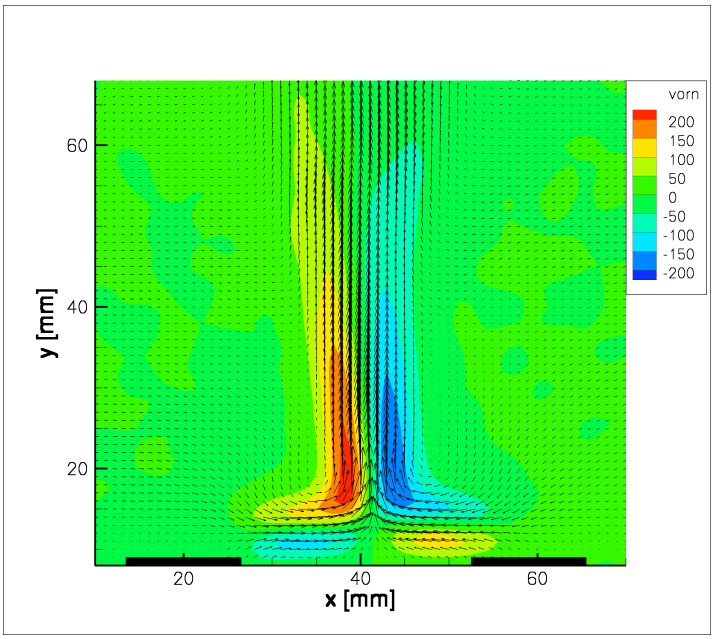

Figure 4.36: Averaged PIV results for pulsing frequency of 500Hz, 1in spacing

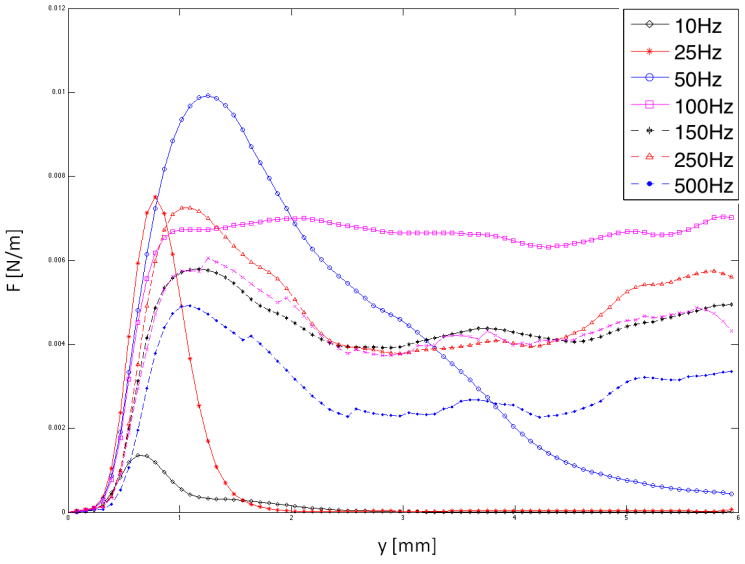

Figure 4.37: Vertical momentum flux induced by a jet vectoring plasma actuator with 1in exposed electrode spacing.

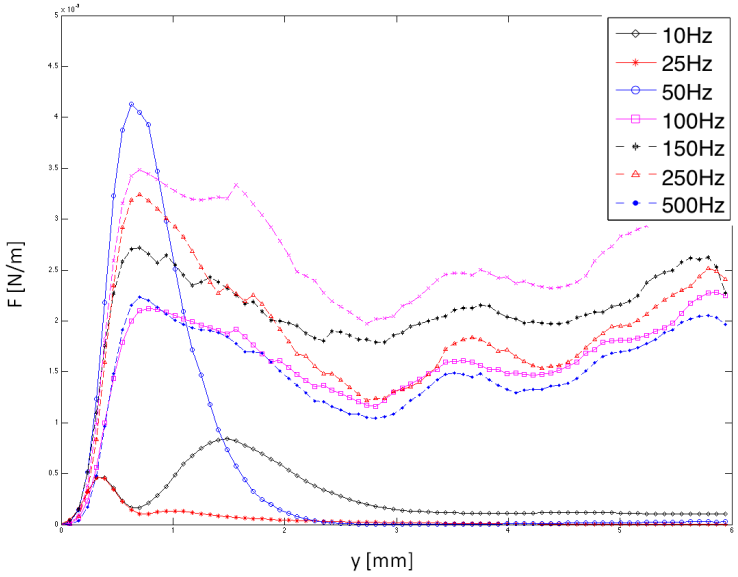

Figure 4.38: Vertical momentum flux induced by a jet vectoring plasma actuator with 3/4in exposed electrode spacing.

at 50%, the duty cycle of the second channel was varied from 0% to 50%, with the phase angle between the two channels at 180° and the operating frequency at 7kHz.

Fig. 4.39 - Fig. 4.44 show averaged PIV results for several different duty cycles. While both channels have a duty cycle of 50%, the jet produced is approximately normal to the wall; the jet is slightly skewed to one side of the actuator in this case, most likely due to a small variation in input power or asymmetric actuator construction. As the duty cycle of one side of the actuator is reduced from 50% to about 40%, the angle of the jet is quickly changed. As the duty cycle of one side of the actuator is decreased from about 40%, the jet direction slowly changes direction.

By varying the duty cycle, one can control the angle at which the jet is produced while decreasing the input power. Fig. 4.45 shows the relationship between the approximate angle, measured from the normal to the wall, and the duty cycle of the second channel, while the first is held at 50%. Near symmetric operation, there are large changes in the angle of jet produced with any change in duty cycle, but lowering

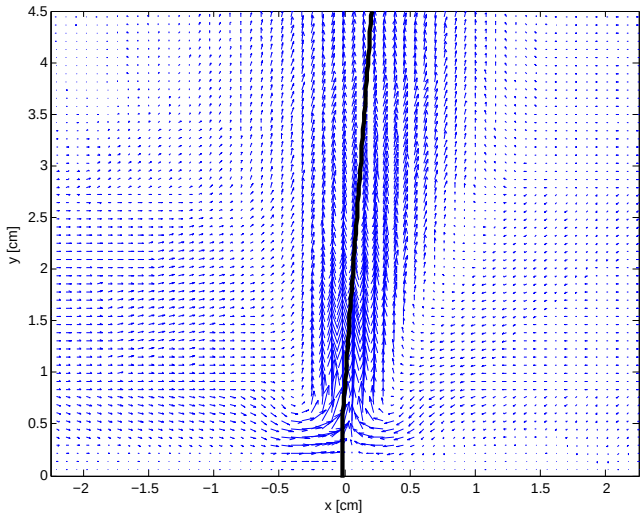

Figure 4.39: Averaged PIV results for duty cycles of 50% and 50%

the duty cycle beyond about 40% shows very little change in the angle of jet created.

4.1.3 Critical Pulsing Frequency

At some pulsing frequency neither a near wall or wall normal jet is created. The pulsing frequency at which this occurs is referred to as the critical pulsing frequency herein. When the pulsing frequency is below the critical pulsing frequency, the flow field produced is similar to two linear plasma actuators acting independently, unaffected by one another, as shown in Fig. 4.52. As one side of the plasma actuator is

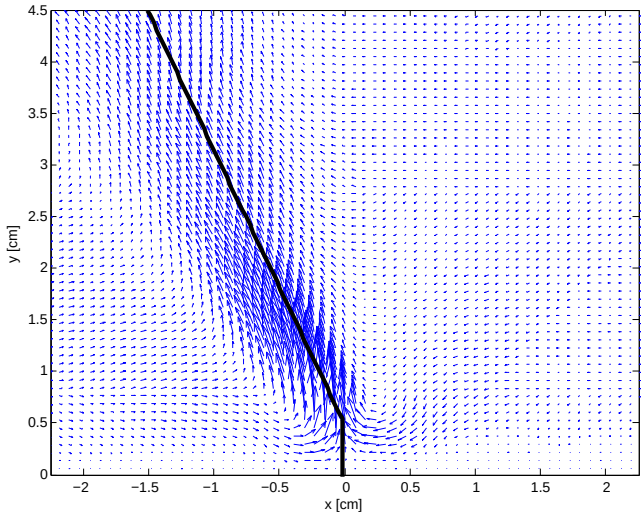

Figure 4.40: Averaged PIV results for duty cycles of 50% and 45%

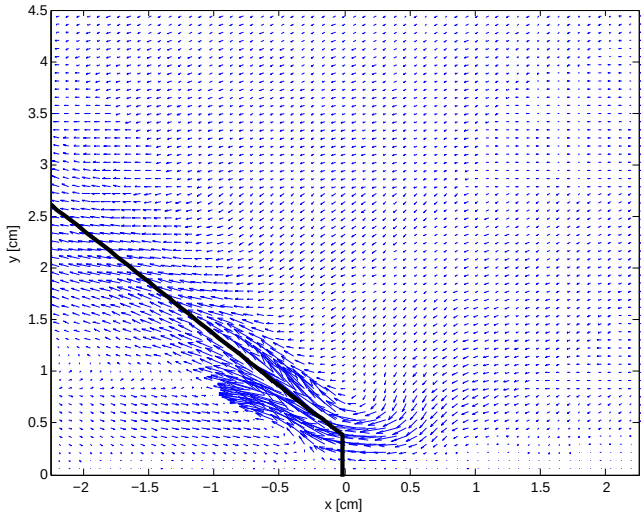

Figure 4.41: Averaged PIV results for duty cycles of 50% and 40%

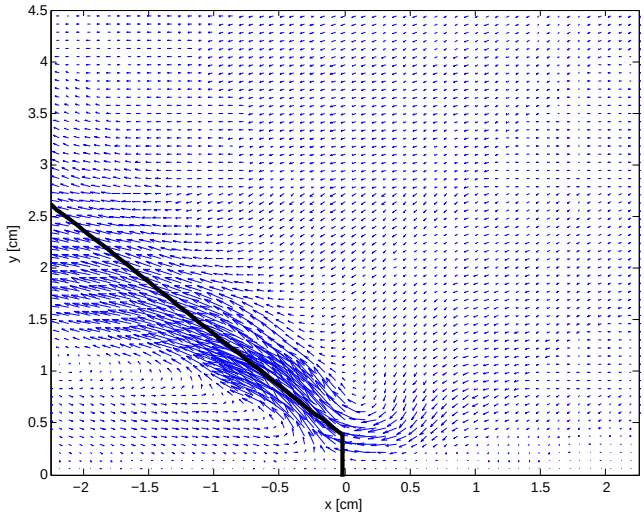

Figure 4.42: Averaged PIV results for duty cycles of 50% and 35%

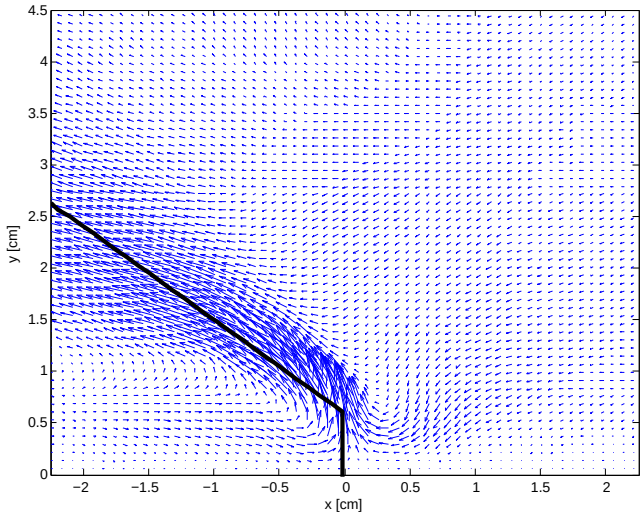

Figure 4.43: Averaged PIV results for duty cycles of 50% and 30%

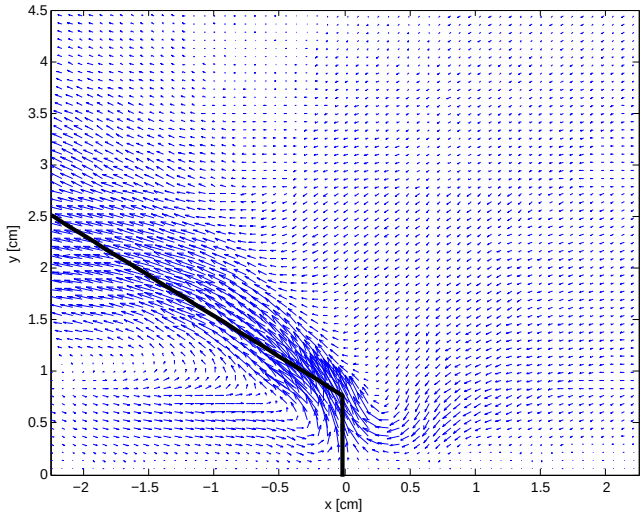

Figure 4.44: Averaged PIV results for duty cycles of 50% and 25%

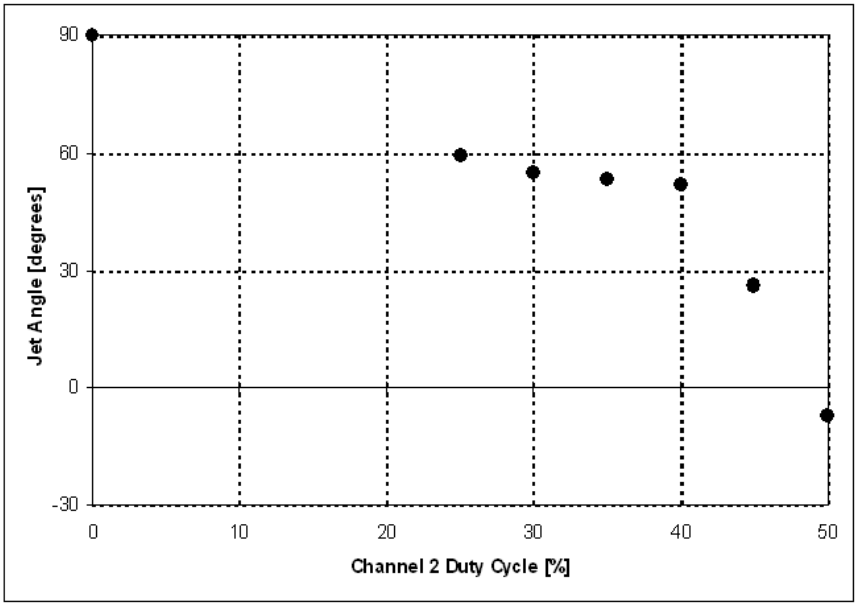

Figure 4.45: Jet angle produced with varying duty cycle.

turned on, it creates a vortex which advects downstream. After the original vortex moves beyond the other side of the plasma actuator, another vortex is created when the second side of the plasma actuator is turned on. This vortex then moves downstream beyond the other side of the actuator, and the process repeats, creating two nearly independent near wall jets.

As the pulsing frequency increases from 10Hz to 150Hz, the absolute maximum jet velocity decreases. As the pulsing frequency increases from 150Hz to 500Hz, the absolute maximum jet velocity increases. It can also be seen that the decay of velocity is slower for higher pulsing frequencies, especially 500Hz. While the pulsing frequency is low, below 150Hz, the maximum jet velocity is fairly high, but only affects the flow near the wall. As the pulsing frequency approaches 150Hz, the area of flow affected is still only near the wall, and the maximum jet velocity is very low. As the pulsing frequency increases beyond 150Hz, the area of the flow field affected extends well beyond that of the lower frequencies.

Fig. 4.50-Fig. 4.51 show how the centerline vertical jet velocity decays over a

distance from the jet vectoring plasma actuator. The three different actuator sizes – 1/2 in, 3/4 in, and 1 in spacing – are shown with the nondimensional vertical jet velocity ($U_{y,CL}/U_{y,MAX}$) against the nondimensional length (scaled with the exposed electrode spacing). For all sizes at low pulsing frequency, 50 Hz, the area affected by the jet is near the wall. As the pulsing frequency is increased beyond the critical frequency, the actuators with 3/4 in and 1 in spacing first begin to affect the flow field farther from the actuator. The actuator with 1/2 in exposed electrode spacing affects only the flow near the wall until much higher frequencies, 250 Hz or 500 Hz. This is especially evident in the 500 Hz case where each of the three cases have very similar centerline velocity decay profiles, reducing to only 0.65-0.75 of the maximum jet velocity at 2.25 actuator widths.

The flow field created when the pulsing frequency is at the critical pulsing frequency is shown in Fig. 4.53. In this case, as one actuator is turned on, a vortex is created, similar to the lower frequency. Unlike the lower pulsing frequency case, a second vortex is created by the other side of the plasma actuator before the first vortex has traveled downstream beyond the other side of the actuator. The two vortices impinge on one another, and create neither a near wall or wall normal jet.

To create a jet that affects the flow beyond the near wall region, it can be seen that the pulsing frequency must be above the critical pulsing frequency, as seen in Fig. 4.54. As in each of the previous two cases, a vortex is created when one side of the actuator is turned on. The other side of the plasma actuator is then turned on, which creates a vortex in the opposite direction. This vortex pushes the original vortex upward; alternately, the first side of the plasma actuator is turned on again, and pushes the previous vortex upward. This continues, quickly producing a wall normal jet.

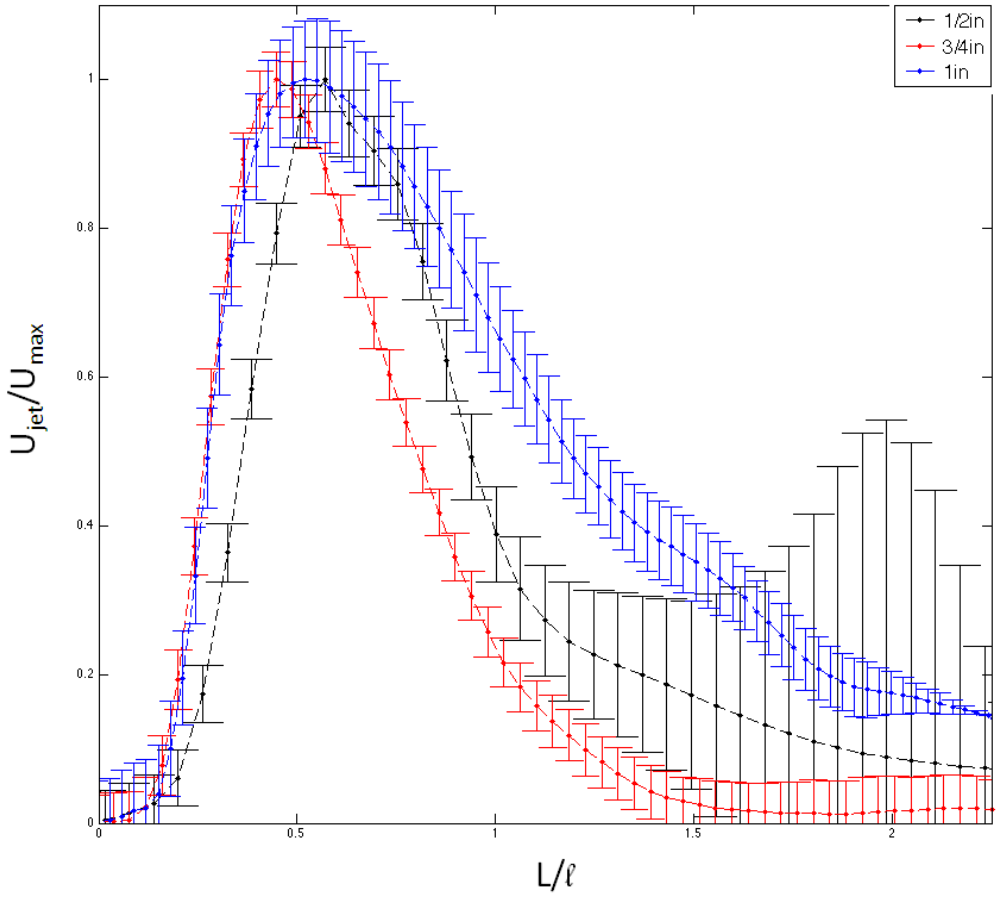

Figure 4.46: Maximum vertical jet velocity decay for 50 Hz pulsing frequency.

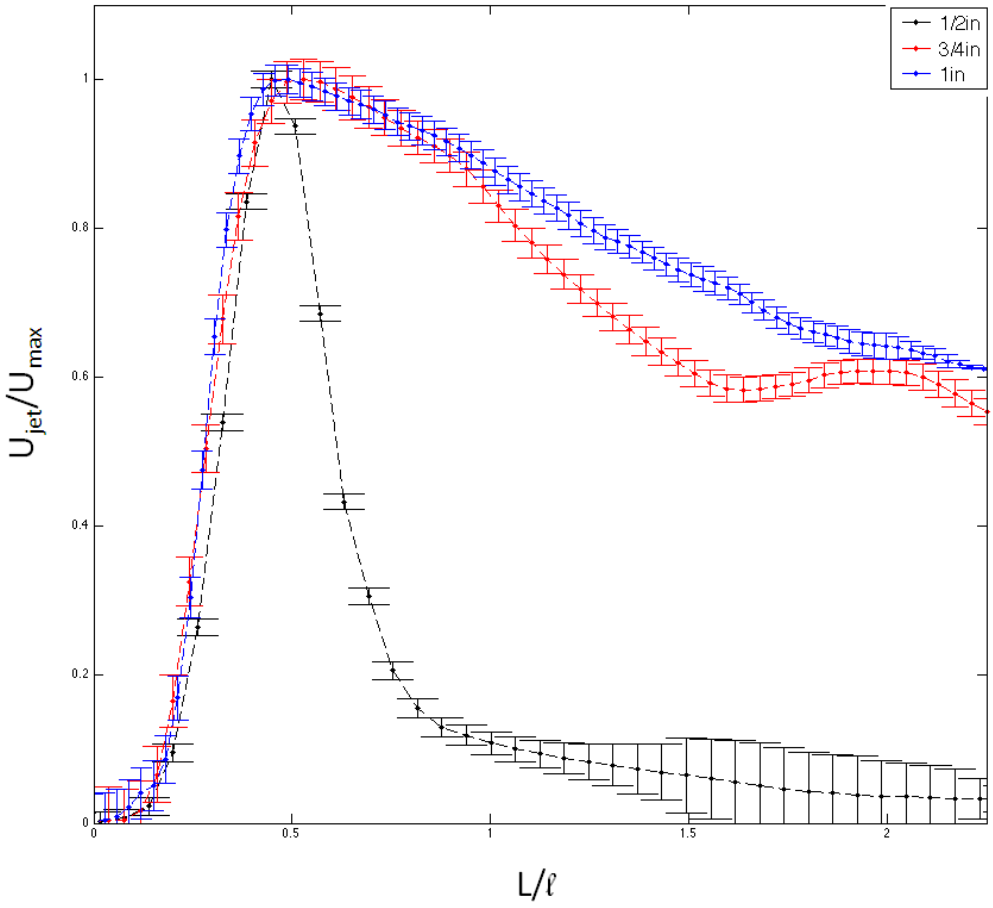

Figure 4.47: Maximum vertical jet velocity decay for 100 Hz pulsing frequency.

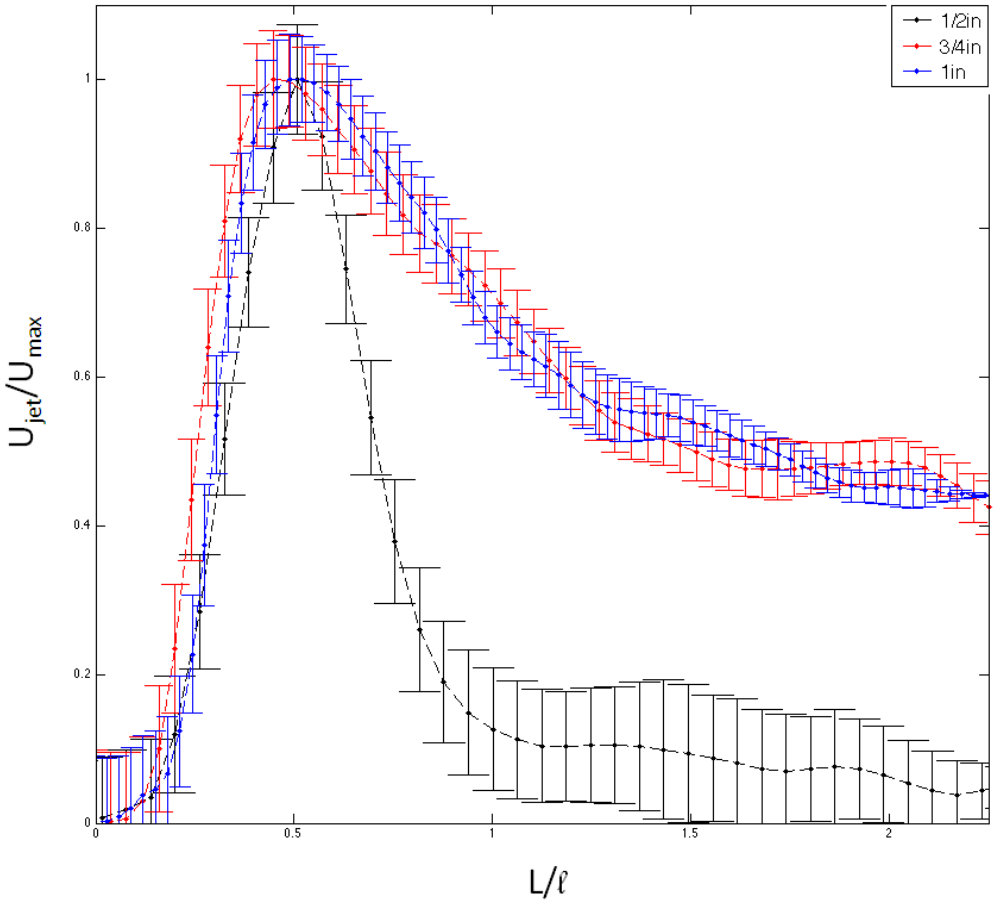

Figure 4.48: Maximum vertical jet velocity decay for 150 Hz pulsing frequency.

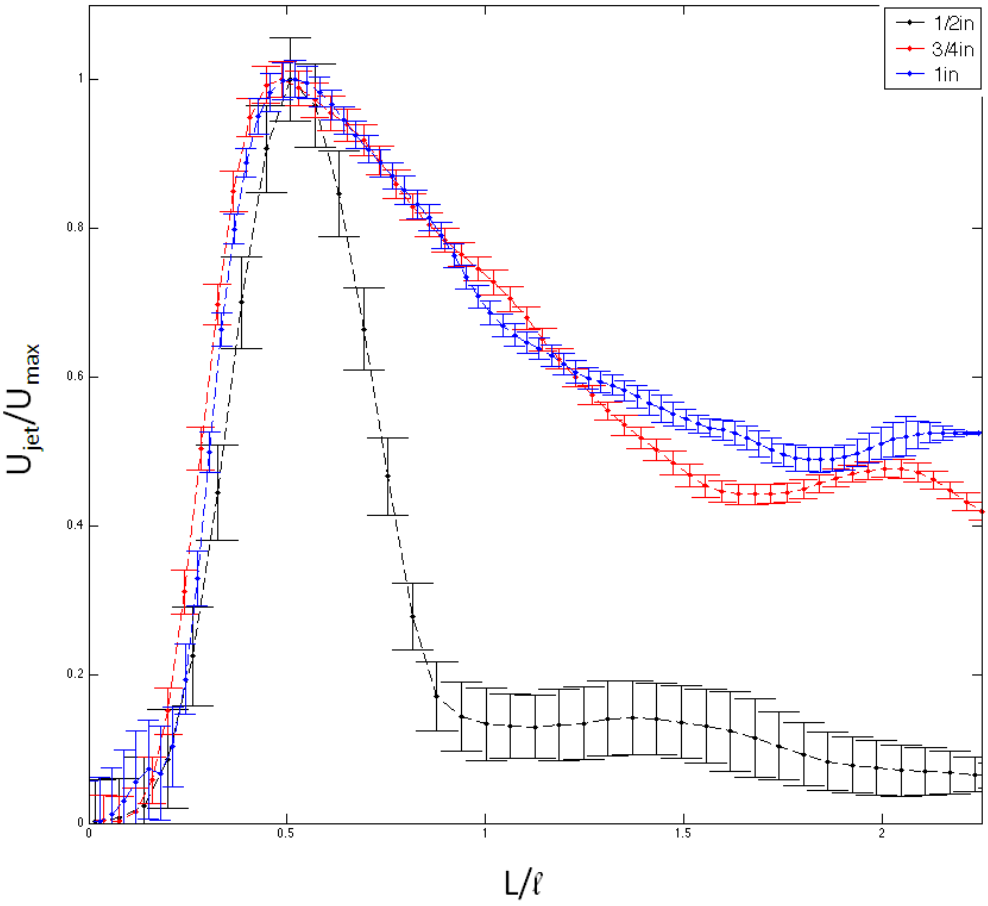

Figure 4.49: Maximum vertical jet velocity decay for 200 Hz pulsing frequency.

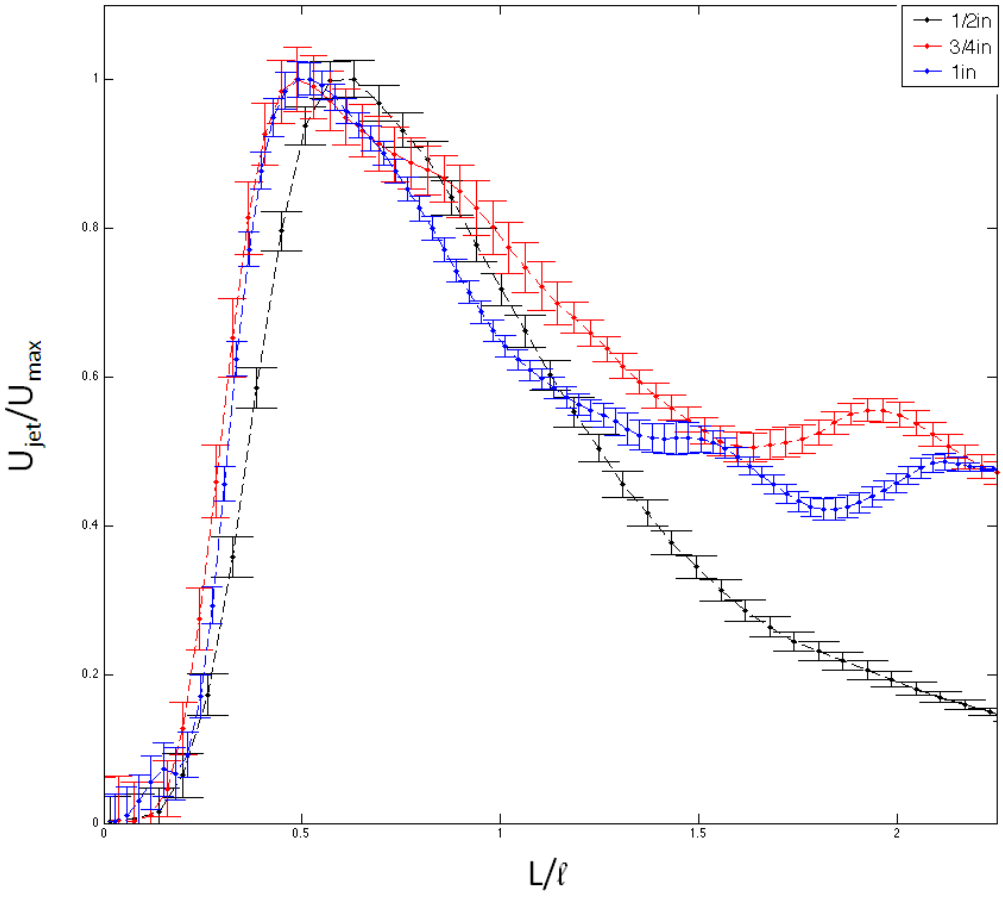

Figure 4.50: Maximum vertical jet velocity decay for 250 Hz pulsing frequency.

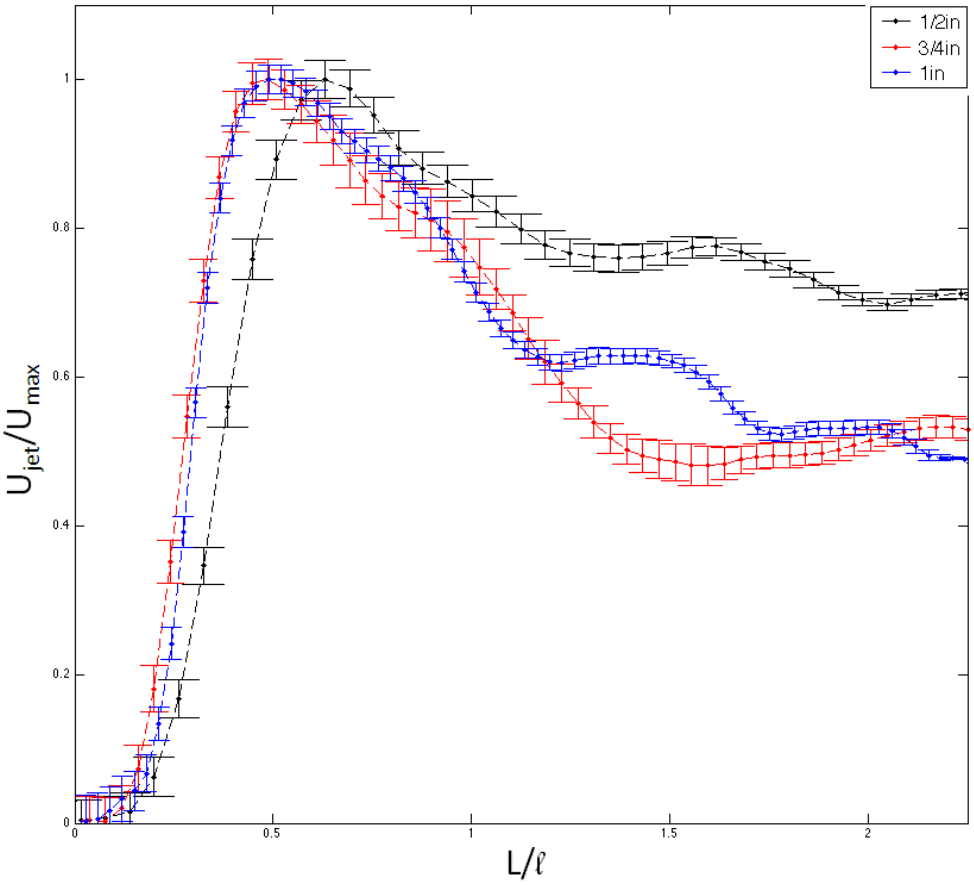

Figure 4.51: Maximum vertical jet velocity decay for 500 Hz pulsing frequency.

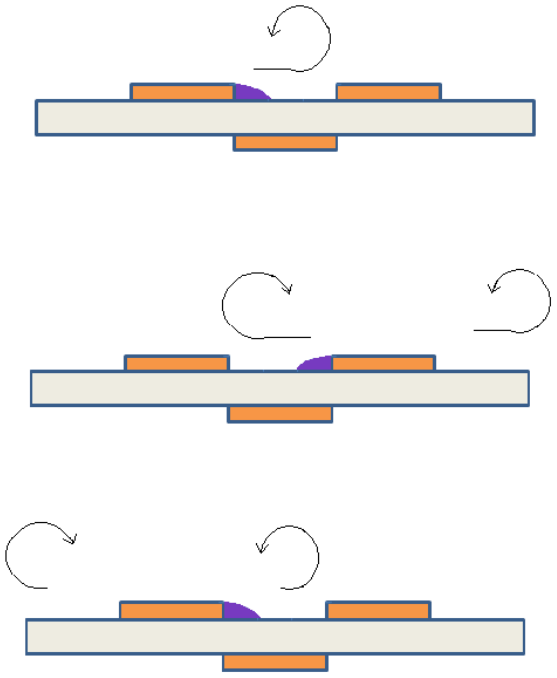

Figure 4.52: Schematic of jet produced at low pulsing frequencies.

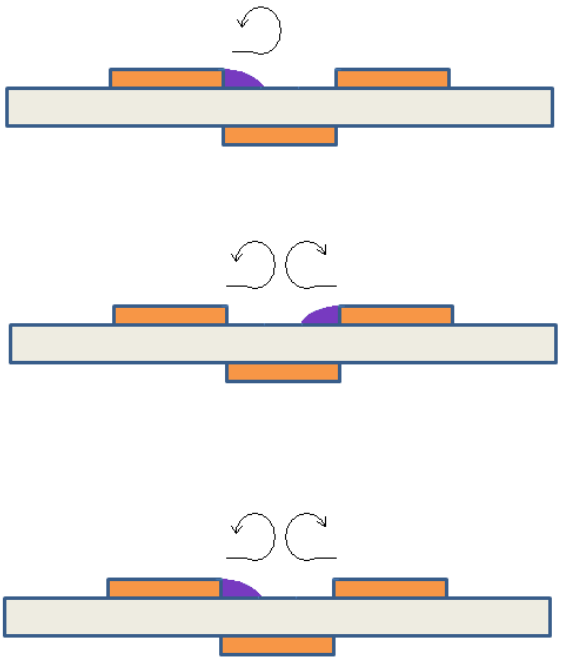

Figure 4.53: Schematic of jet produced at pulsing frequencies near the critical frequency.

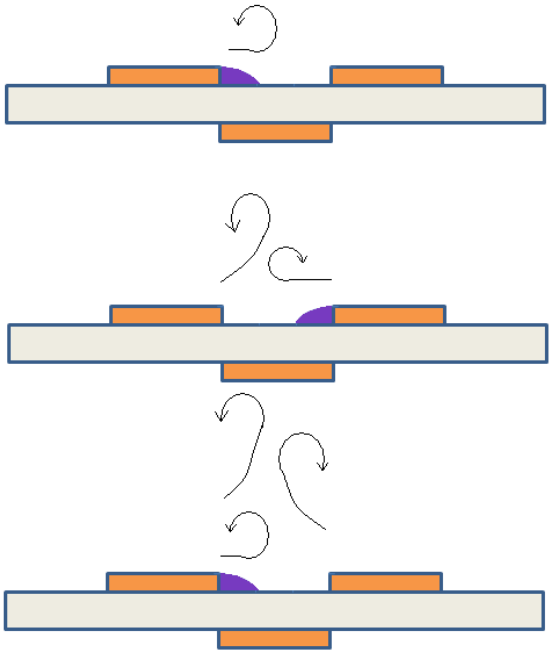

Figure 4.54: Schematic of jet produced at high pulsing frequencies.

4.2 Wind Tunnel

Building on the results gathered from the benchtop experiments, the jet vectoring plasma actuator is tested in a low-speed wind tunnel to determine its effectiveness as a vortex generator jet (VGJ). While the geometry of the actuator is identical for both the benchtop and wind tunnel experiments, the dielectric material used for the wind tunnel tests, for increased robustness, is 0.025 in thick alumina ($\epsilon \sim 10$). The jet vectoring plasma actuator used in the wind tunnel experiments is made up of 1/2 in copper strips for both the embedded and exposed electrodes, with a 1/2 in spacing between the two exposed electrodes. The effects of duty cycle, modulation frequency, yaw angle, and wind tunnel speed on the effectiveness of the jet vectoring plasma actuator as a VGJ are investigated separately. Only unsteady actuation of the jet vectoring plasma actuator is studied for the wind tunnel experiments.

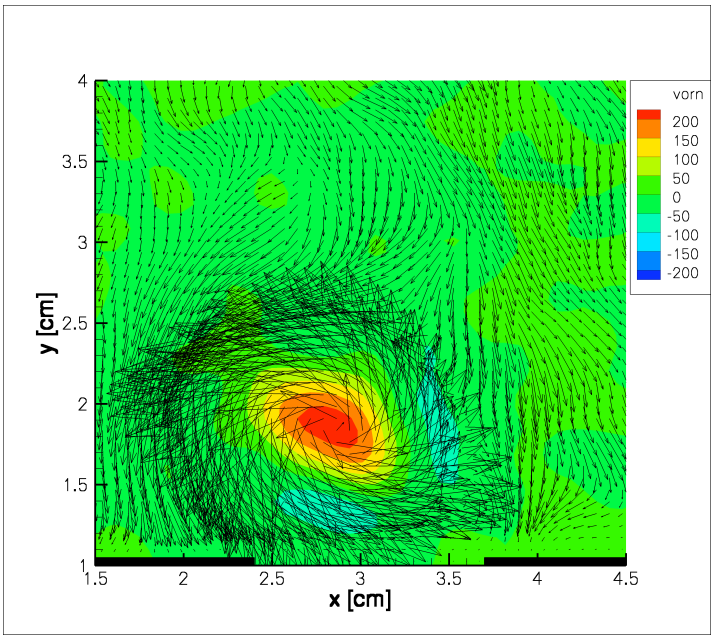

Figure 4.55: Averaged PIV results for both channels operated at 50% DC.

4.2.1 Duty Cycle

To study the effects of duty cycle on the vortex formed by the jet vectoring plasma actuator as a VGJ, the duty cycle of one side of the actuator is held at 50% while the duty cycle of the other side is varied from 10% to 50%. The actuator is placed in the wind tunnel test section with a small yaw angle, approximately 5°, with respect to the direction of flow. The phase angle between the two channels, pulsing frequency, operating frequency, and wind tunnel speed are 180°, 250Hz, 5kHz, and 1.7m/s, respectively.

Fig. 4.55 - Fig. 4.59 show averaged PIV results while the actuator operated while the duty cycle of one channel is varied. The strongest vortex is created when both channels have a duty cycle of 50%, as seen in figure Fig. 4.55. By lowering the duty cycle of one channel, the vortex created is shifted spatially, as shown in Fig. 4.56 - Fig. 4.59

Fig. 4.60 shows the circulation induced by the actuator against radial distance

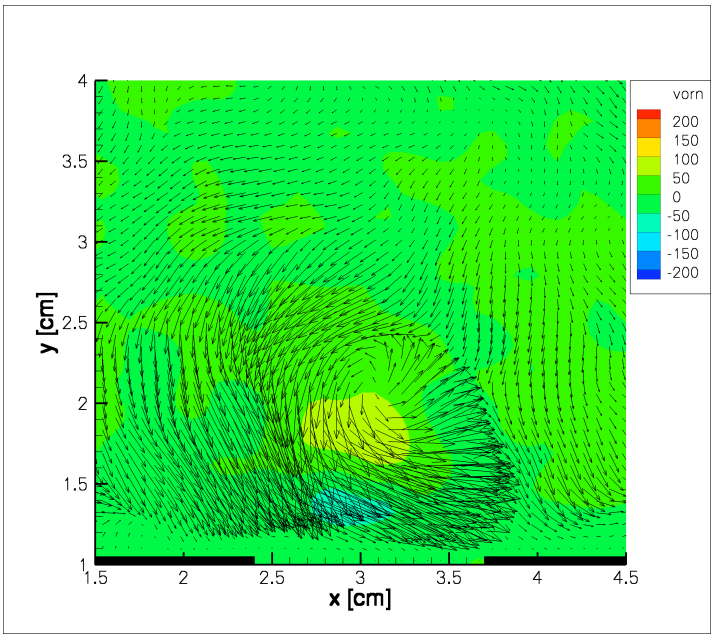

Figure 4.56: Averaged PIV results for one channel at 50% and the other at 40% DC.

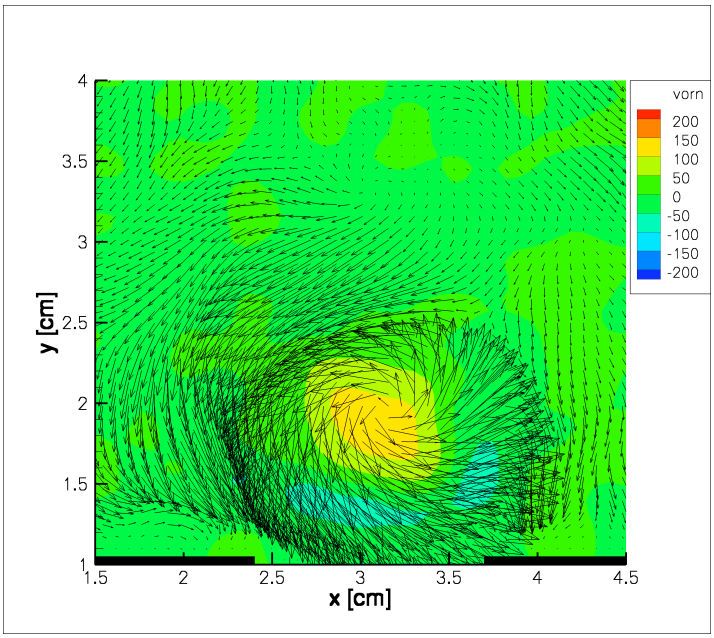

Figure 4.57: Averaged PIV results for one channel at 50% and the other at 30% DC.

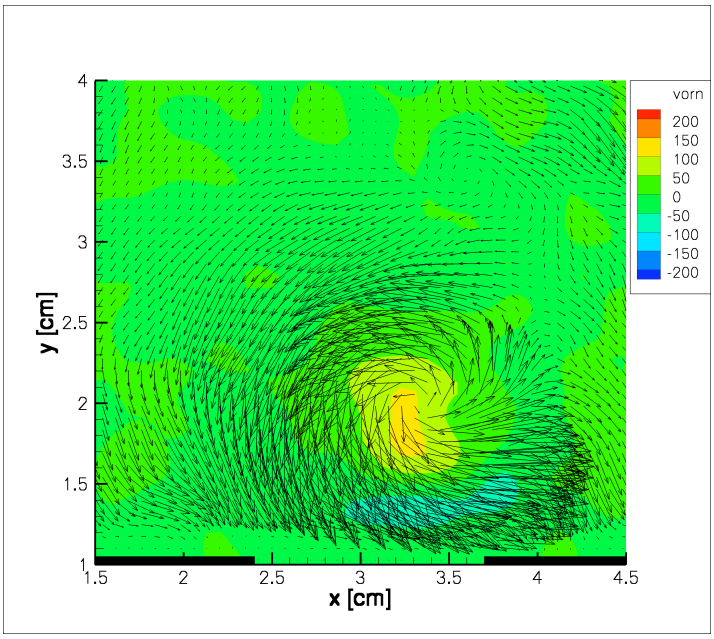

Figure 4.58: Averaged PIV results for one channel at 50% and the other at 20% DC.

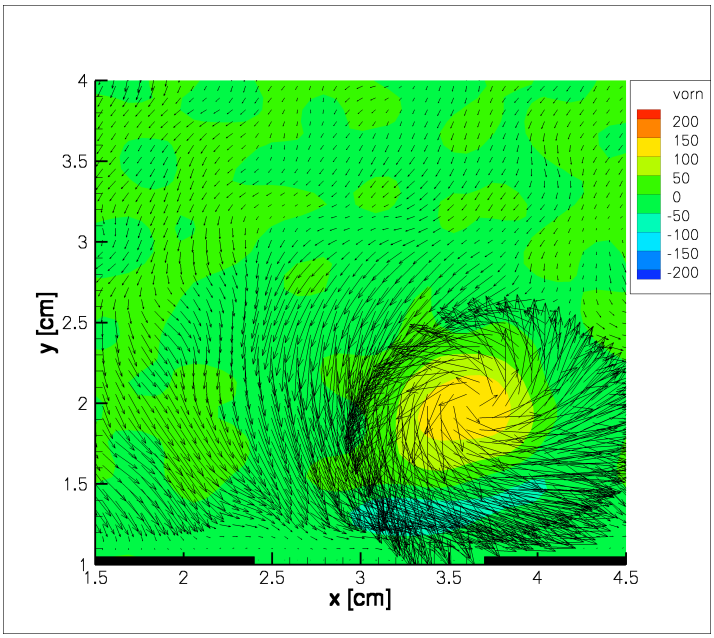

Figure 4.59: Averaged PIV results for one channel at 50% and the other at 10% DC.

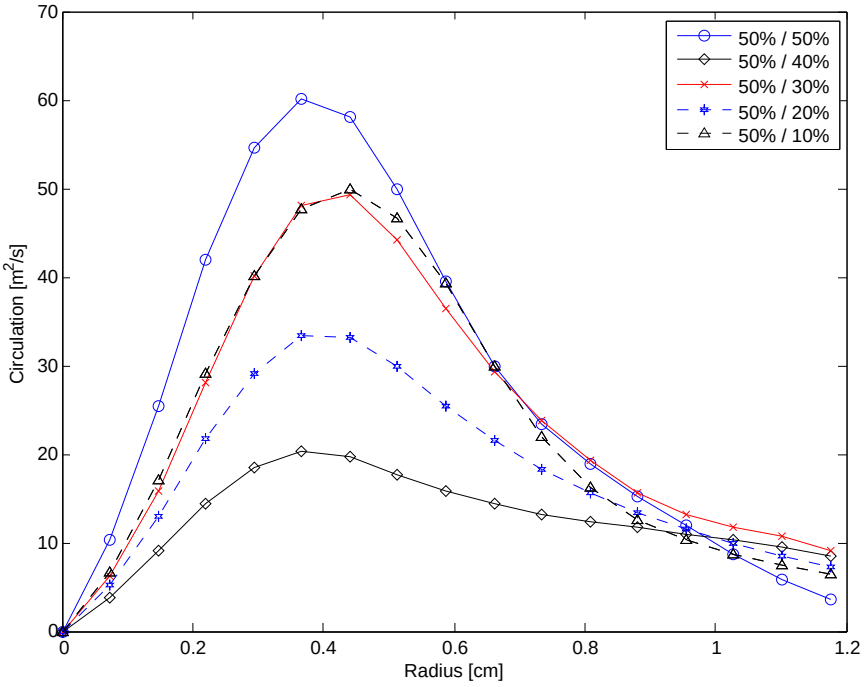

Figure 4.60: Circulation induced by the jet vectoring plasma actuator at a 5° sideslip angle for different duty cycles.

from the center of the vortex. The maximum amount of circulation is attained while the actuator is operated symmetrically.

4.2.2 Pulsing Frequency

The effects of pulsing frequency are studied by varying the pulsing frequency from 1Hz, below the critical frequency, to 250Hz, above the critical pulsing frequency. The two sides of the plasma actuator are varied simultaneously such that each channel has the same pulsing frequency for each run. The actuator is placed in the wind tunnel such that the yaw angle of the actuator relative to the direction of flow is 0°. The phase angle between the two channels, duty cycle of each channel, operating frequency, and wind tunnel speed are 180°, 50%, 5kHz, and 1.7m/s, respectively.

Fig. 4.61, Fig. 4.62, and Fig. 4.63 show the velocity vectors and vorticity contours of averaged PIV results for three different pulsing frequencies, 1Hz, 100Hz, and 250Hz. It was determined during the benchtop tests that the critical pulsing frequency for an actuator with 1/2 in exposed electrode spacing is approximately 100Hz. Fig. 4.61 shows that while the pulsing frequency is below the critical pulsing frequency, the jet produced is similar to that found during benchtop testing. The two sides of the actuator produce vortices that advect beyond the other side of the actuator before another vortex in the opposite direction is created. This creates two near wall jets in opposite directions that interact minimally with each other. While the pulsing frequency is at or near the critical pulsing frequency, as in Fig. 4.62, there is very little vorticity produced. The vortices created by each side of the actuator impinge on one another, and create a very small amount of vorticity in comparison to other pulsing frequency cases. For pulsing frequencies above the critical pulsing frequency, as seen in Fig. 4.63, the jet produced is approximately normal to the wall.

The circulation produced by the plasma actuator for several different pulsing frequencies is shown in Fig. 4.64. For each case, the peak circulation is in approximately

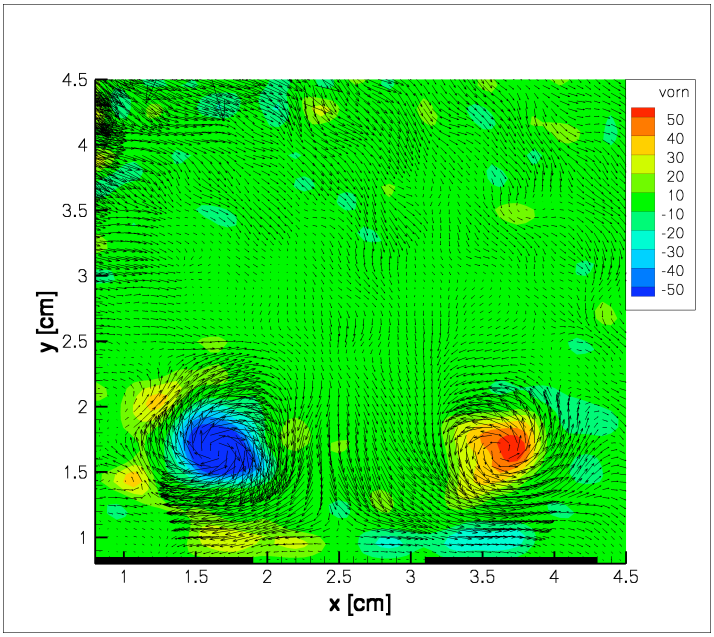

Figure 4.61: Averaged PIV results for 1Hz pulsing frequency (below critical frequency).

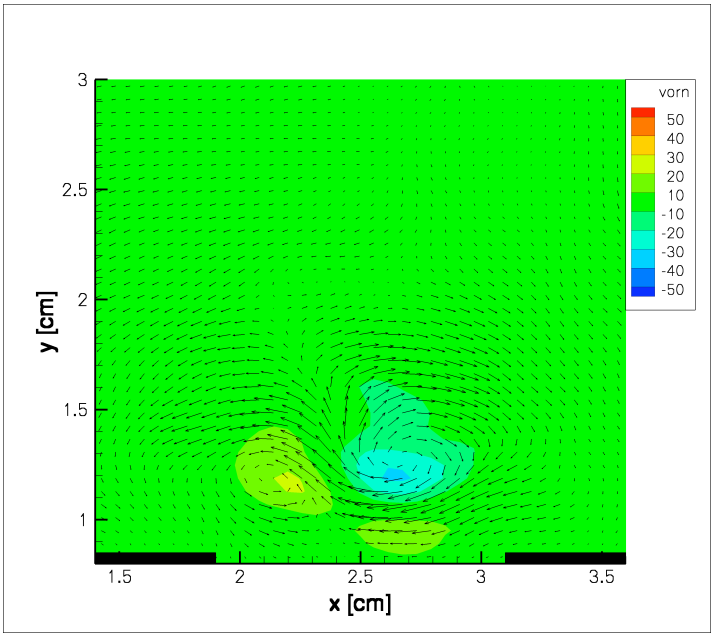

Figure 4.62: Averaged PIV results for 100Hz pulsing frequency (near critical frequency).

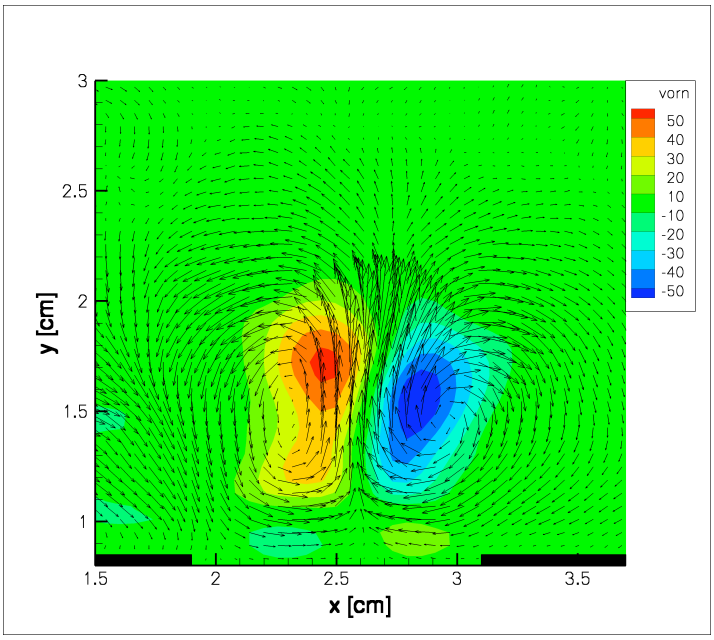

Figure 4.63: Averaged PIV results for 250Hz pulsing frequency (above critical frequency).

the same location, showing that the size of the vortices are similar while the strengths vary. The most circulation produced is while the actuator is pulsed at 500 Hz, about twice that of the lowest pulsing frequency, 10 Hz.

4.2.3 Sideslip Angle

The effects of sideslip angle on the vortex produced by the jet vectoring plasma actuator is examined by varying the sideslip angle from 0° to 10°. While the pulsing frequency is held at 250 Hz, the actuator is tested for two duty cycle conditions, the first is 50% on both channels, and the second is 50% duty cycle on one channel and 20% on the other. The sideslip angles tested are 0°, 5^and°, 10°. Figures 4.65 - 4.67 show the velocity vectors and vorticity contours for the jet vectoring plasma actuator operated under duty cycles of 50% and 50% at different sideslip angles. The same is shown in Fig. 4.68, Fig. 4.69, and Fig. 4.70, except for duty cycles for the two channels of 50% and 20%.

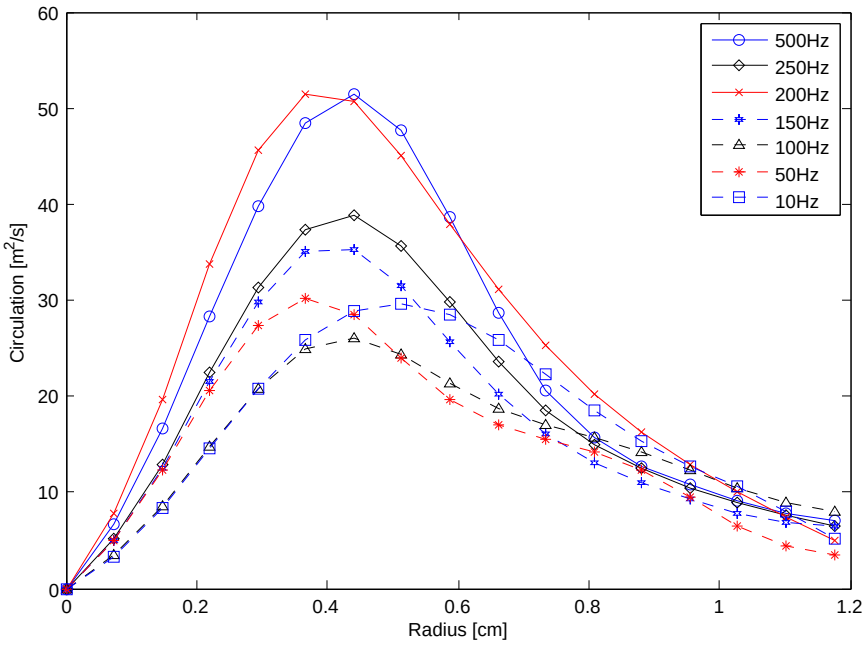

Figure 4.64: Circulation induced by the jet vectoring plasma actuator at a 5° sideslip angle for different pulsing frequencies.

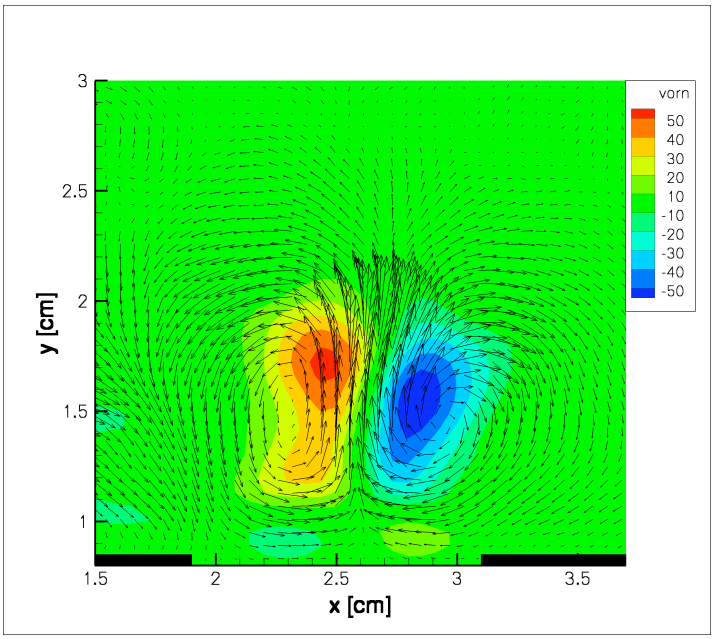

Figure 4.65: Averaged PIV results for both channels at 50% DC, 0° yaw.

Fig. 4.65 shows that with symmetric operation and no sideslip, the jet created is normal to the surface, created a small amount of vorticity. As the sideslip angle is increased to 5° and 10°, the maximum vorticity increases, but when the sideslip angle is increased to 20°, the maximum vorticity decreases. The type of jet produced is also changed from a wall normal jet to a single streamwise vortex.

It is shown in Fig. 4.68 that even at no sideslip, a single streamwise vortex is formed when the actuator is operated with one side at 50% duty cycle and the other at 20%. As the sideslip angle increases to 5° and 10°, the maximum vorticity increases, and the size of the vortex is reduced. As the sideslip angle increases to 20°, the vorticity decreases, similar to that of the previous case. It is observed that at no sideslip, the vortex has the opposite sign of all other cases where sideslip is greater than 0°.

Fig. 4.71 and Fig. 4.72 show the circulation produced by the actuator at three different sideslip angles, and under two different duty cycles. In the case of symmetric operation, there is very little circulation produced with no sideslip, and the highest

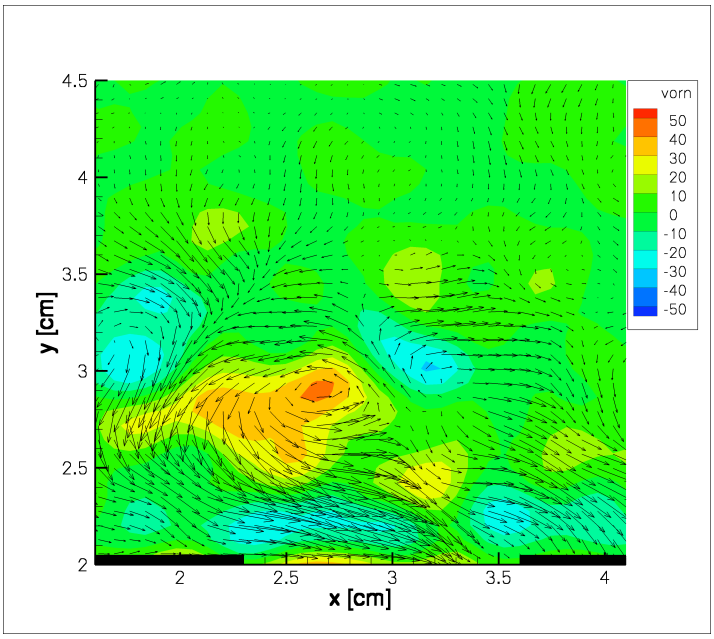

Figure 4.66: Averaged PIV results for both channels at 50% DC, 5° yaw.

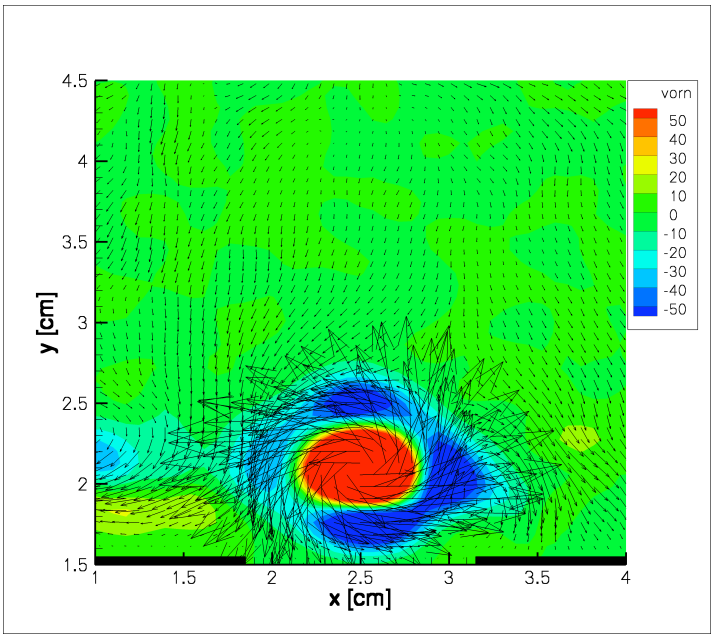

Figure 4.67: Averaged PIV results for both channels at 50% DC, 10° yaw.

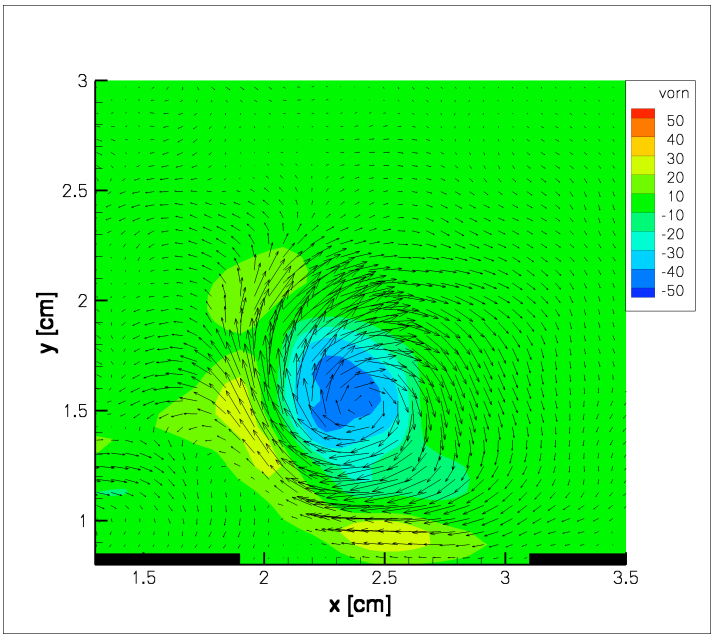

Figure 4.68: Averaged PIV results for two channels at 50% and 20% DC, 0° yaw.

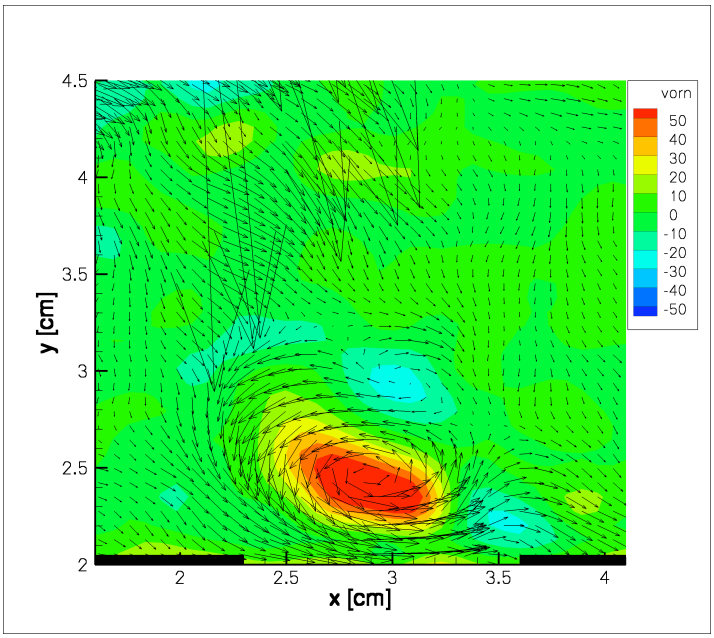

Figure 4.69: Averaged PIV results for two channels at 50% and 20% DC, 5° yaw.

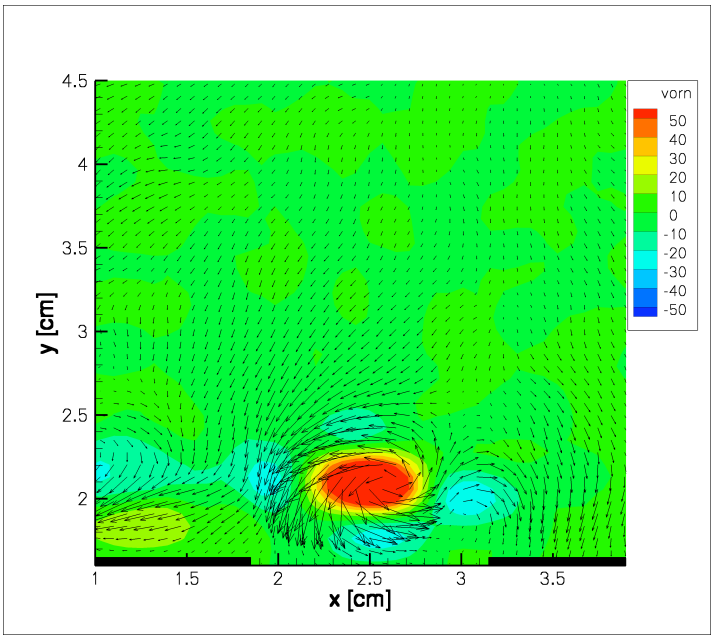

Figure 4.70: Averaged PIV results for two channels at 50% and 20%, 10° yaw.

amount of circulation occurs at a small sideslip angle. The trend is similar for the actuator under asymmetric operation, with the most circulation being produced at a small sideslip angle. Beyond the small sideslip angle of 5°, the amount of circulation produced decreases.

4.2.4 Wind Tunnel Speed

To determine the effects of tunnel speed, two cases cases are studied under two different wind tunnel speeds, 1.7 m/s and 3.4 m/s, giving a U_{jet}/U_{∞} of approximately 0.52 and 0.26, respectively. For all cases in the wind tunnel speed investigation, the two channels of the plasma actuator are pulsed alternately at 250 Hz, and the yaw angle is 0°. The duty cycles of the two channels are 50% and 50% for one case, and 50% and 20% for the other case. Fig. 4.73 and Fig. 4.74 show how the wind tunnel speed affects the jet created by symmetric operation of the jet vectoring plasma actuator. Fig. 4.75 and Fig. 4.76 show the performance of an asymmetrically powered jet vectoring plasma actuator at the two tunnel speeds. For both the symmetric and

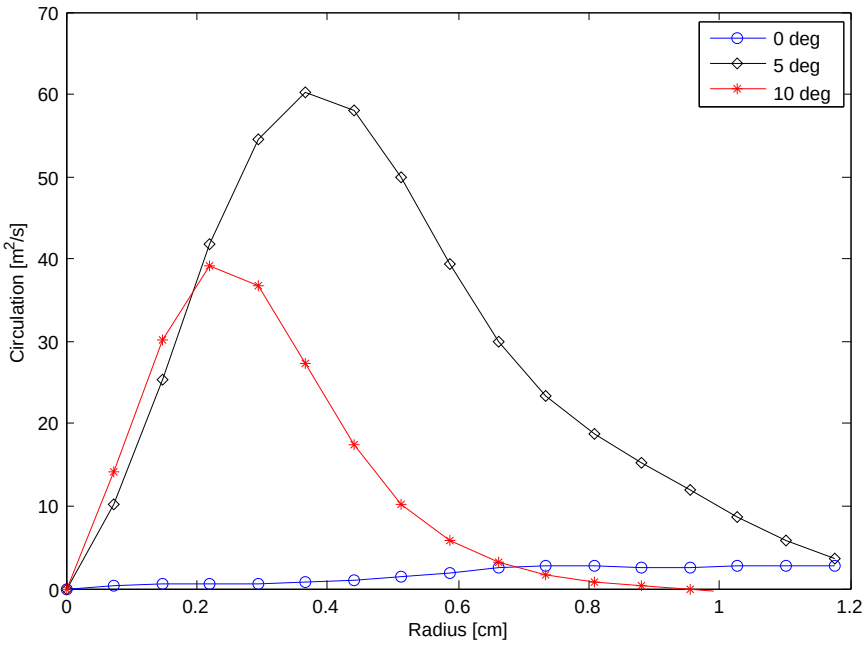

Figure 4.71: Circulation induced by the jet vectoring plasma actuator at different sideslip angles under symmetric operation.

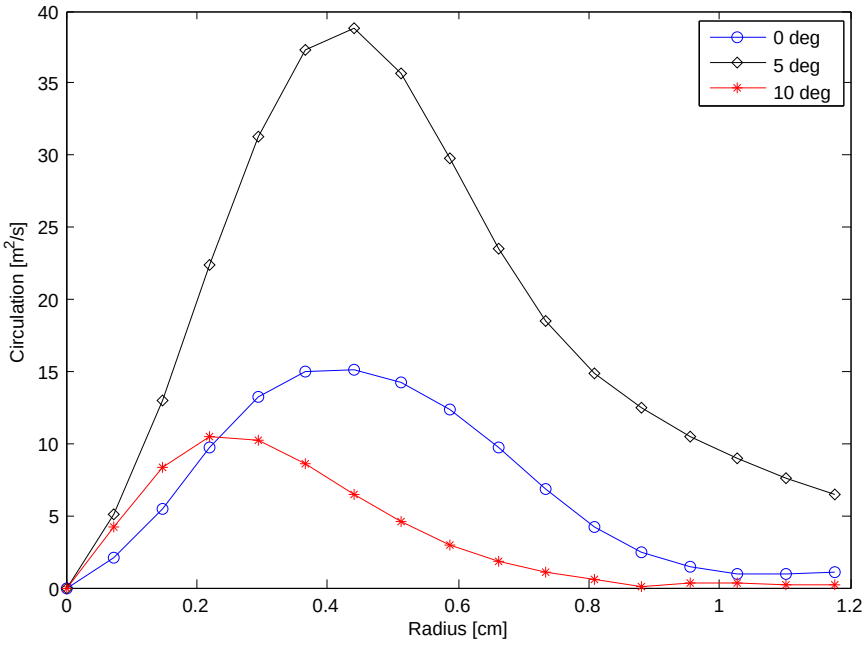

Figure 4.72: Circulation induced by the jet vectoring plasma actuator at different sideslip angles under asymmetric operation (50% and 20% duty cycles).

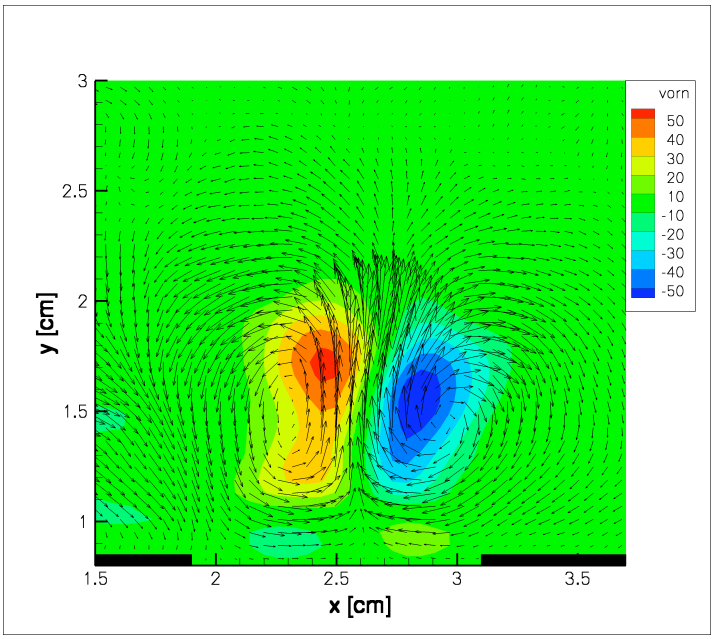

Figure 4.73: Averaged PIV results for both channels at 50%, 1.7m/s tunnel speed.

asymmetric cases, the effectiveness of the plasma actuator is noticeably decreased with an increase in wind tunnel velocity.

Fig. 4.77 shows how the tunnel speed affects the circulation produced by the plasma actuator. While the actuator is operated asymmetrically, the tunnel speed is increased, reducing the circulation created by the actuator. By doubling the tunnel speed, the peak circulation, in this case, is reduced by about half.

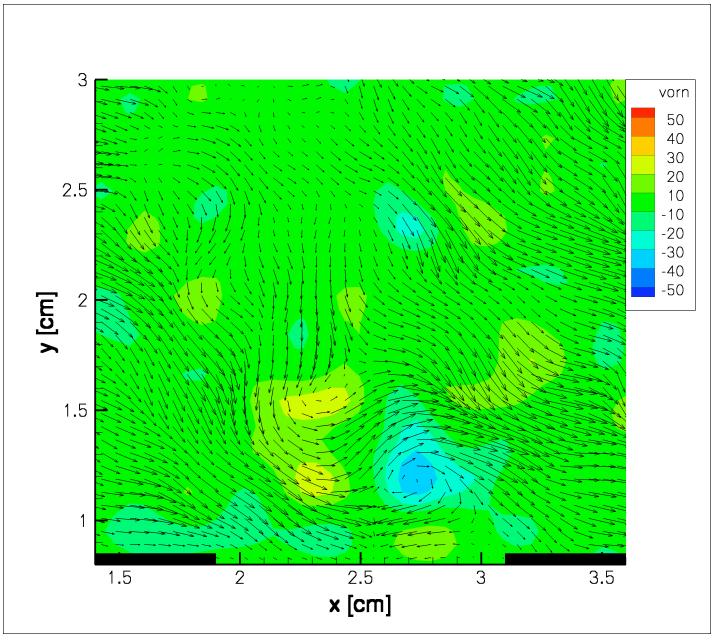

Figure 4.74: Averaged PIV results for two channels at 50%, 3.4m/s tunnel speed.

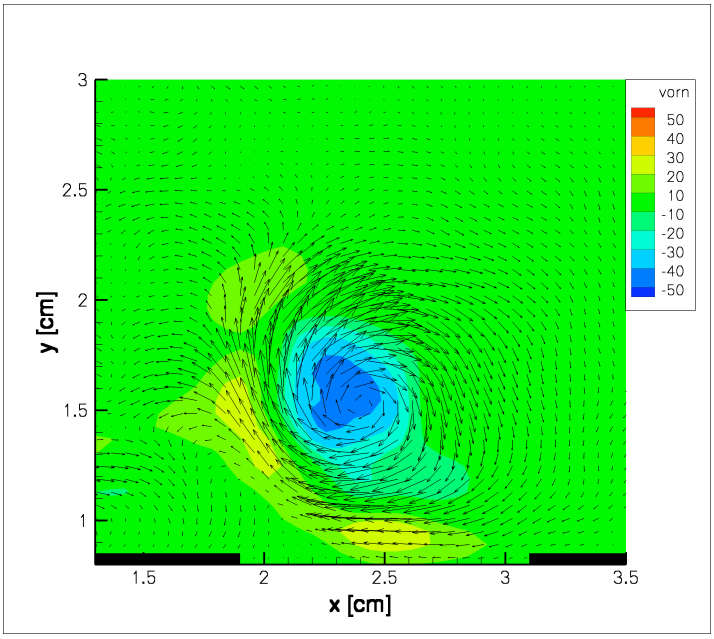

Figure 4.75: Averaged PIV results for two channels at 50% and 20%, 1.7m/s tunnel speed.

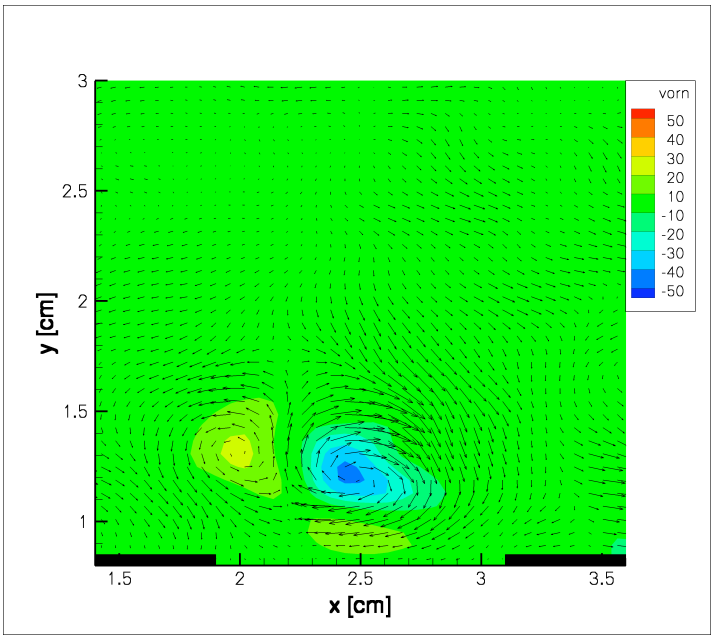

Figure 4.76: Averaged PIV results for two channels at 50% and 20%, 3.4m/s tunnel speed.

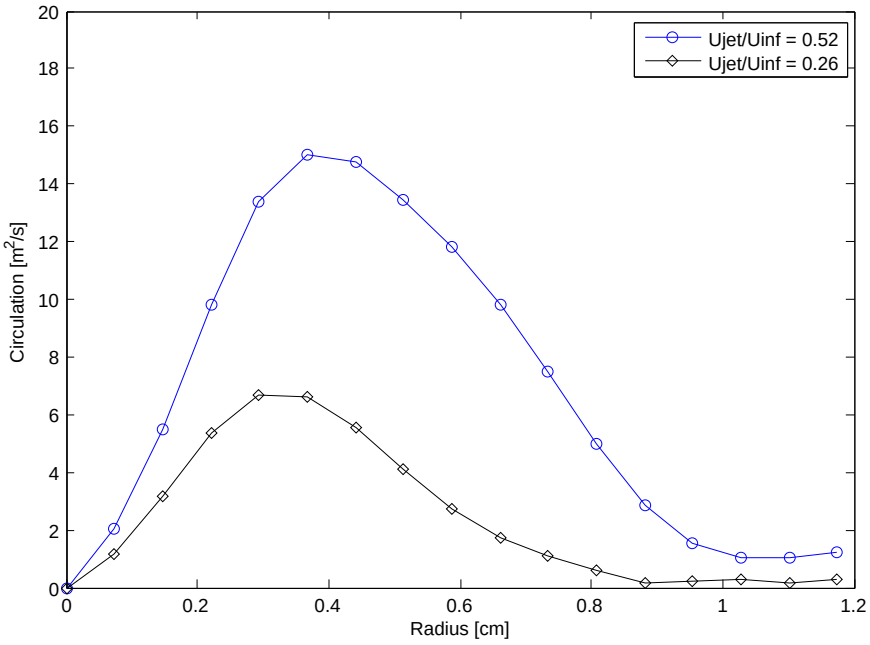

Figure 4.77: Circulation induced by the jet vectoring plasma actuator at different tunnel speeds, under asymmetric operation (50% and 20% duty cycles).

CHAPTER 5

Summary and Conclusions

The effects of input signal and plasma actuator geometry on the type of jet or vortex produced are studied in quiescent conditions as well as a low speed wind tunnel. Both steady and unsteady actuation were studied on the benchtop, while only unsteady actuation was studied in the wind tunnel. The benchtop tests focused on the type of jet produced and angle at which it was produced by varying the input power, operating frequency, duty cycle, exposed electrode spacing, and pulsing frequency. The wind tunnel tests focused on the generation of vortices using the jet vectoring plasma actuator by varying duty cycle, pulsing frequency, and sideslip angle.

It has been shown that the strength of the plasma is directly proportional to the input power; therefore, by varying the input power of one or both sides of the jet vectoring plasma actuator, the resultant induced velocity varies. Using this technique to control the angle of the jet produced results in a jet of any angle over the 180° spectrum. Operated under asymmetric power, the actuator produces a wall normal jet. When the actuator is operated with asymmetric power, the jet produced is either at some non-perpindicular angle to the wall, or parallel to the wall (when only one side of the actuator is powered).

By varying the operating frequency of the plasma actuator, the strength of the plasma is controlled. Similar to varying the input power, this technique produces a wall normal jet during symmetric operation, and a jet non-perpindicular to the wall under asymmetric operation. It is shown that by lowering the operating frequency of one side of the jet vectoring plasma actuator away from its point of maximum plasma

generation (while the other side is held at its point of maximum plasma generation), the angle of the jet produced can be controlled. The momentum induced by the jet is also shown to be affected by the operating frequency of the actuator. By lowering the operating frequency of one side of the actuator, the momentum decreases linearly.

The effects of duty cycle on the jet produced are investigated, and shown to control the angle of jet. While one side of the jet vectoring plasma actuator has a duty cycle of 50%, the other side is varied from 20% to 50%. The angle of the jet produced while varying the duty cycle of one channel was shown to cover the entire span of -90° to 90°. The jet was shown to attach to the wall quickly after after about 30% duty cycle.

Pulsing frequency was varied to each side of the jet vectoring plasma actuator simultaneously, to investigate the effects it has on the type of jet produced. At very low pulsing frequencies, the jet produced is two near wall jets in either direction that are nearly independent of each other. As the frequency is increased to the critical frequency, the vortices formed by either side of the actuator impinge on one another and nearly cancel, producing neither a near wall jet or wall normal jet. As the pulsing frequency is increased beyond the critical frequency, the jet produced is normal to the wall, and resembles a jet under steady operation. Exposed electrode spacing was investigated with the pulsing frequency. It was shown each spacing had a unique critical frequency at which the vortices produced by either side of the actuator would nearly cancel. It was also shown that while the pulsing frequency does not affect the amount of momentum induced by the actuator, the momentum increased as the exposed electrode spacing increased (over the span investigated in the current study).

The investigation conducted in the wind tunnel while varying duty cycle focused on the amount of vorticity created. While keeping the duty cycle of one side of the jet vectoring actuator at 50%, the other side was varied from 10% to 50%. It was shown that the maximum vorticity created was not changed significantly with changes in

duty cycle, but the size and location of the vortex changed with changes in duty cycle.

The effects of sideslip on the vortex produced by the jet vectoring plasma actuator in the wind tunnel were investigated. It was shown that the maximum vorticity increased for all cases of duty cycle (between 10% and 50%) when the sideslip angle was nonzero.

The wind tunnel speed was varied to investigate the effectiveness of the jet vectoring plasma actuator as the speed was increased. Two cases were studied, one in which both channels had a duty cycle of 50% and the second case had 50% duty cycle on one channel and 20% on the other. It was shown that by increasing the tunnel speed, the effectiveness of the actuator diminished.

APPENDIX A

Appendix

A.1 PSJA Arrays

Plasma actuators can be readily arranged such that complex flow structures are created. Fig. **??** shows the creation of a plasma induced synthetic jet by using an annular plasma actuator. These can be pulsed to create vortex rings or run continuously to create a steady zero net mass flux (ZNMF) jet. Unlike synthetic jets, they can easily be reversed to act as suction devices. By modifying the actuator geometry, the plasma induced jets can be arranged such that they create an upward synthetic jet structure or an inverted jet with a downward-then-outward flow, as shown in Fig. A.1.

Also of interest is the use of staging in PSJAs. Currently, with a single actuator under the present configuration, we can achieve velocities in of $\mathcal{O}(1$ m/s). To increase the peak velocity, we are using a staged actuator design where a successive arrangement of concentric actuators is used to continually accelerate the flow to a higher velocity. A cross-section of a 3 stage actuator design is shown in Fig. A.6. Here the letters indicate the annular ring index. A is the outermost ring, B is interior to A,

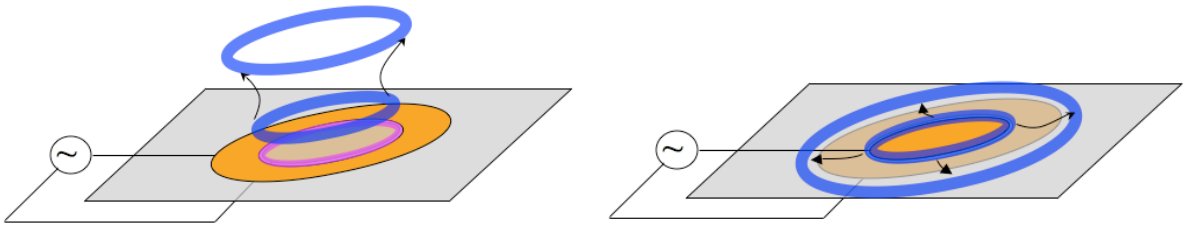

Figure A.1: (a) Plasma ring created by pulsed annular actuator in blowing configuration. (b) Plasma ring created by pulsed annular actuator in suction configuration.

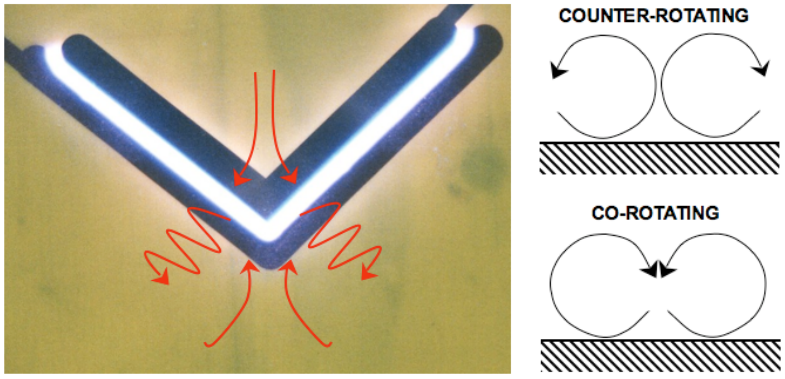

Figure A.2: (a) Vortices induced by chevron actuator. (b) Cross-stream vortex structures.

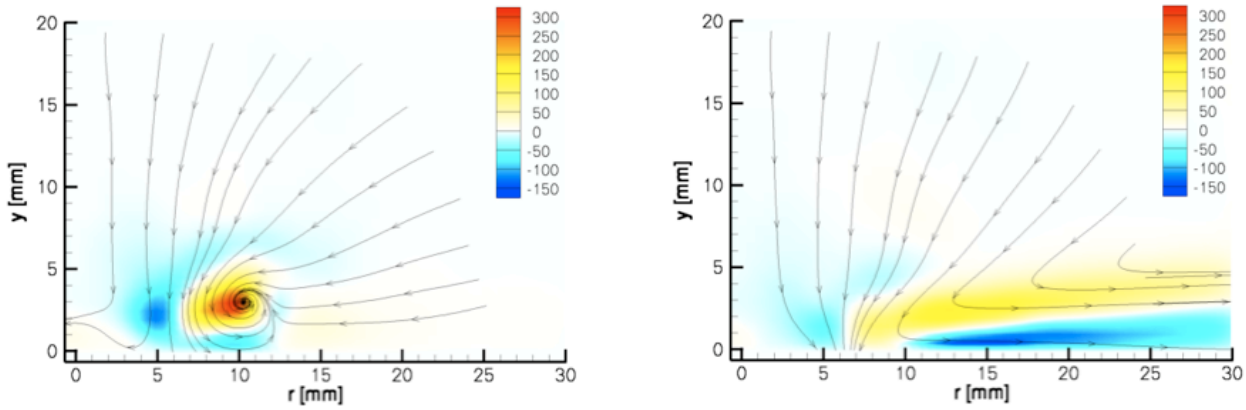

Figure A.3: PIV data of right side of PSJA in suction configuration. Left: phase-locked at $t = 13$ ms. Right: time-averaged.

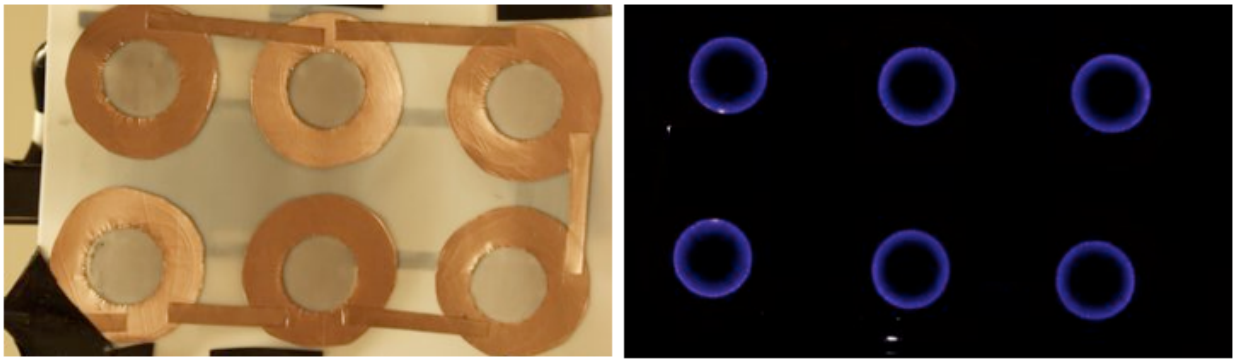

Figure A.4: Array of PSJAs: construction (left) and actuation (right).

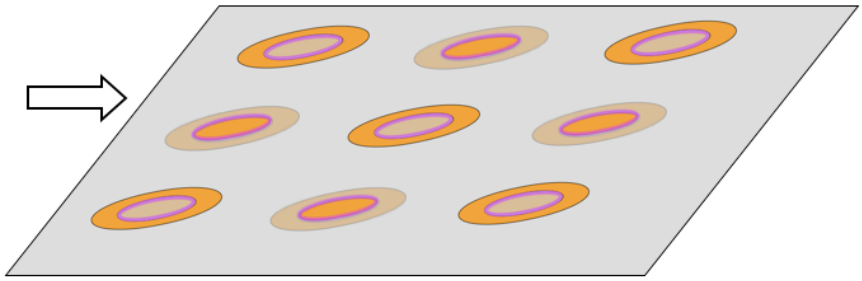

Figure A.5: Grid of alternating blowing and sucking PSJAs.

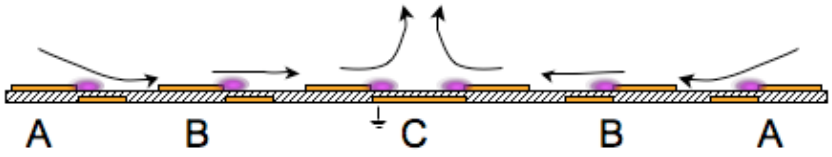

Figure A.6: Cross section of a staged PSJA.

and C is the innermost ring. There are several obvious ways in which that actuator can be actuated. One is to simply have all of the rings actuate simultaneously. In this form, fluid is continually accelerated from the outer region of A to C while both B and C draw additional fluid in from above. In a phased configuration, the A, B and C rings are sequentially actuated, where A is actuated first followed by B and finally C. In this arrangement, the phase lab is determined by the length of time it takes the accelerated fluid parcel to travel from A to B and then from B to C. Note that since this is an annular configuration and the circumference is being reduced as one travels inward, the fluid velocity may increase and thus phase lags are not purely a function of spacing alone. A 2 stage PSJA is shown in Fig. A.7. The outer plasma ring is not continuous to allow the inner ring conductor to pass through without creating non-annular plasma structures. Note that the inner plasma ring is nearing the formation of a plasma disk.

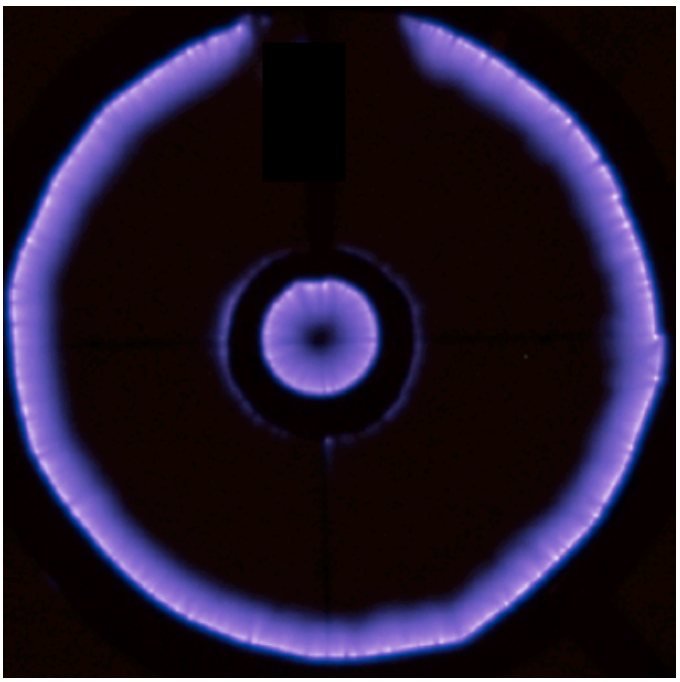

Figure A.7: 2 stage PSJA.

BIBLIOGRAPHY

[1] A. Glezer and M. Amitay, "Synthetic jets," *Annual Rev. of Fluid Mech.*, vol. 34, pp. 503–529, 2002.

[2] M. Malik, L. Weinstein, and M. Hussani, "Ion wind drag reduction," AIAA Paper 83–0231, 21st AIAA Aerospace Sciences Meeting and Exhibit, Reno, NV, Jan. 1983.

[3] C. L. Enloe, T. E. McLaughlin, R. D. VanDyken, K. D. Kachner, E. J. Jumper, and T. C. Corke, "Mechanisms and responses of a single dielectric barrier discharge plasma actuator: Plasma morphology," *AIAA Journal*, vol. 42, no. 3, pp. 589–594, 2004.

[4] C. L. Enloe, T. E. McLaughlin, R. D. VanDyken, K. D. Kachner, E. J. Jumper, T. C. Corke, M. Post, and O. Haddad, "Mechanisms and responses of a single dielectric barrier discharge plasma actuator: Geometric effects," *AIAA Journal*, vol. 42, no. 3, pp. 595–604, 2004.

[5] C. O. Porter, J. W. Baughn, T. E. McLaughlin, C. L. Enloe, and G. I. Font, "Temporal force measurements on an aerodynamic plasma actuator," AIAA Paper 2006–104, 44th AIAA Aerospace Sciences Meeting and Exhibit, Reno, NV, Jan. 2006.

[6] J. W. Gregory, C. L. Enloe, G. I. Font, and T. E. McLaughlin, "Force production mechanisms of a dielectric-barrier discharge plasma actuator," AIAA Paper 2007–0185, 45th Aerospace Sciences Meeting and Exhibit, Reno, NV, Jan. 2007.

[7] J. W. Baughn, C. O. Porter, B. L. Peterson, T. E. McLaughlin, C. L. Enloe, G. I. Font, and C. Baird, "Momentum transfer for an aerodynamic plasma actuator with an imposed boundary layer," AIAA Paper 2006–168, 44th AIAA Aerospace Sciences Meeting and Exhibit, Reno, NV, Jan. 2006.

[8] G. I. Font, "Boundary layer control with atmospheric plasma discharges," AIAA Paper 2004–3574, 40th AIAA/ASME/SAE/ASEE Joint Propulsion Conference and Exhibit, Fort Lauderdale, FL, July 2004.

[9] T. C. Corke and M. L. Post, "Overview of plasma flow control: Concepts, optimization, and applications," AIAA Paper 2005–563, 43rd AIAA Aerospace Sciences Meeting and Exhibit, Reno, NV, Jan. 2005.

[10] M. L. Post and T. C. Corke, "Flow control with single dielectric barrier plasma actuators," AIAA Paper 2005–4630, 35th AIAA Fluid Dynamics Conference and Exhibit, Toronto, Ontario, Canada, June 2005.

[11] T. C. Corke, E. J. Jumper, M. Post, D. Orlov, and T. E. McLaughlin, "Application of weakly-ionized plasmas as wing flow-control devices," AIAA Paper 2002–0350, 40th AIAA Aerospace Sciences Meeting and Exhibit, Reno, NV, Jan. 2002.

[12] C. Porter, T. McLaughlin, C. Enloe, G. Font, J. Roney, and J. Baughn, "Boundary layer control using a dbd plasma actuator," AIAA Paper 2007–0786, 45th Aerospace Sciences Meeting and Exhibit, Reno, NV, Jan. 2007.

[13] T. Segawa, H. Furutani, H. Yoshida, T. Jukes, and K.-S. Choi, "Wall normal jet under elevated temperatures produced by surface plasma actuator," AIAA Paper 2007–0784, 45th Aerospace Sciences Meeting and Exhibit, Reno, NV, Jan. 2007.

[14] A. Santhanakrishnan, K. Ramakumar, and J. D. Jacob, "Characteristics of a plasma synthetic jet," ORAL PRESENTATION, Bulletin of the American Physical Society Fluid Dynamics Division, Annual Meeting, Nov. 2005.

[15] J. R. Roth, D. M. Sherman, and S. P. Wilkinson, "Boundary layer flow control with a one atmosphere uniform glow discharge plasma," AIAA Paper 98–0328, 36th AIAA Aerospace Sciences Meeting and Exhibit, Reno, NV, Jan. 1998.

[16] J. D. Jacob, "Some experiments on boundary layer flow control using ac discharge plasma actuators," Air Force Summer Faculty Fellowship Program Final Report, AFRL, WPAFB, Aug. 2003.

[17] J. D. Jacob, R. Rivir, C. Carter, and J. Estevadeordal, "Boundary layer flow control using ac discharge plasma actuators," AIAA Paper 2004–2128, 2nd AIAA Flow Control Conference, Portland, OR, June 2004.

[18] J. R. Roth and X. Dai, "Optimization of the aerodynamic plasma actuator as an electrohydrodynamic (ehd) electrical device," AIAA Paper 2006–1203, 44th AIAA Aerospace Sciences Meeting and Exhibit, Reno, NV, Jan. 2006.

[19] J. R. Roth, X. Dai, J. Rahel, and D. M. Shermann, "The physics and phenomenology of paraelectric one atmosphere uniform glow discharge plasma (OAUGDP) actuators for aerodynamic flow control," AIAA Paper 2005–781, 43rd AIAA Aerospace Sciences Meeting and Exhibit, Reno, NV, Jan. 2005.

[20] C. Porter, A. Abbas, K. Cohen, T. McLaughlin, and C. Enloe, "Spatially distributed forcing and jet vectoring with a dielectric barrier discharge plasma actuator," AIAA Paper 2008–1374, 46th Aerospace Sciences Meeting and Exhibit, Reno, NV, Jan. 2008.

[21] M. Bolitho and J. Jacob, "Thrust vectoring flow control using plasma synthetic jet actuators," AIAA Paper 2008–1429, 46th Aerospace Sciences Meeting and Exhibit, Reno, NV, Jan. 2008.

[22] M. McQuilling and J. D. Jacob, "Effect of chord location on separation control with vortex generator jets on low pressure turbine blades," AIAAaper 2004–2205, 2nd AIAA Flow Control Conference, Portland, OR, June 2004.

[23] A. Gross and H. Fasel, "Investigation of low-pressure turbine separation control," AIAA Paper 2007-0520, 45th Aerospace Sciences Meeting and Exhibit, Reno, NV, Jan. 2007.

[24] J. P. Bons, L. C. Hansen, J. P. Clark, P. J. Koch, and R. Sondergaard, "Designing low-pressure turbine blades with integrated flow control," ASME Paper gt2005-68962, ASME Turbo Expo 2005, Reno, NV, June 2005.

[25] M. McQuilling, B. Hollon, and J. D. Jacob, "Active separation flow control in a low pressure turbine blade cascade model," AIAA Paper 2003–0615, 41st Aerospace Sciences Meeting and Exhibit, Reno, NV, Jan. 2003.

[26] M. Sholl and O. Savas, "A fast lagrangian piv method for study of general high-gradient flows," AIAA Paper 1997–0493, 35th AIAA Aerospace Sciences Meeting, Reno, NV, Jan. 1997.

[27] A. S. Santhanakrishnan, *Characterization and Flow Physics of Plasma Synthetic Jet Actuators*. PhD thesis, University of Kentucky, 2007.

[28] H. Schlichting and K. Gersten, *Boundary Layer Theory*. New York: Springer-Verlag, 8 ed., 2000.

[29] M. Gad-El-Hak, *Flow Control: Passive, Active, and Reactive Flow Management*. New York: Cambridge University Press, 2000.

[30] J. R. Roth, *Industrial Plasma Engineering, Volume II – Applications to Non-Thermal Plasma Processing.* Bristol and Philadelphia: Institute of Physics Publishing, 2001.

[31] P. B. S. Lissaman, "Low-Reynolds number airfoils," *Annual Rev. of Fluid Mech.*, vol. 15, pp. 223–239, 1983.

[32] T. Mueller and J. DeLaurier, "Aerodynamics of small vehicles," *Annual Rev. of Fluid Mech.*, vol. 35, pp. 89–111, 2003.

[33] E. Stanewsky, "Adaptive wing and flow control technology," *Progress in Aerospace Sciences*, vol. 37, pp. 583–667, 2001.

[34] M. Gad-El-Hak, "Control of low-speed airfoil aerodynamics," *AIAA Journal*, vol. 28, pp. 1537–1552, 1990.

[35] M. Gad-El-Hak, "Flow control: The future," *Journal of Aircraft*, vol. 38, pp. 402–418, 2001.

[36] A. Seifert, T. Bachar, D. Koss, M. Shepshelovich, and I. Wygnanski, "Oscillatory blowing: A tool to delay boundary-layer separation," *AIAA Journal*, vol. 34, pp. 2052–2060, 1993.

[37] A. Seifert, A. Darabi, and I. Wygnanski, "Delay of airfoil stall by periodic excitation," *Journal of Aircraft*, vol. 33, pp. 691–698, 1996.

[38] K. B. M. Q. Zaman, A. Bar-Sever, and S. M. Mangalam, "Effect of acoustic excitation on the flow over a low re airfoil," *J. Fluid Mech.*, vol. 182, pp. 127–148, 1987.

[39] C. A. Lyon, M. S. Selig, and A. P. Broeren, "Boundary layer trips on airfoils at low reynolds numbers," AIAA Paper 1997–0511, 35th AIAA Aerospace Sciences Meeting, Reno, NV, Jan. 1997.

[40] M. F. Kerho and M. B. Bragg, "Airfoil boundary layer development and transition with large leading-edge roughness," *AIAA Journal*, vol. 35, no. 1, pp. 75–84, 1997.

[41] D. Miklosovic, M. Murray, L. Howle, and F. Fish, "Leading-edge tubercules delay stall on humpback whale (*Megaptera novaeangliae*) flippers," *Phys. Fluids*, vol. 16, pp. 39–42, May 2004.

[42] A. Santhanakrishnan and J. D. Jacob, "Effect of regular surface perturbations on flow over an airfoil," AIAA Paper 2005–5145, 35th AIAA Fluid Dynamics Conference and Exhibit, Toronto, Ontario, June 2005.

[43] N. J. Pern, J. D. Jacob, and R. P. LeBeau, "Characterization of zero mass flux flow control for separation control of an adaptive airfoil," AIAA Paper 2006–3032, to be presented at the 3rd AIAA Flow Control Conference, San Francisco, CA, June 2006.

[44] T. Lee and P. Gerontakos, "Investigation of flow over an oscillating airfoil," *J. Fluid Mech.*, vol. 512, pp. 313–341, 2004.

[45] V. J. Modi, "On the moving surface bounday-layer control," AIAA Paper 2000–2238, Fluids 2000 Conference and Exhibit, Denver, CO, June 2000.

[46] A. Santhanakrishnan, N. J. Pern, and J. D. Jacob, "Optimization and validation of a variable camber airfoil," AIAA Paper 2005–1956, 13th AIAA/ASME/AHS Adaptive Structures Conference, Austin, Texas, Apr. 2005.

[47] M. Amitay, D. R. Smith, V. Kibens, D. E. Parekh, and A. Glezer, "Aerodynamic flow control over an unconventional airfoil using synthetic jet actuators," *AIAA Journal*, vol. 39, no. 3, pp. 361–370, 2001.

[48] L. Tsuei and O. Savas, "Treatment of interfaces in particle image velocimetry," *Experiments in Fluids*, vol. 29, pp. 203–214, 1999.

[49] S. El-Khabiry and G. Colver, "Drag reduction by dc corona discharge along an electrically conductive flate plate for small reynolds number flow," *Phys. Fluids*, vol. 9, pp. 587–599, May 1997.

[50] J. R. Roth, D. M. Sherman, and S. P. Wilkinson, "Electrodynamic flow control with a glow-discharge surface plasma," *AIAA Journal*, vol. 38, no. 7, pp. 1166–1172, 2000.

[51] S. Leonov, V. Bityurin, N. Savischenko, A. Yuriev, and V. Gromov, "Influence of surface electrical discharge on friction of plate in subsonic and transonic airfoil," AIAA Paper 2001–0640, 39th AIAA Aerospace Sciences Meeting and Exhibit, Jan. 2001.

[52] M. L. Post, "Phased plasma actuators for unsteady flow control," Master's thesis, University of Notre Dame, 2001.

[53] W. Shyy, B. Jayaraman, and A. Andersson, "Modeling of glow discharge-induced fluid dynamics," *J. Appl. Phys.*, vol. 92, pp. 6434–6443, Dec. 2002.

[54] J. P. Boeuf and L. C. Pitchford, "Electrohydrodynamic force and aerodynamic flow acceleration in surface dielectric barrier discharge," *J. Appl. Phys.*, vol. 97, p. 103307, May 2005.

[55] A. Asghar and E. J. Jumper, "Phase syncrhonization of vortex shedding from multiple cylinders using plasma actuators," AIAA Paper 2003–1028, 41st AIAA Aerospace Sciences Meeting and Exhibit, Reno, NV, Jan. 2003.

[56] L. Hultgren and D. Ashpis, "Demonstration of separation delay with glow-discharge plasma actuators," AIAA Paper 2003–1025, 41st AIAA Aerospace Sciences Meeting and Exhibit, Reno, NV, Jan. 2003.

[57] G. Font, C. Enloe, T. McLaughlin, and D. Orlov, "Plasma discharge characteristics and experimentally determined boundary conditions for a plasma actuator," AIAA Paper 2007–01888, 45th Aerospace Sciences Meeting and Exhibit, Reno, NV, Jan. 2007.

[58] J. List, A. Byerley, T. McLaughlin, and R. V. Dyken, "Using a plasma actuator to control laminar separation on a linear cascade turbine blade," AIAA Paper 2003–1026, 41st AIAA Aerospace Sciences Meeting and Exhibit, Reno, NV, Jan. 2003.

[59] R. Rivir, A. White, C. Carter, B. Ganguly, A. Forelines, and J. Crafton, "Turbine flow control, plasma flows," AIAA Paper 2003–6055, 41st AIAA Aerospace Sciences Meeting and Exhibit, Reno, NV, Jan. 2003.

[60] J. Siegenthaler, E. J. Jumper, and A. Asghar, "A preliminary study in regularizing the coherent structures in a planar, weakly compressible, free shear layer," AIAA Paper 2003–0680, 41st AIAA Aerospace Sciences Meeting and Exhibit, Reno, NV, Jan. 2003.

[61] C. Suchomel, D. V. Wie, and D. Risha, "Perspectives on cataloguing plasma technologies applied to aeronautical sciences," AIAA Paper 2003–3852, 34th AIAA Plasmadynamics and Lasers Conference, Orlando, FL, June 2003.

[62] B. Jayaraman and W. Shyy, "Flow control and thermal management using dielectric glow discharge concepts," AIAA Paper 2003–3712, 33rd AIAA Fluid Dynamics Conference and Exhibit, Orlando, FL, June 2003.

[63] T. C. Corke, C. He, and M. P. Patel, "Plasma flaps and slats: An application of weakly ionized plasma actuators," AIAA Paper 2004–2127, 2nd AIAA Flow Control Conference, Portland, OR, June 2004.

[64] C. L. Enloe, T. E. McLaughlin, R. D. VanDyken, and J. C. Fischer, "Plasma structure in the aerodynamic plasma actuator," AIAA Paper 2004–844, 42nd AIAA Aerospace Sciences Meeting and Exhibit, Reno, NV, Jan. 2004.

[65] R. D. VanDyken, T. E. McLaughlin, and C. L. Enloe, "Parametric investigations of a single dielectric barrier plasma actuator," AIAA Paper 2004–846, 42nd AIAA Aerospace Sciences Meeting and Exhibit, Reno, NV, Jan. 2004.

[66] T. C. Corke and E. Matlis, "Phased plasma arrays for unsteady flow control," AIAA Paper 2000-2323, 30th AIAA Fluid Dynamics Conference and Exhibit, Denver, CO, June 2000.

[67] J. Huang, T. C. Corke, and F. O. Thomas, "Plasma actuators for separation control of low-pressure turbine blades," *AIAA Journal*, vol. 44, no. 1, pp. 51–57, 2006.

[68] G. Artana, R. Sosa, E. Moreau, and G. Touchard, "Control of the near-wake flow around a circular cylinder with electrohydrodynamic actuators," *Experiments in Fluids*, vol. 35, pp. 580–588, 2003.

[69] G. Artana, J. D'Adamo, L. Leger, E. Moreau, and G. Touchard, "Flow control with electrohyrodynamic actuators," *AIAA Journal*, vol. 40, no. 9, pp. 1773–1779, 2002.

[70] M. Forte, L. Leger, J. Pons, E. Moreau, and G. Touchard, "Plasma actuators for airflow control: Measurement of the non-stationary induced flow velocity," *Journal of Electrostatics*, vol. 63, pp. 929–936, 2005.

[71] A. Labergue, L. Leger, E. Moreau, and G. Touchard, "Effect of a plasma actuator on an airflow along an inclined wall: P. i.v and wall pressure measurements," *Journal of Electrostatics*, vol. 63, pp. 961–967, 2005.

[72] E. Moreau, L. Leger, and G. Touchard, "Effect of a dc surface-corona discharge on a flat plate boundary layer for air flow velocity up to 25 m/s," *Journal of Electrostatics*, vol. 64, pp. 215–225, 2006.

[73] R. Sosa and G. Artana, "Steady control of laminar separation over airfoils with plasma sheet actuators," *Journal of Electrostatics*, vol. 64, pp. 604–610, 2006.

[74] J. D. Jacob, "Time resolved piv measurements of plasma based flow control," Air Force Summer Faculty Fellowship Program Final Report, AFRL, WPAFB, July 2004.

[75] M. Samimy, I. Adamovich, J. Kim, B. Webb, S. Keshav, and Y. Utkin, "Active control of high speed jets using localized arc filament plasma actuators," AIAA Paper 2004–2130, 2nd AIAA Flow Control Conference, Portland, OR, June 2004.

[76] T. E. McLaughlin, M. D. Munska, J. P. Vaeth, T. E. Dauwalter, J. R. Goode, and S. G. Siegal, "Plasma-based actuators for cylinder wake vortex control," AIAA Paper 2004–2129, 2nd AIAA Flow Control Conference, Portland, OR, June 2004.

[77] M. L. Post and T. C. Corke, "Separation control using plasma actuators – dynamic stall control on an oscillating airfoil," AIAA Paper 2004–2517, 2nd AIAA Flow Control Conference, Portland, OR, June 2004.

[78] C. L. Enloe, T. E. McLaughlin, G. I. Font, and J. W. Baughn, "Parameterization of temporal structure in the single dielectric barrier aerodynamic plasma

actuator," AIAA Paper 2005–564, 43rd AIAA Aerospace Sciences Meeting and Exhibit, Reno, NV, Jan. 2005.

[79] C. Baird, C. L. Enloe, T. E. McLaughlin, and J. W. Baughn, "Acoustic testing of the dielectric barrier discharge (dbd) plasma actuator," AIAA Paper 2005–565, 43rd AIAA Aerospace Sciences Meeting and Exhibit, Reno, NV, Jan. 2005.

[80] D. M. Orlov and T. C. Corke, "Numerical simulation of aerodynamic plasma actuator effects," AIAA Paper 2005–1083, 43rd AIAA Aerospace Sciences Meeting and Exhibit, Reno, NV, Jan. 2005.

[81] F. O. Thomas, A. Kozlov, and T. C. Corke, "Plasma actuators for landing gear noise reduction," AIAA Paper 2005–3010, 11th AIAA/CEAS Aeroacoustics Conference, Monterey, CA, May 2005.

[82] J. Lopera, T. T. Ng, M. P. Patel, S. Vasudevan, and T. C. Corke, "Aerodynamic control of 1303 uav using windward surface plasma actuators on a separation ramp," AIAA Paper 2007–0636, 45th Aerospace Sciences Meeting and Exhibit, Reno, NV, Jan. 2007.

[83] M. P. Patel, T. T. Ng, S. Vasudevan, T. Corke, M. Post, T. E. McLaughlin, and C. F. Suchomel, "Scaling effects of an aerodynamic plasma actuator," AIAA Paper 2007–0635, 45th Aerospace Sciences Meeting and Exhibit, Reno, NV, Jan. 2007.

[84] J. H. Mabe, F. T. Calkins, B. Wesley, R. Woszidlo, L. Taubert, and I. Wygnanski, "On the use of single dielectric barrier discharge plasma actuators for improving the performance of airfoils," AIAA Paper 2007–3972, 45th Aerospace Sciences Meeting and Exhibit, Reno, NV, Jan. 2007.

[85] D. M. Orlov, T. Apker, C. he Hesham Othman, and T. C. Corke, "Modeling and experiment of leading edge separationo control using sdbd plasma actuators,"

AIAA Paper 2007–0786, 45th Aerospace Sciences Meeting and Exhibit, Reno, NV, Jan. 2007.

[86] N. McMullin and D. Snyder, "Numerical simulation of plasma-based actuator vortex control of a turbulent cylinder wake," AIAA Paper 2007–0936, 45th Aerospace Sciences Meeting and Exhibit, Reno, NV, Jan. 2007.

[87] T. Abe, Y. Takizawa, S. Sato, and N. Kimura, "A parametric experimental study for momentum transfer by plasma actuator," AIAA Paper 2007–0187, 45th Aerospace Sciences Meeting and Exhibit, Reno, NV, Jan. 2007.

[88] M. L. Post, S. L. Greenwade, M. H. Yan, T. C. Corke, and M. P. Patel, "Effects of and aerodynamic plasma actuator on an hsnlf airfoil," AIAA Paper 2007–0638, 45th Aerospace Sciences Meeting and Exhibit, Reno, NV, Jan. 2007.

[89] G. I. Font and W. L. Morgan, "Plasma discharges in atmospheric pressure oxygen for boundary layer separation control," AIAA Paper 2005–4632, 35th Fluid Dynamics Conference and Exhibit, Toronto, Ontario, June 2005.

[90] K. Ramakumar and J. D. Jacob, "Flow control and lift enhancement using plasma actuators," AIAA Paper 2005–4635, 35th AIAA Fluid Dynamics Conference and Exhibit, Toronto, Ontario, June 2005.

[91] Y. B. Suzen, P. G. Huang, J. D. Jacob, and D. E. Ashpis, "Numerical simulation of plasma based flow control applications," AIAA Paper 2005–4633, 35th AIAA Fluid Dynamics Conference and Exhibit, Toronto, Ontario, June 2005.

[92] J. D. Jacob, K. Ramakumar, R. Anthony, and R. B. Rivir, "Control of laminar and turbulent shear flows using plasma actuators," TSFP 4-225, 4th International Symposium on Turbulence and Shear Flow Phenomena, Williamsburg, VA, June 2005.

[93] J. S. Shang, "Electromagnetic field of dielectric barrier discharge," AIAA Paper 2005–5182, 36th AIAA Plasmadynamics and Lasers Conference, Toronto, Ontario, June 2005.

[94] J. S. Shang and C. L. Chang, "Magneto-aerodynamic interaction over airfoil," AIAA Paper 2005–5179, 36th AIAA Plasmadynamics and Lasers Conference, Toronto, Ontario, June 2005.

[95] K. D. Hall, E. J. Jumper, T. C. Corke, and T. E. McLaughlin, "Potential flow model of a plasma actuator as a lift enhancement device," AIAA Paper 2005–783, 43rd AIAA Aerospace Sciences Meeting and Exhibit, Reno, NV, Jan. 2005.

[96] A. Santhanakrishnan and J. D. Jacob, "On plasma synthetic jet actuators," AIAA Paper 2006–0317, 44th AIAA Aerospace Sciences Meeting and Exhibit, Reno, NV, Jan. 2006.

[97] A. Santhanakrishnan, J. D. Jacob, and Y. B. Suzen, "Flow control using plasma actuators and linear/annular plasma synthetic jet actuators," AIAA Paper 2006–3033, 3rd AIAA Flow Control Conference, San Francisco, CA, June 2006.

[98] C. L. Enloe, T. E. McLaughlin, G. I. Font, and J. W. Baughn, "Frequency effects on the efficiency of the aerodynamic plasma actuator," AIAA Paper 2006–166, 44th AIAA Aerospace Sciences Meeting and Exhibit, Reno, NV, Jan. 2006.

[99] G. I. Font, S. Jung, C. L. Enloe, T. E. McLaughlin, W. L. Morgan, and J. W. Baughn, "Simulation of the effects of force and heat produced by a plasma actuator on neutral flow evolution," AIAA Paper 2006–167, 44th AIAA Aerospace Sciences Meeting and Exhibit, Reno, NV, Jan. 2006.

[100] R. Anderson and S. Roy, "Preliminary experiments of barrier discharge plasma actuators using dry and humid air," AIAA Paper 2006–369, 44th AIAA Aerospace Sciences Meeting and Exhibit, Reno, NV, Jan. 2006.

[101] B. E. Balcer, M. E. Franke, and R. B. Rivir, "Effects of plasma induced velocity on boundary layer flow," AIAA Paper 2006–875, 44th AIAA Aerospace Sciences Meeting and Exhibit, Reno, NV, Jan. 2006.

[102] T. C. Corke, B. Mertz, and M. P. Patel, "Plasma flow control optimized airfoil," AIAA Paper 2006–1208, 44th AIAA Aerospace Sciences Meeting and Exhibit, Reno, NV, Jan. 2006.

[103] S. Roy, H. Kumar, D. V. Gaitonde, and M. Visbal, "Effective discharge dynamics for plasma actuators," AIAA Paper 2006–374, 44th AIAA Aerospace Sciences Meeting and Exhibit, Reno, NV, Jan. 2006.

[104] M. Visbal and D. V. Gaitonde, "Control of vortical flows using simulated plasma actuators," AIAA Paper 2006–505, 44th AIAA Aerospace Sciences Meeting and Exhibit, Reno, NV, Jan. 2006.

[105] Y. B. Suzen and P. G. Huang, "Simulations of flow separation control using plasma actuators," AIAA Paper 2006–877, 44th AIAA Aerospace Sciences Meeting and Exhibit, Reno, NV, Jan. 2006.

[106] D. M. Orlov, T. C. Corke, and M. P. Patel, "Electric circuit model for aerodynamic plasma actuator," AIAA Paper 2006–1206, 44th AIAA Aerospace Sciences Meeting and Exhibit, Reno, NV, Jan. 2006.

[107] B. Goksel, D. Greenblatt, I. Rechenberg, C. N. Nayeri, and C. O. Paschereit, "Steady and unsteady plasma wall jets for separation and circulation control," AIAA Paper 2006–3686, 3rd AIAA Flow Control Conference, San Francisco, CA, June 2006.

[108] K. Ramakumar, "Active flow control of low pressure turbine blade separation using plasma actuators," Master's thesis, University of Kentucky, Lexington, Kentucky, May 2006.

[109] A. Santhanakrishnan and J. D. Jacob, "Flow control with plasma synthetic jet actuators," *J. Phys. D: Appl. Phys.*, vol. 40, 2007.

[110] A. Santhanakrishnan and J. D. Jacob, "Characteristics of plasma synthetic jet actuators in crossflow," ORAL PRESENTATION, Bulletin of the American Physical Society Fluid Dynamics Division, 59th Annual Meeting, Nov. 2006.

[111] A. Santhanakrishnan and J. D. Jacob, "Effect of plasma morphology on flow control using plasma synthetic jet actuators," AIAA Paper 2007–0783, to be presented at the 45th AIAA Aerospace Sciences Meeting and Exhibit, Reno, NV, Jan. 2007.

[112] A. Santhanakrishnan and J. D. Jacob, "Formation and scaling of plasma synthetic jet actuators," AIAA Paper 2007–0940, to be presented at the 45th AIAA Aerospace Sciences Meeting and Exhibit, Reno, NV, Jan. 2007.

[113] H. J. Hussein, S. P. Capp, and W. K. George, "Velocity measurements in a high reynolds number, momentum conserving, axisymmetric, turbulent jet," *J. Fluid Mech.*, vol. 258, pp. 31–75, 1994.

[114] R. D. James, J. W. Jacobs, and A. Glezer, "A round turbulent jet produced by an oscillating diaphragm," *Phys. Fluids*, vol. 8, pp. 2484–2495, Sept. 1996.

[115] M. Amitay, B. L. Smith, and A. Glezer, "Aerodynamic flow control using synthetic jet technology," AIAA Paper 98–0208, 36th AIAA Aerospace Sciences Meeting and Exhibit, Reno, NV, Jan. 1998.

[116] B. L. Smith and A. Glezer, "The formation and evolution of synthetic jets," *Phys. Fluids*, vol. 10, pp. 2281–2297, Sept. 1998.

[117] O. . K. Rediniotis, J. Ko, X.Yue, and A. Kurdilla, "Synthetic jets, their reduced order modeling and applications to flow control," AIAA Paper 99–1000, 37th AIAA Aerospace Sciences Meeting and Exhibit, Reno, NV, Jan. 1999.

[118] M. Amitay, B. L. Smith, and A. Glezer, "Aerodynamic flow control using synthetic jet technology," AIAA Paper 98–0208, 36th AIAA Aerospace Sciences Meeting and Exhibit, Reno, NV, Jan. 1998.

[119] J. C. Bera, M. Michard, N. Grosjean, and G. Comte-Bellot, "Flow analysis of two-dimensional pulsed jets by particle image velocimetry," *Experiments in Fluids*, vol. 31, pp. 519–532, 2001.

[120] J. E. Cater and J. Soria, "The evolution of round zero-net-mass-flux jets," *J. Fluid Mech.*, vol. 472, pp. 167–200, 2002.

[121] R. Mittal and P. Rampunggoon, "On the virtual aeroshaping effect of synthetic jets (brief communication)," *Phys. Fluids*, vol. 14, pp. 1533–1536, Apr. 2002.

[122] M. B. Chiekh, J. C. Bera, and M. Sunyach, "Synthetic jet control for flows in a diffuser: Vectoring, spreading and mixing enhancement," *Journal of Turbulence*, vol. 32, pp. 1–12, 2003.

[123] B. L. Smith and G. W. Swift, "A comparison between synthetic jets and continuous jets," *Experiments in Fluids*, vol. 34, pp. 467–472, 2003.

[124] R. Mittal, R. B. Kotapati, and L. N. Cattafesta, "Numerical study of resonant interactions and flow control in a canonical separated flow," AIAA Paper 2005–1261, 43rd AIAA Aerospace Meetings & Exhibits, Reno, NV, Jan. 2005.

VITA

Michael Bolitho

Candidate for the Degree of

Master of Science

Thesis: JET VECTORING AND VORTICITY GENERATION USING PLASMA ACTUATORS

Major Field: Mechanical Engineering

Biographical:

Personal Data: Born in Kansas City, MO, USA on March 10, 1983.

Education:

Received the B.S. degree from Oklahoma State University, Stillwater, OK, USA, 2006, in Mechanical Engineering

Completed the requirements for the degree of Master of Science with a major in mechanical engineering at Oklahoma State University in May, 2008.

Name: Michael Bolitho Date of Degree: May, 2008

Institution: Oklahoma State University Location: Stillwater, Oklahoma

Title of Study: JET VECTORING AND VORTICITY GENERATION USING PLASMA ACTUATORS

Pages in Study: 101 Candidate for the Degree of Master of Science

Major Field: Mechanical Engineering

The current study examines the use of plasma actuators as flow control devices, including synthetic jet actuators, jet vectoring, and vortex generation. The study of the plasma actuators applied to flat plates is conducted in quiescent conditions, as well as in the wind tunnel. There are two arrangements of plasma actuators investigated, one of which consists of an inner circular electrode embedded under a dielectric material and an outer annular electrode exposed to the atmosphere, and is used to create flow structures similar to that of a conventional synthetic jet actuator. The other arrangement is made up of a single linear electrode embedded within a dielectric material with a linear electrode on either side exposed to the atmosphere, and is used to create vectored jets and generate streamwise vortices. To create the plasma, the embedded electrode in each case is grounded while a high voltage, high frequency signal is applied to the exposed electrode(s). The benchtop experiments conducted primarily focus on the parametric study of jet vectoring, investigating the effects of the variation of input signal and geometry. The experiments conducted in the wind tunnel expand upon the benchtop, studying the uses of the jet vectoring plasma actuator in cross-stream flow, especially the use as a vortex generator jet (VGJ). For both the benchtop and wind tunnel investigations, the method of experimentation was done through PIV. It was found that through variations in the input signal, including voltage drop, frequency, and duty cycle, the jet created by the jet vectoring plasma actuator can be controlled over the entire 180° spectrum. While the plasma actuator investigated here demonstrates this ability, the attainable thrust vectoring angles are approximately 40° with respect to the surface. Varying pulsing frequency affects the type of jet produced by the jet vectoring plasma actuator. At low frequencies, the actuator produces two near wall jets in opposite directions, and at high frequencies, it produces a wall normal jet. There is a critical pulsing frequency at which the vortices created by each side of the actuator impinge on each other and nearly cancel. The portion of this study that was completed in the wind tunnel focused on the use of the plasma actuator previously discussed as a VGJ. The plasma actuator was placed on a flat alumina ceramic plate, and the effects of duty cycle, pulsing frequency, sideslip angle, and wind tunnel speed are investigated. The pulsing frequency is found to change the type of vortex or jet produced, similar to the benchtop results. Varying the sideslip angle slightly increases the vorticity created, but higher sideslip angles produce much less streamwise vorticity.

ADVISOR'S APPROVAL: Dr. Jamey Jacob